EXPERIMENTAL STUDY OF UNBONDED FIBER REINFORCED ELASTOMERIC BEARINGS

EXPERIMENTAL STUDY OF UNBONDED FIBER REINFORCED ELASTOMERIC BEARINGS

By

MICHAEL DE RAAF, B.Eng.

A Thesis

Submitted to the School of Graduate Studies

in Partial Fulfillment of the Requirements

for the Degree

Master of Applied Science

McMaster University

Master of Applied Science (2009)
(Civil Engineering)

McMaster University
Hamilton, Ontario

TITLE: Experimental Study of Unbonded Fiber Reinforced Elastomeric Bearings

AUTHOR: Michael de Raaf

SUPERVISOR: Dr. Michael J. Tait

NUMBER OF PAGES: 121 pages (i-xiv, 1-107)

Abstract

Multilayer elastomeric bearings are a type of seismic isolation device that mitigates seismic damage by lengthening the fundamental period of a low-rise structure. Carbon fiber reinforced elastomeric isolators (FREIs) have been identified as a cost effective alternative to bearings reinforced with steel shims. The stable unbonded fiber reinforced elastomeric isolator (SU-FREI) is an evolution of the FREI. In an attempt to reduce costs even further, FREI bearings of a specific aspect ratio and shape factor have been investigated in an unbonded application with successful results. SU-FREI bearings have shown potential as a viable solution for a more affordable and efficient method of seismic base isolation. Several experimental test procedures were employed in this thesis to further investigate the performance of SU-FREI bearings.

The first objective of this research was to compare the dynamic properties of unscragged SU-FREI bearings at parallel and diagonal orientations. Square ¼ scale SU-FREI bearings were subjected to cyclic excitation under design axial load at 0° (parallel) and 45° (diagonal) orientations. Square SU-FREI bearings achieved acceptable base isolation characteristics at both orientations despite subtle differences in their mechanical properties. Stable rollover (SR) deformation was observed for both orientations.

The stability of SU-FREI bearings under dynamic excitation was the next topic investigated in this thesis. To achieve this, ¼ scale square SU-FREI bearings were subjected to cyclic testing under incrementally increasing lateral displacement amplitudes and axial loads. It was found that the critical buckling load under dynamic excitation decreases with increasing lateral excitation amplitude. SU-FREI bearings exhibited acceptable performance at axial loads well in excess of expected design axial loads.

In addition, an ultimate shear properties test was performed in order to investigate rollout instability in SU-FREI bearings. Rollout was not observed in bearings tested in this study. Test results did however highlight the stiffening effect of vertical facial contact throughout roll over deformation.

Finally, SU-FREI bearings underwent cyclic testing under serviceability and fatigue conditions. Serviceability tests were performed on ¼ scale SU-FREI bearings at lateral displacement amplitudes corresponding to those expected from a 1 in 10 year return period wind pressure. Fatigue testing was performed on ¼ scale bearings at a lateral displacement amplitude equal to the total design displacement (D_{TD}) as required by ASCE 7-05. SU-FREI bearings displayed adequate scragged performance under both serviceability and fatigue testing. Both effective stiffness and damping remained within acceptable limits throughout these tests.

Acknowledgements

First and foremost I would like to thank my graduate supervisor Dr. Michael Tait for his support, guidance and encouragement throughout this research.

I would also like to express my gratitude to Dr. Hamid Toopchi-Nezhad whose advice and assistance have been invaluable.

I would like to thank the technical staff at both the ADL and JHE, specifically: Mr. Peter Koudys, Mr. Dave Perrett, and Mr. Kent Wheeler. Their assistance and advice has been greatly appreciated.

I would also like to thank my friends and colleagues for their support helpful discussion and encouragement.

Finally I would like to thank my family for their understanding and their support during this process.

Table of Contents

List of Tables

List of Figures

Chapter 1. Introduction

This chapter presents an introduction to the theory behind base isolation and a review of the literature surrounding the topic. The types of base isolation systems in use today are discussed with specific attention paid to the multilayer elastomeric bearing system. Several examples of structures that use base-isolation around the world are presented.

1.1 Introduction

The earliest proposals for base isolation technology date back over 100 years (Chopra, 2007, p. 741). Early examples of this technology provided protection to motion sensitive mechanical equipment by isolating the equipment from structural vibrations. They were also used to minimize vibration effects of equipment on structural supports (Connor & Clink, 1996, p.197). Significant progress has been made in the field of base isolation in the past couple of decades (Connor & Clink, 1996, p.198). There are two primary types of isolation systems currently in use. The first method involves the use of reinforced elastomeric bearings and the second method involves the use of a sliding system. Both systems work by modifying the dynamic properties of the structural system to deflect earthquake energy. All base isolation methods attempt to introduce a layer of low lateral stiffness at the base of the structure, between the foundation and superstructure.

1.2 Theory of Base Isolation

Base isolation is effective in cases where a building has a fundamental frequency that is within the high frequency range of earthquake ground motion for a given region. The isolation system introduces a layer of low lateral stiffness between the foundation and superstructure, which changes the fundamental frequency of the structural system. This acts to decouple the building from the horizontal components of earthquake ground motion. The fundamental frequency of the isolated structure is much lower than both the fixed-base period of the structure and the predominant frequency range of earthquake ground motion.

The Uniform Hazard Spectra (UHS) for 3 major Canadian cities is provided in Figure 1.1. It can be seen in this figure that spectral acceleration during an earthquake is commonly at its highest between periods of 0.1 – 0.5 seconds. Low rise structures with fundamental periods in this range amplify these accelerations. This leads to increased inter-story drift, resulting in structural damage. In order to avoid structural damage it is advantageous to lengthen the fundamental period of the structural system. This can be accomplished by introducing a layer of low lateral stiffness at the base of a structure between the superstructure and foundation. This is the origin of the term base isolation. The introduction of the isolation layer changes the first mode of the structure so that displacements occur predominantly in the isolation layer. Base isolation minimizes the inter-story drift as well as ground floor accelerations. The displacement during earthquake ground motion is effectively deflected to the isolation layer at the base of the structure.

1.3 Application of Base Isolation

Base isolation technology is used predominantly for projects of high value, buildings with historical significance and structures housing expensive equipment or essential services. The reason for this limitation is due to the cost of manufacturing and installing these devices. For smaller projects, like residential structures, it is not economically feasible to manufacture and install a base isolation system. For the same economic reasons, it is difficult for developing countries to adopt base isolation technology. Despite these constraints, there are numerous examples of base isolated structures worldwide.

A typical layout of a base isolation system installed in a structure is provided in Figure 1.2 for the Foothill Communities Law and Justice Center (FCLJC) in Rancho Cucamonga San Bernardino County. An isolator is placed underneath each column in between the superstructure and the foundation. In cases where the isolation layer is below grade, a clearance or "seismic gap" is required. The seismic gap is dependent on the ultimate expected displacement of the isolation system (Taylor & Igusa, 2004). In the case of the FCLJC the seismic gap measures 16" around the entire structure (Kelly J. M., 1997). The seismic gap requires special considerations such as flexible utility connections and cover plates capable of carrying pedestrian loads (Taylor & Igusa, 2004).

The FCLJC, completed in 1985, was the first base-isolated structure built in the United States, and was designed to withstand a magnitude 8.3 earthquake. The isolation system for this building consists of 98 natural rubber isolators reinforced with steel plates (Naiem & Kelly, 1999). This marked the first structure in the world to use high-damping natural rubber bearings for base-isolation. The isolators used were developed from highly filled natural rubber which exhibited high shear stiffness at low strain and 4-5 times less shear stiffness at high strains (Naiem & Kelly, 1999). At shear strains greater than 100% the bearings begin to stiffen again. For wind loading and low level earthquakes the stiffness in the isolation layer is relatively high. The stiffness in the isolation layer drops as the load increases which in turn lengthens the period of the structure. These properties are ideal for a base-isolated structure that will need to perform under wind loading in addition to strong earthquake events.

Base isolation is not limited to inclusion in the initial design of a structure. Alternatively, these bearings may be used in cases of seismic retrofit where it may be desirable to protect existing high value structures from earthquake damage. One example of such a retrofit is the San Francisco City Hall. Designed in 1911, it is listed in the National Register of Historic Places. In 1989 the structure sustained significant damage from the Loma Prieta Earthquake. As part of the seismic retrofit strategy, 530 lead-plug rubber bearings were installed just above the existing foundation. The installation of the isolation system involved a complicated process of shoring and cutting columns while the load was transferred to temporary supports (Naiem & Kelly, 1999).

Other examples include: the Emergency Operations Centre in California, the San Francisco City Hall, the Los Angeles City Hall, and the West Japan Postal Centre. All of these examples are high value structures such as government buildings and medical centers. In order to expand the application of isolation systems to practical use in common structures and developing countries, it is necessary to reduce the costs involved in both their manufacture and installation. This study explores the feasibility through experimental testing of one such cost saving alternative to current base isolation practices; the Stable Unbonded - Fiber Reinforced Elastomeric Isolator SU-FREI.

1.4 Base Isolation Systems

There are two basic types of isolation systems in use today; the most common type involves elastomeric bearings; the other is a low-friction sliding system. Elastomeric bearings began as large rubber blocks consisting of a damped natural gum rubber or neoprene (Naiem & Kelly, 1999). The first evolution of the elastomeric bearing is the multilayer elastomeric bearing which consists of alternating layers of rubber and lateral reinforcement sheets that provide additional axial stiffness which was found lacking in previous rubber block designs (Naiem & Kelly, 1999). Thin steel plates, also referred to as shims, are the typical choice of reinforcement for multilayer elastomeric isolators. The second type of base isolation involves the use of a sliding system. A number of sliding systems have been developed and installed around the world. Some examples of sliding systems include the friction pendulum system, and the shape memory system. Both systems provide a layer of low lateral stiffness between the foundation and superstructure of the building. This study deals with the multilayer elastomeric base isolator.

1.4.1 Multilayer Elastomeric Base Isolators

Elastomeric base isolation systems began as large rubber blocks with no reinforcement, steel or otherwise. These bearings had a vertical stiffness of only a couple times that of their horizontal stiffness, resulting in axial compression of up to 25% under the weight of the structure alone (Naiem & Kelly, 1999). This led to the development of elastomeric base isolators with reinforcing sheets in order to increase the vertical stiffness to hundreds of times the horizontal stiffness. This also limited the bulging of elastomeric isolators under axial load.

Multilayer elastomeric bearings started as alternating layers of low damped natural rubber or synthetic rubber (neoprene) with steel shims for additional vertical stiffness. Lateral stiffness and damping of these isolators are dependent on the rubber material used. Low damping elastomeric bearings have the advantage of being well understood, as well as being easy to manufacture and easy to model. However, isolation systems with low damping require elaborate supplementary damping systems (Naiem & Kelly, 1999). Supplementary damping systems will incur additional costs, which are not necessary when sufficient damping can be developed by the isolators themselves.

Additional damping can be achieved by either adding a hole and lead-plug to the isolator or by using a high damping natural rubber or neoprene. A lead-plug core can be added to a steel reinforced bearing by simply placing a cylindrical lead-plug to the centre of the bearing. The lead core is forced to displace by the interlocking steel sheets. Lead was chosen based on its availability and energy dissipating capabilities (Robinson, 1982). A study performed by Aiken et al. (1992) involved a comparative test between two types of high damping rubber bearings and one lead-rubber bearing. Acceptable damping ratios were achieved for all three bearing types. Both methods are widely accepted as methods for adding damping to multilayer elastomeric isolators.

Conventional steel reinforced elastomeric base isolators (SREIs) are currently the most widely used and recognized multilayer elastomeric bearings for base isolation purposes worldwide. However, the application of these bearings is limited by manufacturing and installation costs. A number of methods are being explored to find a more cost effective multilayer elastomeric bearing design.

1.4.2 Flexible Reinforcement in Multilayer Elastomeric Isolators

There are two main disadvantages of using steel plates for reinforcing elastomeric base isolators. The first is the weight of the SREI unit and the second is the total cost to manufacture and install. The manufacturing of SREI bearings requires steel plates to be cut, sand blasted, and acid cleaned. The plates and compounded sheets of rubber need to be pressed in a mold and heated for several hours. In addition, vulcanization must be performed under high pressure and temperature. The steel reinforcement in SREIs is rigid in both extension and flexure. The weight of the isolator is mainly due to the weight of these steel plates. Decreasing the cost and weight of reinforced elastomeric isolators is particularly important for application viability in developing countries subjected to high levels of seismic activity.

A light weight, versatile, and cost effective alternative would be ideal for use in seismically active regions of the developing world where SREI bearings are not an affordable option. For this reason, a variety of flexible light weight reinforcements have been investigated as alternatives for multilayer elastomeric base isolators. Fiber Reinforced Elastomeric Isolators (FREIs) are the result of this research. In comparison, fiber reinforcement is more flexible in extension and has no flexural rigidity. The fiber reinforcement in FREIs consists of a matrix of woven strands. These strands straighten out when in-plane tension is applied thereby increasing the tensile modulus of the bearing.

Experimental testing has been performed on bearings with fiber layers composed of glass fiber (Mordini & Strauss, 2008), Kevlar (Kelly & Takhirov,

2001) or more commonly, carbon fiber. Woven carbon fiber fabric is the most researched alternative that has shown promise as a viable alternative to steel. FREI bearings have displayed performance equal to or better than SREI bearings under test conditions in several studies (Kelly, 1999; Kelly & Takhirov, 2001; Moon et al., 2002; Campbell, 2004; Ashkezari et al., 2008). Moon et al. (2002) compared a carbon fiber reinforced elastomeric bearing directly to a steel reinforced bearing of the same dimensions and found that while the effective stiffness of the two bearings were comparable; the FREI bearing provided nearly twice the effective damping of the SREI bearing.

When an FREI bearing is displaced laterally, tension is developed in the reinforcing sheets through the curvature of the bearing. The individual strands in each fiber bundle slip against each other leading to frictional damping, which adds to the damping of the elastomer (Kelly J. M., 1999). When designing an FREI, the added damping from the fibers themselves can be taken advantage of making more elaborate damping techniques unnecessary. For example, the addition of a lead-plug for additional damping becomes unnecessary. A study by Kang et al. (2003) directly compared an FREI isolator to a SREI isolator and an FREI isolator with a lead plug installed. The results of experimental and analytical research showed that fiber reinforcement has a high likelihood of being a good replacement for steel reinforcement. Additionally, it was found that the hole and lead-plug have little effect on the effective stiffness and damping of FREI bearings.

Another benefit of carbon fiber reinforcement is the possibility of creating large sheets of FREI Isolator, which could be cut to the required size. It is important to investigate the feasibility of this manufacturing process and how the production costs compare to SREI bearings, a concern mentioned by Kelly and Takhirov (2001). However, in a following study (Kelly & Takhirov, 2002) Dongil Rubber Belt Company Ltd. in Pusan Korea manufactured examples of long strip isolators reinforced with carbon fiber fabric. The resulting experimental testing showed acceptable performance even though the fiber fabric was of poor quality with many gaps. The possibility for constructing large sheets of FREI bearing exists.

1.4.3 Scragging

A rubber compound in its natural untested state is subject to what is called the Mullins Effect. This occurs when an unfilled or particle reinforced rubber, in its unscragged state, is subjected to cyclic loading at a constant amplitude under tensile, compressive, or shear loading. The stress required on reloading is less than that of the initial loading for deformations up to a maximum of those previously achieved (Dorfmann & Ogden, 2004). These stress differences are typically largest during the first and second cycles and become negligible after 6 to 10 cycles (Dorfmann & Ogden, 2004). Once a bearing has been deformed to a certain elongation, it is scragged up to and including that elongation. Cycling the same bearing at greater amplitudes than those previously tested will result in unscragged behaviour. The term scragging is defined by ASCE (2005) as "Cyclic loading or working of rubber products, including elastomeric isolators, to effect a reduction in stiffness properties, a portion of which will be recovered over time". This study is concerned with exploring the reduction in effective stiffness of SU-FREIs under repeated cycling. Recovered effective stiffness over time is not investigated in this study. The difference between scragged and unscragged load-displacement hysteresis is illustrated in Figure 1.4. Effective stiffness of each loop is measured as the slope of the line made between the largest positive and negative lateral load and displacement in each loop. A drop in effective stiffness is clearly seen in the scragged second cycle of lateral displacement at the same amplitude. This phenomenon is referred to throughout the rest of this study when comparing the properties of the first cycle of an unscragged bearing to subsequent cycles at the same amplitude.

1.4.4 Unbonded Boundary Conditions

Using FREI bearings in an unbonded application would reduce the cost of installation by removing the need of thick steel mounting plates commonly used in practice. There are a variety of connection methods currently in use. Table 1.1 provides a chart comparing current bearing connection methods based on the provisions of ISO (2005) with the inclusion of Type SU (Stable Unbonded). The Type I and Type II connections involve bonding the isolator to thick steel plates which are then bolted in place. In a Type III connection the isolator is bonded to steel plates which are either connected to mounting plates with dowelled pins or recessed rings. All three of these methods involve thick steel plates which are both costly and heavy, requiring significant effort to install. FREIs installed in an unbonded application are placed directly between the foundation and superstructure without any connection to these boundaries.

1.4.5 Rollover

This term was first used by Toopchi-Nezhad et al. (2008a) to describe the behaviour of square FREI bearings without bonding between the contact surfaces and the test platens. The lack of flexural rigidity accompanying the use of carbon fiber fabric is also necessary for rollover deformation. As a result of unbonded boundary conditions, FREI bearings "rollover" under lateral displacement. The top and bottom surfaces of the bearing begin to lose contact with the upper and lower surfaces as the bearing is displaced laterally (Figure 1.3). This behaviour is typically undesirable in elastomeric base isolators due to the loss of stability that normally accompanies it. However, the loss of lateral stiffness accompanying rollover increases the efficiency of an isolation system so long as stability can be maintained. Toopchi-Nezhad et al. (2008a) found that unbonded FREI bearings with a certain aspect ratio and shape factor were able to achieve stable stiffness properties throughout lateral sinusoidal displacement under a constant axial design load.

1.4.6 Stable Unbonded - Fiber Reinforced Elastomeric Isolators

Stable unbonded fiber reinforced elastomeric isolator (SU-FREI) refers to an FREI bearings with no bonding at the contact surfaces (platen), and with an aspect ratio (R) and shape factor (S) such that stable rollover (SR) deformation occurs (Toopchi-Nezhad, Tait, & Drysdale, 2008a). The behaviour of an unbonded FREI bearing is defined as "stable" when positive incremental load-resisting capacity is achieved throughout each fully reversed cycle of lateral displacement. Toopchi-Nezhad et al. (2008a) tested two bearings with aspect ratios of $R = 1.9$ and shape factors of $S = 10.6$ which resulted in unstable behaviour. Two bearings were then cut from the initial specimens with aspect ratios of $R = 2.5$ and $R = 2.9$ respectively. Cyclic lateral testing of SU-FREI bearings with these aspect ratios resulted in stable hysteretic behaviour. In addition, a strength hardening and increased stiffness was observed in the bearings at the largest lateral displacements. This occurred when the two vertical faces of the bearing perpendicular to the direction of excitation began to make contact with the upper and lower platens.

This facial contact is only possible in an elastomeric bearing with flexible reinforcement in an unbonded application. The hardening behaviour is advantageous as it acts to limit the maximum lateral displacement of the isolation system. The bearings cut from the original specimens were labeled as SU-FREI bearings due to their stable performance and unique characteristics. A subsequent study by Toopchi-Nezhad et al. (2008b) was conducted on ¼ scale SU-FREI bearings with aspect ratio $R = 2.8$ and shape factor $S = 11$. Stable hysteretic behaviour and hardening at large lateral displacements were observed. It was found that SU-FREIs could be effectively used for seismic isolation purposes based on design code provisions of ASCE 7-05.

It has been demonstrated through experimental testing that SU-FREIs show suitable behaviour for seismic isolation purposes. The use of FREI bearings in a stable unbonded application shows promise as a low-cost and light weight alternative to current seismic isolation practices. However, more research is necessary to better understand the behaviour of these bearings. This study is a continuation of experimental research of SU-FREI bearings.

1.5 Organization of Thesis

Chapter 2 describes the objectives and methodology of the experimental testing performed. The details of the test setup and the construction process and specification of the ¼ scale bearing samples are discussed.

Chapter 3 investigates the dynamic properties of ¼ scale SU-FREIs under cyclic excitation at a wide range of excitation amplitudes. Effective stiffness and effective damping are compared for sample bearings at two orientation angles with respect to the direction of excitation.

Chapter 4 explores the stability of ¼ scale SU-FREI bearings under cyclic lateral displacement and increasing axial load. Rollout stability in ¼ scale SU-FREI bearings is also investigated in this chapter.

Chapter 5 reports on the serviceability and fatigue performance of ¼ scale SU-FREI bearings. Test performance is compared to the requirements of ASCE 2005.

Chapter 6 summarizes the conclusions of the experimental research performed in this study and outlines recommendations for further study.

Table 1.1 Base isolator classification by connection type including bolted, dowelled, recessed, and stable unbonded. (ISO, 2005).

<table>
<tr><td>Type I</td><td>Isolator is bonded to connecting flanges which are in turn bolted to the mounting flanges</td><td>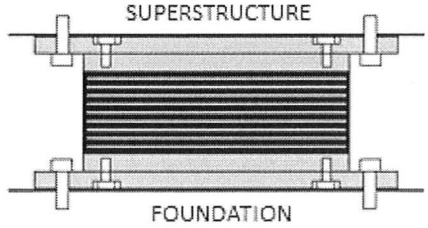
</td></tr>
<tr><td>Type II</td><td>Isolator is bonded directly to the mounting flanges</td><td>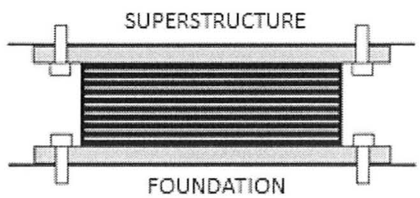
</td></tr>
<tr><td rowspan="2">Type III</td><td>Isolator connected to the base with recessed rings</td><td>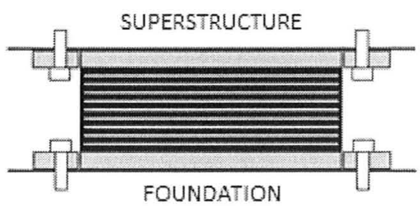
</td></tr>
<tr><td>Isolator connected to the base with dowelled pins</td><td>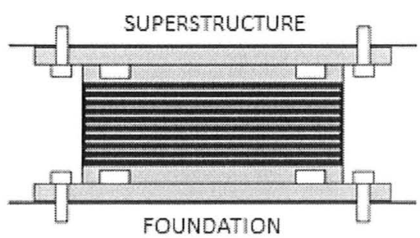
</td></tr>
<tr><td>Type SU</td><td>Isolator is placed directly between superstructure and foundation with no bonding</td><td>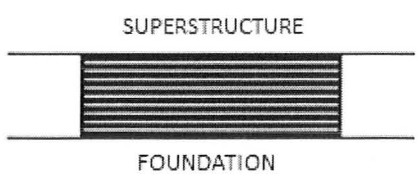
</td></tr>
</table>

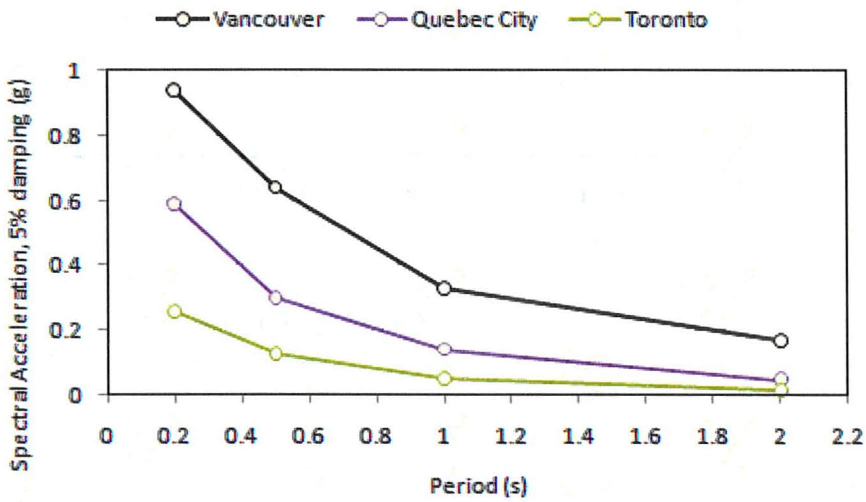

Figure 1.1 Uniform Hazard Spectra (UHS) for three major Canadian cities. Values obtained for 5% damped horizontal spectral acceleration for 0.2, 0.5, 1.0, and 2.0 second periods form the NBC 2005 for each city.

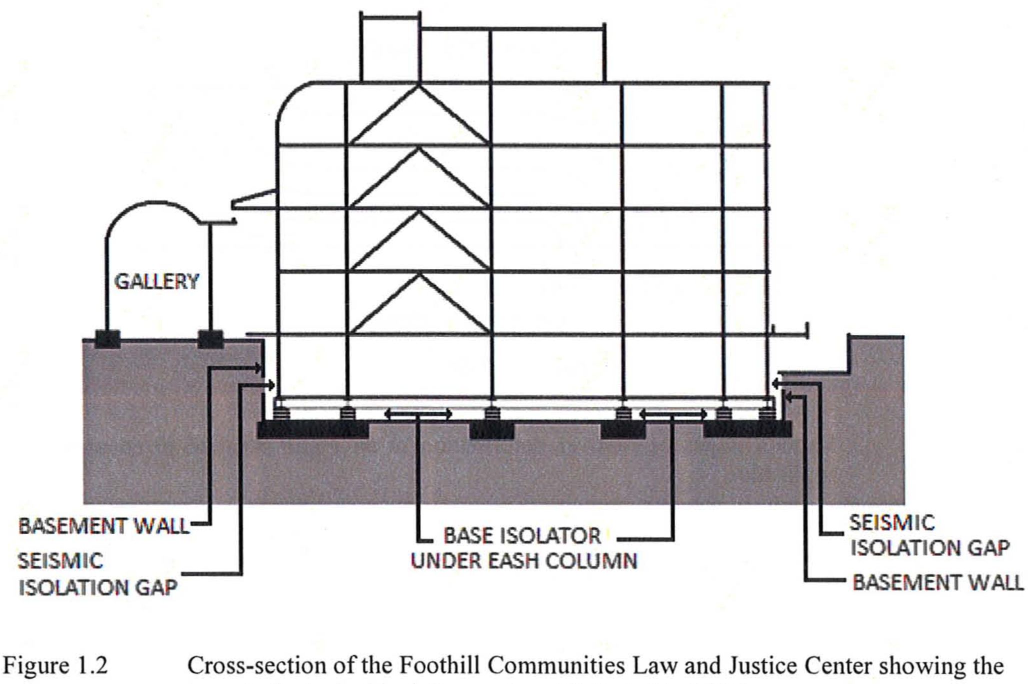

Figure 1.2 Cross-section of the Foothill Communities Law and Justice Center showing the layout of a typical isolation system (Kelly J. M., 1997).

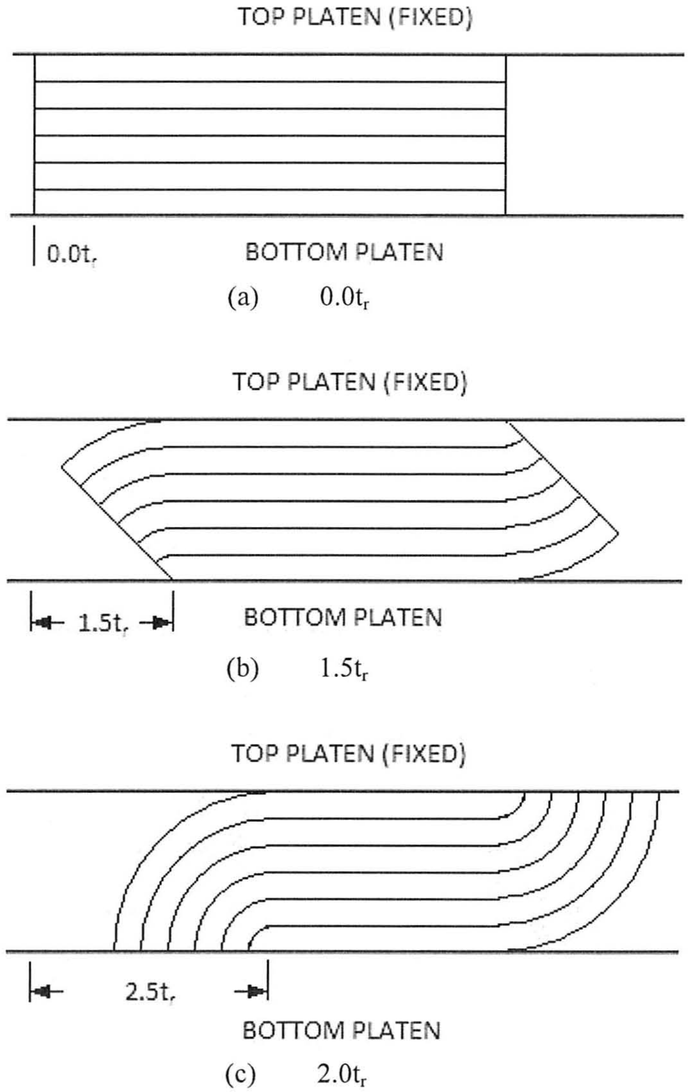

Figure 1.3 Various stages of rollover deformation in an FREI installed in an unbonded application

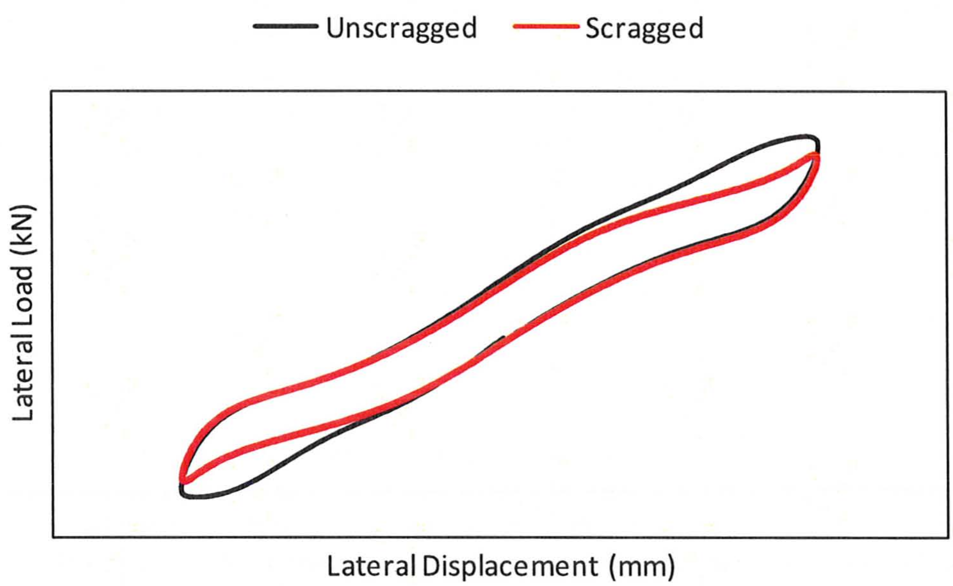

Figure 1.4 Load-displacement hysteresis from cyclic lateral testing on a unscragged SU-FREI bearing. Two fully reversed cycles at the same amplitude were performed under constant axial load.

Chapter 2. Objectives, Test Setup and Sample Specifications

This chapter describes the specifications of the ¼ scale SU-FREI bearings investigated in this study. The test setup and layout are detailed and an introduction to the objectives of this study is provided. Topics explored in this study include: effect of orientation on the dynamic properties of bearings under cyclic lateral testing; investigation of stability of SU-FREI bearings; and the performance of SU-FREI bearings under fatigue and serviceability conditions. Specific details regarding test procedure and experimental results are provided in subsequent chapters.

2.1 Sample Specification

This study involves experimental testing and evaluation of the performance of ¼ scale square SU-FREI bearings. The bearings constructed for this test were manufactured to the same specifications as those tested by Toopchi-Nezhad et al. (2008b). The bearings were constructed in sheets using the same process and equipment as Toopchi-Nezhad et al. (2008b) in an attempt to maintain consistent properties. A total of three sheets of fiber-reinforced elastomeric isolator were constructed for this study labeled MB1, MB2, and MB3. Each sheet measured 200 x 200 x 24 mm consisting of 12 layers of soft unfilled neoprene rubber and 11 layers of bidirectional (0/90 degree orientation) plain weave carbon fiber. Four ¼ scale bearings were cut from each sheet with dimensions of 70x70x24mm. Sheet plan dimensions as well as the location (labeled 1 through 4) and dimensions of the individual bearings cut from a typical sheet are provided in Figure 2.1. Each bearing tested in this study is labeled based on the sheet it was cut from and the location from which it was cut. For example, bearing MB1-1 is a bearing cut from sheet MB1 from position 1 (top left corner). As illustrated in Figure 2.1, each bearing sheet yielded 4 bearings for a total of 12 model scale bearing samples for testing purposes.

A side view of a typical ¼ scale bearing specimen is provided in Figure 2.2, which shows the alternating layers of rubber and carbon fiber. Rubber layers are 1.59 mm thick giving a total thickness of rubber of $t_r \approx 19$ mm. The neoprene rubber used has a measured hardness of 37 ± 5 Durometer, Shore A (ASTM 2005). The supplier specified nominal tensile modulus of the rubber is 1.2 MPa at an elongation of 100%. The carbon fiber layers are composed of 0/90 degree bi-directional plain weave carbon fiber fabric. The carbon fiber fabric was pretensioned in both the 0 and 90 degree direction to achieve a uniform amount of tautness prior to being bonded to the rubber sheets. Bonding of the carbon fiber to a layer of neoprene was accomplished using two even coats of a cold vulcanizing rubber cement. This process was repeated for each subsequent layer of carbon fiber and neoprene.

Kelly and Takhirov (1987) have indicated that the exposed edges of isolator samples cut from a strip isolator of FREI bearing are prone to delamination. Significant delamination was observed by Toopchi-Nezhad et al.(2008a) during testing of a full scale unbonded FREI bearing with exposed edges. In a following study performed on ¼ scale SU-FREI bearings (Toopchi-Nezhad et al., 2008b), two coatings of rubber cement were applied to the exposed surfaces of the ¼ scale bearing after it was cut to the appropriate dimensions. This coating prevented delamination during cyclic testing. The same process was used on bearings cut from sheets MB1, MB2, and MB3 in this study. Figure 2.3 depicts a ¼ scale SU-FREI bearing during the construction process with one exposed edge and another edge coated with rubber cement.

2.2 Test Setup and Instrumentation

An overview of the test setup, provided in Figure 2.4, shows a number of different views of the setup. The test setup and instrument layout is detailed in Figure 2.5 and Figure 2.6 with cross-section views. This setup is a modified version of the test setup used by Toopchi-Nezhad et al. (2007a; 2008a; 2008c). Delrin brackets were added at the bolted connections between the housing for the horizontal actuator to the upper platen as seen in Figure 2.4a & Figure 2.5. This provided a nearly frictionless surface at the bolted connections between the arms of the upper platen. In addition, a new load cell was installed to measure lateral shear forces during cyclic testing at high axial loads, which were beyond the capabilities of the existing horizontal load cell.

The bottom plate is moved laterally by the horizontal actuator (Figure 2.4b) under displacement control. The displacement rate and amplitude are controlled via an input displacement signal generated using MatLAB, which is sent to a 406 controller (Figure 2.7a). Feedback is provided by the linear variable displacement transducer (LVDT) at the back of the setup shown in Figure 2.5. Corresponding lateral displacements are measured using the string-pot located adjacent to the feedback LVDT. Safety precautions required the installation of limit switches to prevent any unexpected extreme lateral displacements. Shear forces are measured from one of two locations by either horizontal load cell No. 1 or 2 (HLC No.1 and No.2) as seen in Figure 2.4b and Figure 2.4c respectively.

The lateral force measured using horizontal load cell No.1 (Figure 2.4b & Figure 2.5) included frictional forces developed by the linear bearings under the bottom platen as it was cycled laterally and inertia forces related to the mass of the bottom platen. Horizontal load cell No. 2 (Figure 2.4c & Figure 2.6) directly measures the shear at the top surface of the bearing. This load cell was calibrated at axial loads up to 120 kN under cyclic shear. Both cells record lateral shear forces simultaneously and the results were compared and verified at design axial loads between the two horizontal load cells. Horizontal load cell No.2 provides accurate shear measurements for cyclic testing of bearings under axial loads up to 120 kN. The introduction of an additional horizontal load cell was necessary for dynamic stability testing described later in this report. During lateral cyclic testing under design load the original lateral load cell designated as HLC No.1 was used. Shear was measured by HLC No.2 for all other experimental testing.

The vertical actuator is operated under load control and feedback is provided by four 10,000lb load cells (VLC No.1 – No.4) placed between the actuator and the upper platen of the test set up as depicted in Figure 2.4d and Figure 2.5. Similar to the horizontal actuator, MatLAB is used to generate the vertical signal. This signal is sent to a 406 controller which maintains the desired load by comparing the input signal to the measured load on the sum of the four vertical load cells. In order to measure vertical displacements, four laser displacement transducers (LDTs) were installed along the perimeter of the upper and lower platens. Two of the LDTs are attached to the bottom platen (LDT #1 & 2), while the other two are attached to the top platen (LDT # 3 & 4) as shown in Figure 2.5.

A total of 12 channels are measured and recorded simultaneously during each test. These channels are filtered at 10 Hz using an anti-aliasing filter (Figure 2.7b). This allowed for multi-channel conditioning and amplification with dynamic recording. All data was recorded at a sampling rate of 250 Hz (one sample every 0.004 seconds) and digitally filtered at 6 Hz using LabVIEW software. Both the original data filtered at 10 Hz and the digitally filtered data at 6 Hz were recorded separately. The data filtered at 10 Hz was stored as a backup while all calculations were performed using the data filtered digitally at 6 Hz.

2.3 Experimental Tests and Objectives

The objective of this study is to continue investigation into the properties of SU-FREI bearings using a wide variety of experimental tests. Previous studies have established that SU-FREI bearings achieve effective stiffness and damping properties, which are sufficient for base isolation (Toopchi-Nezhad et al., 2007a; 2008a; 2008b). This objective was accomplished by subjecting ¼ scale SU-FREI bearings to a series of experimental tests. These tests cover a wide range of subjects including orientation during cyclic testing, stability, serviceability and fatigue. The topics discussed here have not been explored using SU-FREI bearings prior to this study.

2.3.1 Dynamic Properties

The dynamic properties of interest, which can be obtained from lateral cyclic testing under constant axial pressure, are the effective stiffness and the effective damping of the base isolator. Once these properties are determined through experimental testing, the response of the base isolation system can be predicted. The provisions of ASCE 7-05 can be used to estimate the response of an isolation system composed of SU-FREI bearings with the same properties as those tested in this study. There are a number of factors which influence effective stiffness and effective damping. For example, a rubber compound performs differently when it is cycled from its unscragged state than it does if it has been previously deformed (scragged).

In previous studies, this effect was documented during cyclic testing of SU-FREI bearings by Toopchi-Nezhad et al. (2008a; 2008b). It was found that the "unscragged" first cycle provided higher stiffness and damping than the second and third cycles. The differences in the second and third cycles were negligible and the effective stiffness and damping appeared to be stable. The results of the second and third cycles were labeled as the scragged properties of the SU-FREI bearings. Toopchi-Nezhad et al.(2008b) investigated the performance of ¼ scale SU-FREI bearings under sinusoidal lateral displacement and constant axial load. These cyclic tests were performed along 0°, 90°, and 45° orientations with respect to the direction of excitation (Toopchi-Nezhad et al., 2008b). The bearings tested at 0° (parallel orientation) were unscragged bearings; whereas the bearings tested at 45° (diagonal orientation) had been rigorously tested prior to being cycled at a 45° orientation. These bearings had first been used to investigate the effects of vertical pressure on lateral response as well as a number of other cyclic tests including rate sensitivity. As a result, a direct comparison between the unscragged properties of SU-FREI bearings at parallel and diagonal orientations was not possible. The unscragged properties of SU-FREI bearings cycled at a diagonal orientation have not been explored prior to this study.

In this study, the lateral response of unscragged SU-FREI bearings tested along both a parallel and diagonal orientation will be evaluated. The results of parallel cyclic testing obtained in this study will be directly compared to the results achieved by Toopchi-Nezhad et al. (2008b) on an SU-FREI bearing of the same specifications tested under identical conditions. This will ensure continuity between the manufactured bearing specimens of this study with those of the previous study. It is expected that unscragged bearings subjected to cyclic testing at a diagonal orientation will achieve much greater effective stiffness and effective damping than those tested by Toopchi-Nezhad et al.(2008b). This is primarily due to the amount of testing the bearings in the previous study underwent prior to diagonal cyclic testing.

The specifics of cyclic testing performed on SU-FREI bearings are discussed in greater detail in Chapter 3. This chapter provides the lateral response characteristics obtained from cyclic testing in terms of effective stiffness and effective damping. These values are then used to determine the displacement of the isolation layer and the effective base isolated period at this displacement based on provisions of ASCE 7-05.

2.3.2 Stability Under Dynamic Excitation

A number of studies, both analytical and experimental, have been performed on multi layer elastomeric isolators in order to determine the buckling load. According to International Standard ISO 22762 (2005), a seismic-protection isolator is considered to have undergone buckling when it has lost stability under a combination of compression-shear loading. This occurs when the lateral stiffness becomes zero. A force-displacement curve is provided in Figure 2.8 which illustrates stable and unstable conditions. Several different test procedures were investigated before a buckling test program was developed that would best suit SU-FREI bearings.

A previous study by Buckle and Liu (1994) examined the buckling load of several steel reinforced elastomeric bearings. Bolted connections were used to attach each bearing to the upper and lower platens of the test set up. Each bearing was first scragged at a specified displacement and then held at this displacement while an increasing axial load was applied. Once the lateral shear force became negative the test was stopped. This was repeated at several displacements and the results were used to construct force-displacement curves from which the buckling load could be obtained. This provided critical loads under which the bearing is constrained from any additional lateral displacement. The data was then analyzed to determine the equivalent unconstrained critical loads. This procedure was deemed unsuitable for testing SU-FREI bearings due to the unbonded boundary conditions. It was decided that analyzing stability under dynamic lateral excitation was representative of conditions which are expected to be experienced by an SU-FREI bearing. Dynamic testing provides insight into both the stability of SU-FREI bearings as well as the effect of high axial load on the dynamic properties.

Stanton et al. (1990) investigated the stability of steel-laminated elastomeric bearings in a number of different experimental tests. One of the experimental tests examined the dependence of transverse stiffness on compressive load. Each test subjected a bearing stack to a constant axial load followed by cyclic lateral displacement. This process was repeated at the same amplitude at increasing levels of axial load. This was done for a number of orientations of stacked bearings and various displacement amplitudes. Transverse stiffness K_t was defined as the tangential stiffness obtained at zero displacement from the force-displacement hysteresis. It was found that transverse stiffness decreased with increasing axial load for every combination of lateral displacement amplitude and bearing stack orientation. Furthermore, as the axial load increased the hysteresis increased but the loops remained stable. The influence of axial load on the transverse stiffness of SU-FREI bearings has not been investigated prior to this study. The study by Stanton et al. (1990) looked at a limited range of axial loads where instability was not encountered. It is apparent that if the axial load were increased further it may be possible to achieve negative transverse stiffness corresponding to buckling.

In an Earthquake Engineering Research Center (EERC) report by Koh and Kelly (1987) four different square multilayer elastomeric bearing types were tested. One set of 1/2 scale bearings was tested with and without a lead core along with three sets of 1/5 scale bearings with varying steel shim and rubber layer thicknesses. Each test subjected a bearing sample to a sinusoidal cycle of lateral displacement under a constant axial load. Each bearing was subjected to several tests at the same lateral amplitude and subsequently greater axial loads. This process was repeated for up to three incrementally increasing excitation amplitudes. The purpose of this investigation was to investigate the effect of axial load on the dynamic properties of several types of multilayer elastomeric isolators. The dynamic properties calculated in the report were the effective stiffness and effective damping obtained from the lateral force-displacement hysteresis. Results showed a decrease in effective stiffness accompanied by an increase in effective damping as the axial load was increased. The 1/5 scale bearings were tested at axial loads ranging from 20-130 kN. Approximately 20 tests were performed on each bearing in total. Results showed that the effective stiffness decreased by half while effective damping increased by 2-3 times. Prior to this investigation ¼ scale SU-FREI bearings had undergone cyclic testing at axial loads up to approximately 15 kN (Toopchi-Nezhad et al., 2008a). The effects of axial loads in excess of twice the design axial load have not been explored using SU-FREI bearings.

The testing procedure used in this study is an evolution of the procedure used by Stanton et al.(1990) and the procedure used by Koh and Kelly(1987). Stability of an SU-FREI bearing is evaluated based on the force-displacement hysteresis. A stable hysteresis loop maintains positive incremental force resisting capacity throughout each full reversed cycle. This study aims to determine the critical axial load at which the lateral stiffness becomes zero in an SU-FREI bearing for different excitation amplitudes. This axial load represents the critical buckling load under dynamic excitation. In addition these tests will provide insight into the effective stiffness and damping of SU-FREI bearings under a wide range of axial loads. The specifics of the dynamic buckling test used in this study are discussed in greater detail in Chapter 4.

2.3.3 Rollout

In addition to stability tests performed during dynamic lateral excitation, a more traditional stability test was performed on SU-FREI bearings subjected to constant design axial load. The ultimate shear properties test is performed to determine the displacement at which a bearing either breaks or buckles as described by ISO-22762 (2005). Each bearing is subjected to its design axial load which is held constant. Next the bearing is displaced laterally at a constant rate until failure occurs. The method of failure is dependent on the boundary conditions of the bearing. Bearings with bolted connections are susceptible to breaking failure, while dowelled and recessed bearings are at risk of rollout instability (ISO, 2005). The force-displacement curve shown in Figure 2.8 is representative of an ultimate shear properties test during which a bearing has undergone rollout instability. The lateral displacement δ_{max} represents the onset of buckling due to rollout instability where the lateral stiffness has become zero. This failure mode may occur at very large lateral displacement, when the resultant of the vertical contact pressure falls beyond the horizontal contact area of the bearing.

Due to their unbonded boundary conditions, SU-FREI bearings will rollover as they are laterally displaced. Rollover behaviour is unique to SU-FREI bearings and occurs as soon as the bearing is displaced laterally and the vertical faces perpendicular to the direction of excitation begin to roll over. Rollover behaviour is not to be confused with rollout instability, as rollover is not a failure mode. Rollover results in a significant decrease in the lateral stiffness of the bearing, which is desirable since it also lengthens the effective base isolated period. However unlike standard elastomeric bearings, the SU-FREI bearings investigated in this study are designed to undergo SR (Stable Rollover) deformation (Toopchi-Nezhad et al., 2008a). As the SU-FREI bearing undergoes rollover it maintains positive incremental load resisting capacity. At large lateral displacements, when the vertical faces of the bearing perpendicular to the direction of excitation begin to make contact with the upper and lower contact surfaces, stiffening is observed (Toopchi-Nezhad et al., 2008a). For this reason it is suggested that these bearings can undergo significantly large lateral displacement before rollout instability may be observed.

The objective of this test is to investigate the performance of these bearings under the ultimate shear properties test. This test has not been investigated prior to this study on SU-FREI bearings. It is possible that a failure mode unique to SU-FREI bearings may occur. Two bearings were displaced to predetermined lateral displacements in excess of any of the other tests conducted in this study to examine their response. Details of the testing procedure used as well as results of testing are provided in Chapter 4.

2.3.4 Serviceability

To investigate the lateral response of SU-FREI bearings under wind as a service load, ¼ scale bearings were cycled at a range of lateral displacements that bracket the equivalent lateral displacement generated by the design wind force. The difference between this test and previous cyclic tests is the number of cycles and the amplitude of lateral excitation. ASCE 7-05 requires 20 fully reversed cycles of lateral excitation for serviceability testing. Furthermore, the design wind force is not expected to generate a large displacement in the isolation layer of a typical low-rise structure. SU-FREI bearings maintain relatively high lateral stiffness under wind loading, which is expected to generate small displacements. The results are analyzed to ensure acceptable dynamic performance is achieved as per the ASCE (2005). Serviceability testing is discussed in greater detail in Chapter 5.

2.3.5 Fatigue

The fatigue testing procedure used in this study was taken from ASCE 7-05. Similar to serviceability testing, fatigue tests subject a bearing to a high number of fully reversed lateral cycles and constant design axial load. However the amplitude of lateral displacement for fatigue testing is equal to the total design displacement of the isolation layer. The objective of this test is to ensure that the effective stiffness and damping of the bearing does not fall below the acceptable limits outlined by ASCE 7-05. Details and results of fatigue testing are provided in Chapter 5.

2.4 Testing Sequence

The series of experimental tests performed on each ¼ scale SU-FREI bearing is provided in Table 2.1, Table 2.2, and Table 2.3 for bearings cut from sheet MB1, MB2, and MB3, respectively. It was desirable to group bearings by the sheet they were cut from. The three bearings cycled at a parallel orientation under design axial pressure were cut from sheet MB1 (MB1-1, MB1-2, and MB1-4). Two unscragged bearings, cut from sheet MB3 (MB3-1 & MB3-4), were used to explore the unscragged properties of SU-FREI bearings cycled at a diagonal orientation. The bearings tested at a parallel orientation were then used in a preliminary study into buckling while the bearings tested at a diagonal orientation were used for fatigue testing.

The remaining unscragged bearings from sheet MB1 (MB1-3) and MB3 (MB3-2 & MB3-3) were used along with two unscragged bearings from sheet MB2 to explore stability of SU-FREI bearings. By the end of the dynamic buckling test program these bearings were unusable for further testing. This is due to the volume of cycles at high axial load and lateral displacement combinations these bearings are subjected to during the testing process.

Serviceability and fatigue testing was investigated next using the remaining unscragged bearings cut from MB2 (MB2-2 & MB2-3). These bearings along with the two bearings that underwent cyclic testing at a diagonal orientation (MB3-1 & MB3-4) were then used to investigate fatigue. Both of these testing programs are non-destructive tests under design axial load. For this reason, bearings MB2-2 and MB2-3 were used to investigate the ultimate shear properties of SU-FREI bearings.

Ultimate shear property tests were performed last on MB2-2 and MB2-3 after they had undergone serviceability testing and fatigue testing. Both serviceability and fatigue testing "scragged" the bearing up to deformations equal to the design displacement. This was not a major concern since the rollout tests deform the bearing to approximately twice this displacement. It was expected that these bearings would still exhibit unscragged properties once the lateral displacement in the rollout test surpassed design displacement.

Table 2.1 Testing sequence and descriptions for model scale bearings from sheet MB1

Test No.	Model Scale Bearing Set MB1			
	MB1-1	MB1-2	MB1-3	MB1-4
1	*Cyclic test 0 ° unscragged ascending amp. 3 cycles per amp. P = 7.84kN*	*Cyclic test 0 ° unscragged ascending amp. 3 cycles per amp. P = 7.84kN*	*Dynamic buckling test unscragged amp. = 0.50tr, 1.00tr 1.50tr, 2.00tr P = 7.84, 30, 60, 75/90, 120 kN*	*Cyclic test 0 ° unscragged ascending amp. 3 cycles per amp. P = 7.84kN*

Table 2.2 Testing sequence and descriptions for model scale bearings from sheet MB2

Test No.	Model Scale Bearing Set MB2			
	MB2-1	MB2-2	MB2-3	MB2-4
1	*Dynamic buckling test unscragged amp. = 1.00tr, 1.50tr, 2.00tr P = 7.84, 30, 60, 75/90kN*	*Serviceability test 0º unscragged amp. = 015tr, 0.35tr P = 7.84kN*	*Serviceability test 0º unscragged amp. = 0.15tr, 0.35tr P = 7.84kN*	*Dynamic buckling test unscragged amp. = 1.00tr, 1.50tr, 2.00tr P = 7.84, 30, 60, 75/90kN*
2		*Fatigue test 90º scragged to 0.35tr amp. = 1.50tr P = 7.84kN*	*Fatigue test 90º scragged to 0.35tr amp. = 1.50tr P = 7.84kN*	
3		*Rollout test 0º scragged to 1.50tr disp. = 2.75tr P = 7.84kN*	*Rollout test 0º scragged to 1.50tr disp. = 3.00tr P = 7.84kN*	

Table 2.3 Testing sequence and descriptions for model scale bearings from sheet MB3

Test No.	Model Scale Bearing Set MB3			
	MB3-1	MB3-2	MB3-3	MB3-4
1	*Cyclic test 45 ° unscragged ascending amp. 3 cycles per amp. P = 7.84kN*	*Dynamic buckling test unscragged amp. = 1.00tr, 1.50tr, 2.00tr P = 7.84, 30, 60, 75/90 kN*	*Dynamic buckling test unscragged amp. = 1.00tr, 1.50tr, 2.00tr P = 7.84, 30, 60, 75/90 kN*	*Cyclic test 45 ° unscragged ascending amp. 3 cycles per amp. P = 7.84kN*
2	*Fatigue test 0º scragged amp. = 1.50tr P = 7.84kN*			*Fatigue test 0º scragged amp. = 1.50tr P = 7.84kN*

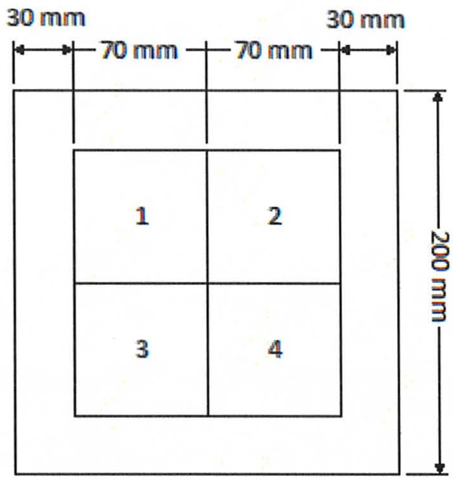

Figure 2.1 SU-FREI bearing sheet with the location and dimensions of ¼ scale samples

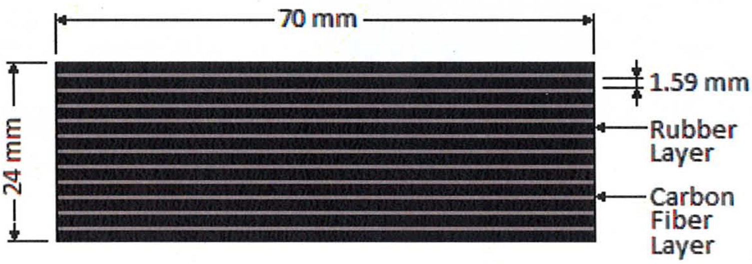

Figure 2.2 Side view of ¼ scale SU-FREI bearing with dimensions of width height and rubber layer thickness specified

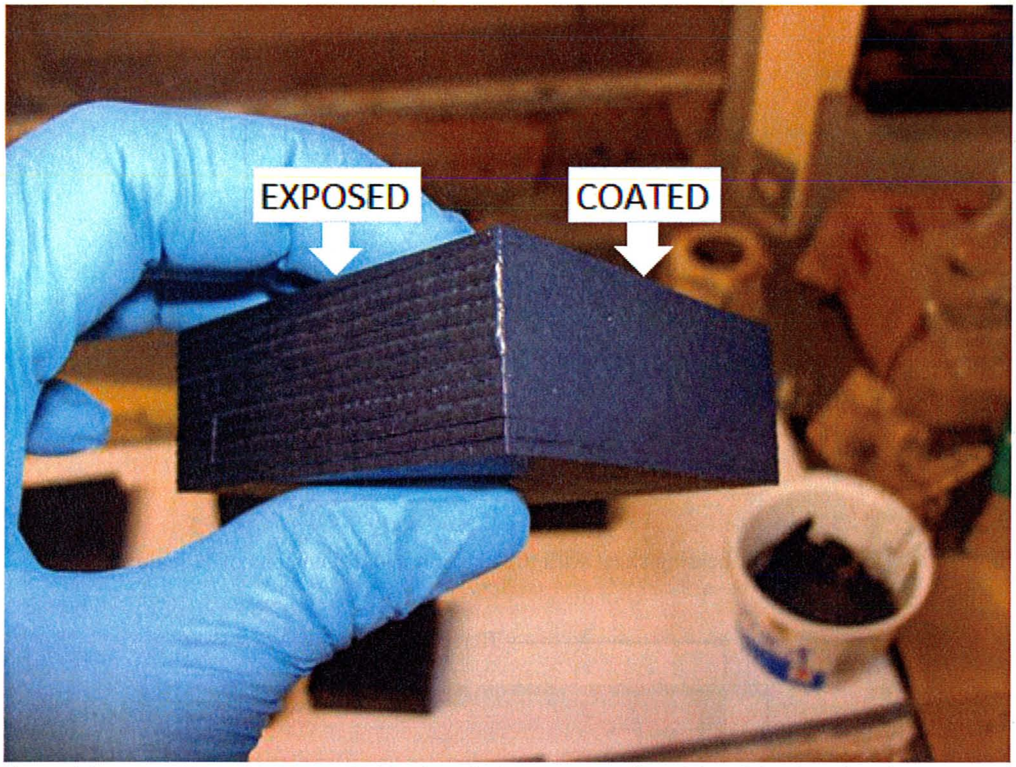

Figure 2.3 ¼ scale SU-FREI bearing during construction. The right face has been coated with rubber cement and the left face has not.

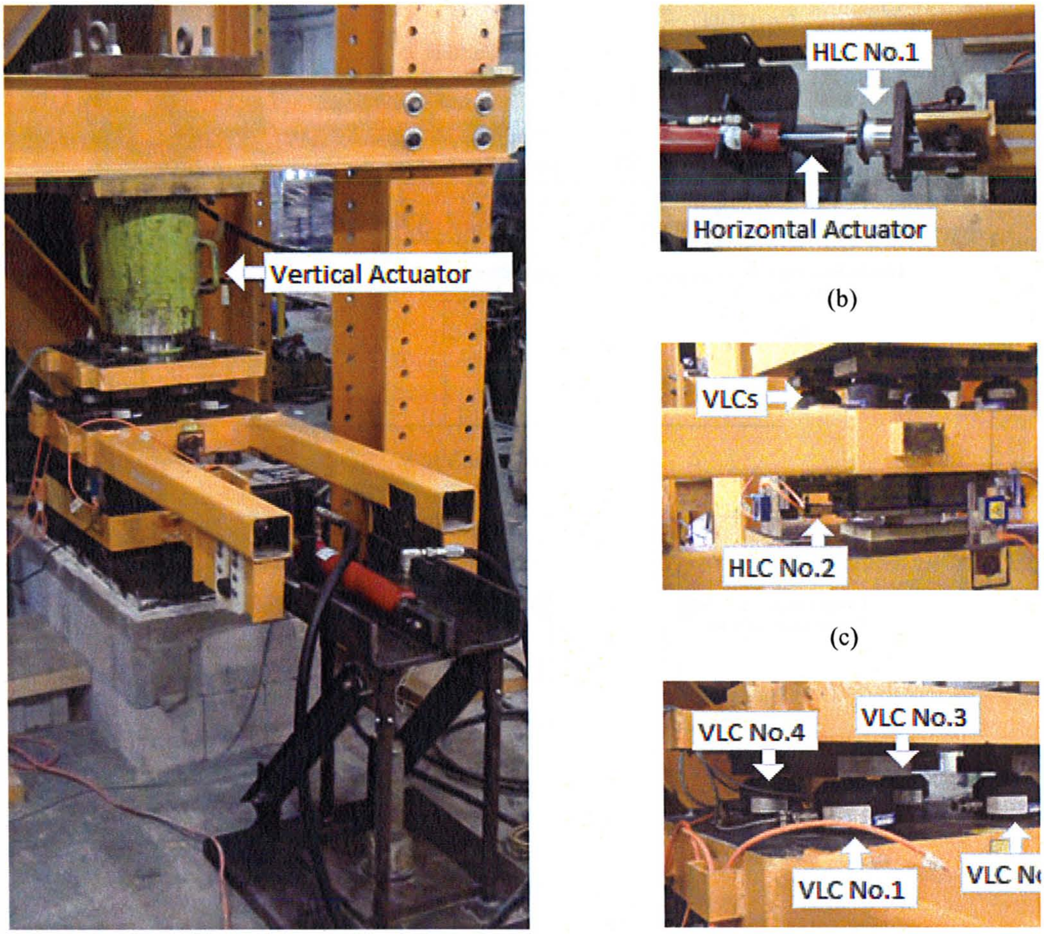

(a) (b) (c) (d)

Figure 2.4 Test setup orientation: (a) Overview of test setup; (b) Top view of the horizontal actuator and horizontal load cell No.1; (c) Side view including the vertical load cells as well as horizontal load cell No. 2; (d) Vertical load cell orientation

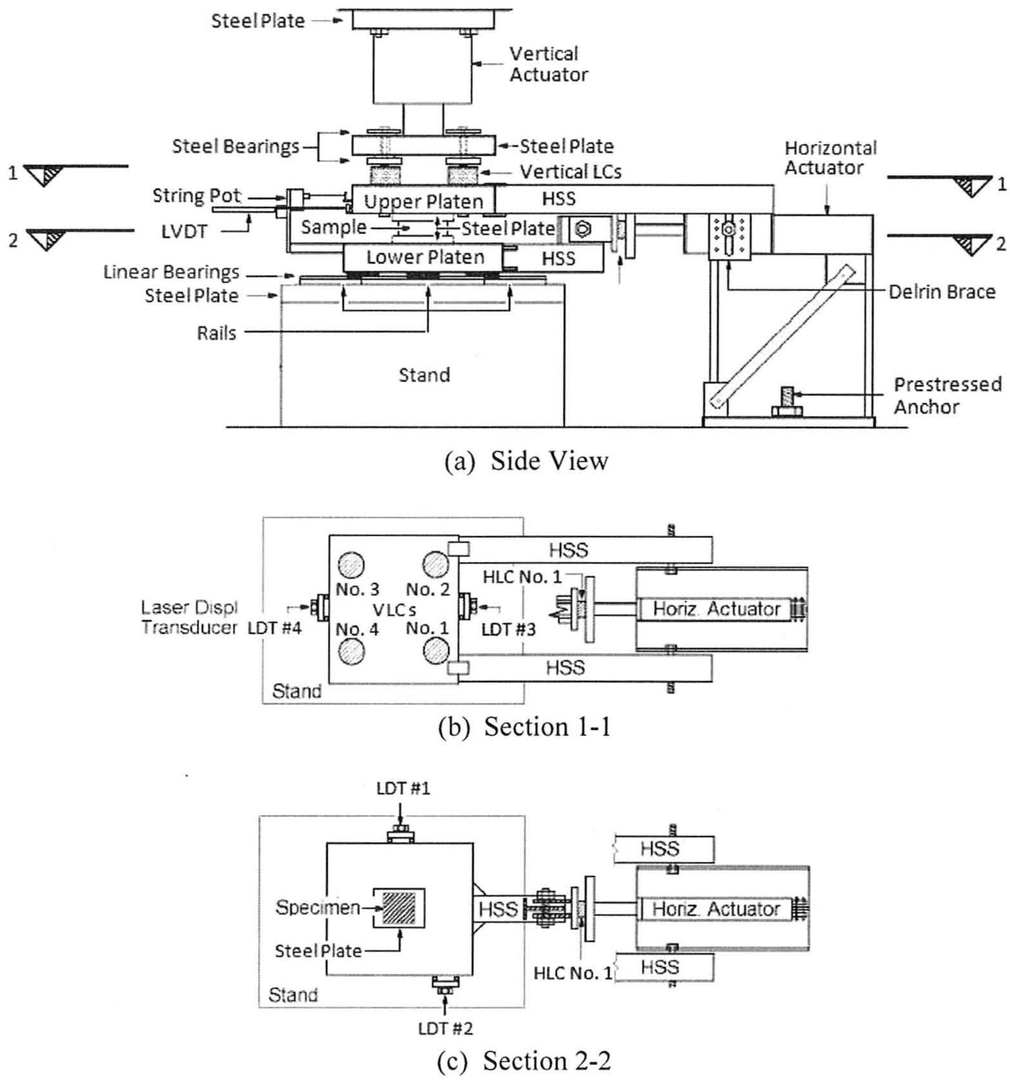

Figure 2.5 Test setup and instrumentation layout modified from Toopchi-Nezhad et al. (2008a).

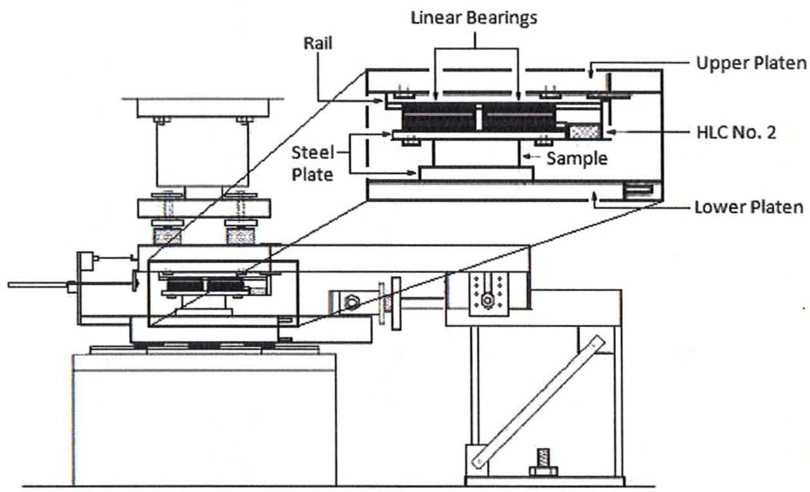

Figure 2.6 Test setup detailing the inclusion of the second horizontal load cell

(a) (b)

Figure 2.7 Overview of signal control and acquisition equipment: (a) Computer for data acquisition and 406 controllers for vertical and horizontal actuators; (b) Signal filters (12 channels), power supply for LDTs, and sumer box for vertical load cells

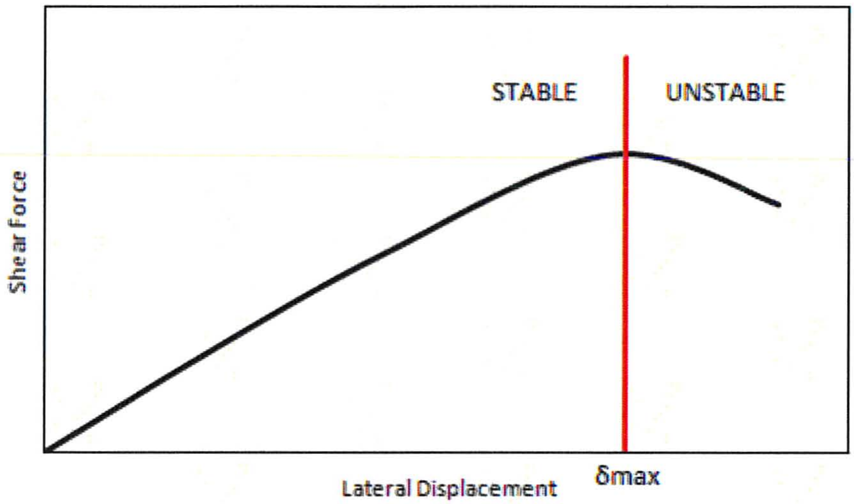

Figure 2.8 Example of a typical force-displacement curve showing stable and unstable behaviour as well as the critical displacement (Buckle & Liu, 1994)

Chapter 3. Cyclic Testing

This chapter reports on cyclic tests performed on ¼ scale SU-FREI bearings. Out of the twelve bearings manufactured, five were used to investigate dynamic properties under sinusoidal (cyclic) lateral excitation. A total of six incremental lateral displacement amplitudes were investigated. The effective horizontal stiffness and effective damping of each bearing was determined for each cycle. Bearings were tested at angles of 0° (parallel) and 45° (diagonal) with respect to the direction of lateral displacement as illustrated in Figure 3.1 and Figure 3.2. The effects of SU-FREI bearing orientation are explored in terms of calculated dynamic properties and code evaluated response characteristics.

The two response characteristics of importance that can be determined from experimental cyclic testing are the lateral effective stiffness and effective damping. In order to estimate the lateral response of an isolation system composed of SU-FREI bearings, code evaluation is performed using ASCE 7-05. The specific provisions that will be looked at in this section relate to the calculation of the displacement of the isolation layer as well as the effective base isolated period. These calculations are performed for both the design basis earthquake (DBE) and the maximum considered earthquake (MCE) for the region of study.

Previous tests on ¼ scale square SU-FREI bearings were performed at parallel, perpendicular and diagonal orientations with respect to the direction of excitation (Toopchi-Nezhad et al., 2008b). The bearings tested in the previous study at a diagonal orientation were scragged (previously tested) bearings. The unscragged properties of SU-FREI bearings tested at a 45° orientation have not yet been investigated. This study provides further insight into the dynamic response of unscragged SU-FREI bearings at parallel and diagonal orientations. A comparison between the results of this study and the results of previous studies on ¼ scale square SU-FREI bearings is carried out between tests performed at a parallel orientation to compare properties between bearings. Following this, the influence of orientation on the dynamic properties of unscragged SU-FREI bearings is explored along with scragging effects.

3.1 Testing Procedure

Cyclic tests were performed under a specified axial design pressure of 1.6 MPa (≈7.8 kN). This axial load was applied to each bearing and held constant throughout the horizontal excitation. The lateral displacement signal used for this test is composed of six amplitudes taken with respect to the total thickness of rubber (t_r). These excitation amplitudes were applied in ascending order: $0.25t_r$, $0.50t_r$, $0.75t_r$, $1.00t_r$, $1.50t_r$ and $2.00t_r$. Three fully reversed cycles were performed at each of the six excitation amplitudes in sequence resulting in a total of 18 fully reversed cycles (see Figure 3.3). The manufacturer specified rubber sheet thickness is 1.59 mm. Given that each bearing consists of 12 layers of rubber, the total thickness of rubber in a given bearing was taken as 19.05 mm. Once the sinusoidal lateral cycling was completed the axial load was removed from the bearing.

The average rate of displacement throughout these tests was maintained at 76.2 mm/s. In an ideal situation the bearing would be cycled at the fundamental frequency corresponding to the specific excitation amplitude. This was not possible due to the limitations of the horizontal actuator used. At the largest amplitudes of displacement, it would be necessary for the actuator to move at a rate outside its capability to reach the natural frequency of the bearing. Rate sensitivity tests were performed with the same test setup on ¼ scale SU-FREI bearings of the same composition and dimensions in a previous study (Toopchi-Nezhad et al., 2008b). In this study, two bearings were cycled at different frequencies ranging from 0.16 to 0.66 Hz. The resulting variation in effective stiffness and damping was negligible. It was determined that, at a rate of 76.2 mm/s, an excitation frequency of approximately 1 Hz was achieved at an amplitude of 1.0 t_r. This is sufficiently close to the bearing's natural frequency at the design displacement.

The results obtained from cyclic testing were used to determine the effective stiffness and effective damping of the bearings for each fully reversed cycle of displacement. Using these calculated parameters it is then possible to evaluate the lateral displacement of the isolation layer and the effective isolated period at design lateral displacement as specified by ASCE 7-05.

3.2 Effective Stiffness and Effective Damping

There are two mechanical characteristics of interest that can be obtained from lateral cyclic testing of isolator units. These properties are the effective stiffness (K_{eff}) and the equivalent viscous damping (β_{eff}). These properties are commonly used to evaluate the response of seismic isolation devices. ASCE 7-05 is a commonly used code for evaluating and designing base isolation systems. It provides expressions for the evaluation of K_{eff} and β_{eff} which are used here. Effective stiffness is calculated using the following equation (ASCE 2005):

$$K_{eff} = \frac{|F_{max}| + |F_{min}|}{|\Delta_{max}| + |\Delta_{min}|} \tag{3.1}$$

where F_{max} and F_{min} represent the maximum positive and maximum negative lateral force respectively. Similarly, Δ_{max} and Δ_{min} are the maximum positive and maximum negative displacements in a hysteresis loop. An example of a typical hysteresis loop, with the location of the maximum displacements and maximum lateral loads identified, can be found in Figure 3.4.

Effective damping is dependent on the total area enclosed by the load-displacement hysteresis loop and is calculated using the following equation (ASCE 2005):

$$\beta_{eff} = \frac{2}{\pi} \frac{E_{\text{loop}}}{K_{eff}(|\Delta_{max}| + |\Delta_{min}|)^2} \qquad 3.2$$

where the energy dissipated in an isolator unit during a full cycle E_{loop} is measured by the area enclosed by the load-displacement hysteresis loop.

3.3 Code Evaluation

Once the effective stiffness and effective damping are determined for each fully reversed cycle of lateral displacement, the displacement of the isolation layer and effective isolated period of the isolation layer at this displacement can be estimated. The design provisions of ASCE (2005) were used to evaluate the design lateral displacement (D_D) and the effective period of the bearing at the design displacement (T_D). Evaluation was performed for a full-scale structure with an isolation system composed of four full-scale bearings. The design lateral displacement is determined using the following equation:

$$D_D = \frac{gS_{D1}T_D}{4\pi^2 B_D} \qquad 3.3$$

where S_{D1} represents the spectral response acceleration for the design basis earthquake (DBE) taken as 2/3 of the maximum considered earthquake (MCE). Specifically, $S_{D1} = \frac{2}{3}S_{M1}$, and S_{M1} is a factor of the site class effects and MCE spectral response acceleration for a period of 1 second (S_1). The MCE represents ground motion with a probability of exceedence of 2% in 50 years (ASCE 2005). B_D is a numerical coefficient for the effective damping measured at the design displacement. Similar to the design displacement calculation, the maximum displacement D_M is calculated using Equation 3.3 replacing: B_D with B_M, T_D with T_M, and S_{D1} with S_{M1}. For the calculation of the response under MCE: B_M is the effective damping of the bearing at D_M and T_M is the base isolated period at D_M.

The effective period of the structure at the design displacement (D_D) was calculated using the following equation from ASCE (2005):

$$T_D = 2\pi\sqrt{\frac{W}{K_{Dmin}g}} \qquad 3.4$$

where W is the effective seismic weight of the structure and K_{Dmin} is the minimum effective stiffness of the isolation system at the design displacement in the horizontal direction under consideration. The design vertical pressure of p = 1.6 MPa implies W = 124.4 kN for the full-scale structure. The effective period of the isolated structure at the maximum displacement (T_M) is calculated using Equation 3.4 with K_{Mmin} replacing K_{Dmin}, where K_{Mmin} is the minimum effective stiffness at a displacement of D_M.

Effective stiffness values were obtained through linear interpolation of experimental test result. Since the calculations required the full scale effective stiffness of the SU-FREI bearings, a scale factor $S_L = 4$ was applied to yield the equivalent full-scale effective stiffness values. The full scale effective stiffness was then multiplied by 4 to represent the effective stiffness of an isolation layer composed of 4 full-scale SU-FREI bearings.

For calculation purposes ground motion values for Vancouver are used from the NBC (2005) with $S_1 = 0.34$. This yields $S_{M1} \cong 0.5$ and $S_{D1} \cong 0.33$ for Site Class D, assuming unknown soil properties. Due to the nature of Equation 3.3 and 3.4, an iterative process was employed in order to determine D_D/D_M and. T_D/T_M. The effective damping and minimum effective stiffness are dependent on the amplitude of excitation for a given bearing. It is necessary to first select an arbitrary initial estimate for displacement. From there it is possible to determine K_{min} and B through linear interpolation between the two points bracketing the initial estimate for D. These values can then be input into Equations 3.3 and 3.4 and a new displacement will be calculated based on the values of K_{min} and B. The process is then repeated replacing the initial input displacement with the calculated displacement. It is then necessary to iterate until convergence is achieved between the input and the calculated displacement. The final result yields D_D/D_M and T_D/T_M for a particular bearing.

3.4 Test Specimen Adequacy

Test specimen adequacy is determined using the provisions of ASCE 7-05. The provisions that are used in this study describe test specimen adequacy of bearings tested at three fully reversed cycles of lateral displacement under design axial load at increasing intervals of displacement amplitude based on the design displacement. ASCE 7-05 states that for each test specimen the difference between the effective stiffness of each of the three cycles and the average stiffness at the same amplitude should not be greater than 15%. Furthermore, when comparing two different specimens of a common type and size, the difference between the effective stiffness of each cycle and the average effective stiffness taken over all three cycles of both bearings should not be greater than 15%. Adequacy of the test specimens based on the effective damping is not specified in the code. However, the same 15% difference is used in this study to evaluate the effective damping result. Additionally, it is necessary that the force-displacement hysteresis show positive incremental force resisting capacity throughout each fully reversed cycle (ASCE 7-05). This is evaluated by ensuring that the tangential stiffness of the force displacement-hysteresis remains positive.

3.5 Results of Parallel Cyclic Testing

Cyclic lateral tests were performed on a total of three unscragged SU-FREI bearings (MB1-1, MB1-2, and MB 1-4) at a parallel orientation. The lateral force-displacement hysteresis for bearing MB1-1 can be found in Figure 3.5a. Bearings MB1-2 and MB1-4 displayed similar hysteretic behaviour. Acceptable response characteristics can be observed from these hysteresis loops for stable-rollover behaviour. The displaced shape of an SU-FREI bearing during parallel cyclic testing is provided for amplitudes of $0.5t_r$, 1.0tr, 1.5tr, and 2.0tr in Figure 3.6a to Figure 3.9a. These figures show the various stages of rollover experienced by the SU-FREI bearings at different stages of lateral displacement. The bearings show positive incremental force resisting capacity (stability) throughout each fully reversed cycle, satisfying test specimen adequacy outlined in ASCE 7-05. The response characteristics of these bearings are evaluated using the calculated values of effective stiffness and effective damping.

The calculated values of effective stiffness and effective damping for each cycle are provided in Table 3.1 for the bearings tested at a parallel orientation. It can be observed, from these results and the lateral force-displacement hysteresis (Figure 3.5a) that the effective stiffness of the first (unscragged) cycle is larger than that of the 2^{nd} and 3^{rd} cycles (scragged) for any given lateral displacement amplitude. This is further highlighted in Figure 3.10 which compares both the mean scragged and unscragged effective stiffness against displacement amplitude. The scragged effective stiffness is between 5-10% less than the unscragged effective stiffness. The average percentage drop in effective stiffness increases as the excitation amplitude increases, the largest difference (10%) occurring at the largest displacement ($2.0t_r$). The effective stiffness of each cycle is well within 15% of the mean effective stiffness over all three cycles.

Figure 3.10 also shows that both the scragged and unscragged effective stiffness are within 15% of the mean effective stiffness averaged over all three cycles of all three bearings. The effective stiffness satisfies test specimen adequacy for test specimens of a common type and size according to ASCE 7-05. Similar to the effective stiffness, the effective damping (Table 3.1) decreases with increasing excitation amplitude. The mean scragged and unscragged effective damping versus excitation amplitude is provided in Figure 3.11. There is a 5-13% difference in the scragged and unscragged effective damping. Aside from the first amplitude of displacement ($0.25t_r$) the results show a drop in effective damping between the unscragged results and the scragged results. At $0.25t_r$ all three bearings showed an average 6% increase in effective damping between the first cycle and the following cycles at this amplitude. The effective damping of each cycle is within 15% of the mean taken over all three cycles and all three bearings at each increment of lateral displacement. This is illustrated in Figure 3.11 which shows that both the unscragged and scragged effective damping fit within the 15% bounds. Fiber reinforcement has been discussed previously as a source of energy dissipation in SU-FREI bearings by Toopchi-Nezhad et al. (2008b). The manufacturer specified nominal damping of the elastomer used in these bearings was approximately 5% at 100% elongation. The measured effective damping of SU-FREI bearings during cyclic testing at a parallel orientation ranges from 8% to 14%. Kelly (1999) postulated that curvature in the fiber reinforcing sheets due to rollover deformation causes individual fiber strands to slip against each other leading to additional energy dissipation in the bearing.

As expected, these results show that effective stiffness decreases with increasing displacement amplitude. This is one of the desirable properties attributed to rollover behaviour since a decrease in stiffness creates a longer fundamental period for the system. An additional noteworthy observation is the increase in effective stiffness between 1.5t_r and 2.0t_r. This increase in stiffness is due to the end faces of the bearing making contact with the upper and lower platens of the test set-up at the largest displacement amplitude. This is illustrated in Figure 3.8a and Figure 3.9a. From these images it is clear that the edge faces of the SU-FREI bearing perpendicular to the direction of excitation have began to make contact with the upper and lower platens of the test setup at a displacement of 2.0t_r. This led to the development of additional force resisting capacity in the bearing at extreme lateral displacement. This behaviour is desirable since it acts to limit the maximum displacement of the isolation layer.

3.5.1 Parallel Response

Once the effective stiffness and damping values were calculated for the bearings tested along a parallel orientation they were used to estimate the response of the isolation system using ASCE 7-05. For the parallel response, K_{min} and B were interpolated from the 3rd cycle results of testing performed on bearing MB1-4. These results represent the lowest effective stiffness values obtained during parallel cyclic testing, which provided a conservative estimate for displacement of the isolation layer. At DBE convergence was achieved using Equation 3.3 and 3.4, resulting in a lateral design displacement of D_D = 88 mm ($\approx$1.2t_r) and a base isolated period of T_D = 1.29 s. At MCE the resulting maximum displacement and the corresponding effective base isolated period are calculated as D_M = 146 mm ($\approx$1.9t_r) and T_M = 1.37 s, respectively. For both the DBE and the MCE the effective isolated period has been increased to greater than 1 second. These bearings would effectively lengthen the effective period of a typical low rise structure so that it is outside the range of dominant earthquake accelerations.

3.5.2 Comparison to Previous Study

Once the characteristics of SU-FREI bearings tested at a parallel orientation in this study were compiled it was possible to compare them to the results of previous testing performed by Toopchi-Nezhad et al. (2008b). In the previous study one unscragged SU-FREI bearing (B1-3) was tested under the same testing sequence allowing for a direct comparison to be made. The results of testing performed on SU-FREI bearing B1-3 are provided in Figure 3.12, which shows the effective stiffness versus lateral excitation amplitude. Figure 3.13 shows the effective damping versus lateral excitation amplitude. In both figures the unscragged and scragged values are shown separately. These results have been plotted with $\pm$15% of the mean effective stiffness over all three cycles averaged between the bearings test in this study (MB1-1, MB1-2, & MB1-4) and bearing B1-3 (from the previous study). The results show that both the effective stiffness and effective damping resulting from the previous study fit well within 15% of the mean. This satisfies test specimen adequacy outlined by ASCE 7-05 regarding test specimens of a common type and size. This comparison was performed to show continuity between the specimens tested in this study and those tested in the previous study.

3.6 Results of Diagonal Cyclic Testing

Two unscragged bearings, MB3-1 and MB3-4, were used to evaluate the unscragged response along a diagonal (45°) orientation. The load-displacement hysteresis for a bearing under diagonal excitation is shown in Figure 3.5b for bearing MB3-1. Similar to the parallel tests, the results show a drop in restoring force after the first cycle. The larger loops represent the first unscragged cycle at that amplitude. This loss of stiffness is further supported by the calculated effective stiffness values in Table 3.2. This is also illustrated in Figure 3.14 which shows the effective stiffness at a diagonal orientation versus the lateral excitation amplitude for both the unscragged and scragged cycles separately. The effective stiffness of each cycle for each bearing fit within 15% of the mean effective stiffness between all three cycles of both bearings. This satisfies the conditions for test specimen adequacy outlined by ASCE 7-05. The unscragged effective stiffness is an average of 5-10% greater than the scragged effective stiffness. Once again the largest percentage difference was measured at the greatest excitation amplitude.

Both the scragged and unscragged effective stiffness values obtained from cyclic testing at a diagonal orientation were 12% to 15% greater than those achieved by ¼ scale SU-FREI bearings tested at a parallel orientation. The one exception is the effective stiffness at a displacement of $2.0t_r$ at which the effective stiffness in the parallel bearings is an average of 7% greater than the diagonal bearings. At both orientations, there is a significant drop in effective stiffness as the excitation amplitude increases and the top and bottom faces of the bearing lose contact with the upper and lower platens. At a parallel orientation this stiffness increases between amplitudes of $1.5t_r$ and $2.0t_r$. This is not the case in the diagonal direction. Both samples show the effective stiffness continuing to decrease between $1.5t_r$ and $2.0t_r$. It is postulated that this is due to the amount of facial contact made by the edge face of the bearing perpendicular to the direction of excitation at each orientation. At a diagonal orientation, the corner edge of the bearing makes limited contact with the end plates at a lateral displacement of $2.0t_r$. Conversely at a parallel orientation the edge faces of the bearing will make substantial contact with the end plates. This is supported by Figure 3.9 which compares a side profile of an SU-FREI bearing at a displacement of $2.0t_r$ for both a diagonal and parallel orientation. The bearing at a parallel orientation has clearly made significantly more facial contact with the upper and lower platens.

The effective damping for diagonal testing is provided in Table 3.2 and plotted in Figure 3.15. The results obtained from both SU-FREI bearings are consistent and show a decrease in effective damping up to an excitation amplitude of $1.0t_r$. At greater excitation amplitudes the unscragged cycles show an increase in effective damping while the scragged cycles show an almost constant effective damping up to $2.0t_r$ whereas the parallel results show a notable decrease in effective damping between $1.5t_r$ and $2.0t_r$. In general the effective damping values achieved by bearings tested at a diagonal orientation were 4-8% greater than bearings tested at a parallel orientation. The exception to this occurs at an amplitude of $2.0t_r$ where diagonal tests show an average of 23% greater effective damping than parallel tests. It was previously suggested that the curvature of reinforcing sheets creates additional energy dissipation in FREI bearings in an unbonded application (Kelly J. M., 1999). The fiber used in the SU-FREI bearings tested here has a 0/90 degree over under weave. At a parallel orientation, only the fibers parallel to the direction of excitation will undergo curvature during cyclic testing. At a diagonal orientation, the fibers in both directions will undergo curvature during rollover deformation. It is postulated that slip between individual fiber strands in both directions causes the additional damping observed in bearings tested at a diagonal orientation. The effective damping measured at each cycle for each bearing is within 15% of the mean of all three cycles of both bearings. The effective damping results are well within the adequacy constraints for this study.

3.6.1 Diagonal Response

Similar to the parallel calculations, the results from the 3rd cycle of bearing MB3-4 were used to estimate D and T for the diagonal response. The 3rd cycle from tests run on bearing MB3-4 provided the lowest effective stiffness for the diagonal tests. At DBE the resulting lateral displacement of the centre of rigidity of the isolation system and the effective base isolated period were D_D = 78.5 mm ($\approx 1.0t_r$) and T_D = 1.17 s, respectively. At MCE the resulting maximum displacement and the corresponding effective base isolated period are calculated as D_M = 138 mm ($\approx 1.8t_r$) and T_M = 1.37 s respectively. The higher effective stiffness achieved by bearings tested at a diagonal orientation has resulted in effective isolated periods that are shorter than those achieved at a parallel orientation. However, for both the DBE and the MCE the effective isolated period has been lengthened to greater than 1 second. At a diagonal orientation, these bearings would effectively lengthen the effective period of a typical low rise structure so that it is outside the range of dominant earthquake accelerations.

3.7 Summary and Concluding Remarks

In this chapter, lateral cyclic testing was performed on ¼ scale SU-FREI bearings at parallel and diagonal orientations with respect to the direction of excitation. At each orientation the mechanical properties of effective stiffness and effective damping were analyzed. This study is a continuation of research conducted on ¼ scale SU-FREI bearings. For this reason, it was desirable to compare the properties of the bearings used in this study with those used in the previous study (Toopchi-Nezhad et al., 2008a & 2008b). The difference in effective stiffness and damping between bearings from both studies was within 15% of the mean. This satisfied the provisions for test specimen adequacy as laid out by ASCE 7-05 with regards to bearings of a common type and size. The mechanical properties of ¼ scale SU-FREI bearings from both studies were in agreement.

At both a parallel and diagonal orientation it was found that SU-FREI bearings were able to achieve greater effective stiffness and damping at lower lateral displacement amplitudes. This is beneficial for reducing displacement in the isolation layer caused by minor seismic activity and wind loads. Increased lateral displacement was accompanied by a significant drop in effective stiffness. This is attributed to rollover behaviour caused by the unbonded boundary conditions and lack of flexural rigidity inherent to SU-FREI bearings. The most significant reduction in effective stiffness is observed at lateral displacements in the range of $1.0t_r$ to $2.0t_r$. This range corresponds to the typical design displacement of SU-FREI bearings. A decrease in effective stiffness results in a longer effective period of the isolation layer improving the efficiency of SU-FREI bearings as seismic isolators. Tests performed at parallel and diagonal orientations satisfied the code requirements of ASCE 7-05.

Comparison between orientation angles at amplitudes of $0.25t_r$ to $1.5t_r$ revealed that higher effective stiffness and damping is generally achieved when square SU-FREI bearings are cycled at a diagonal orientation. Effective stiffness was measured at 12-15% greater and effective damping is 4-8% greater than bearings tested at a parallel orientation. Between lateral displacements of 1.5tr and 2.0tr there is a noteworthy increase in the effective stiffness of bearings tested along a parallel orientation. This is caused by the onset of facial contact between the vertical faces of the bearing perpendicular to the direction of excitation and the upper and lower test platens. Bearings tested along a diagonal orientation did not display stiffening in the same manner. This is attributed to the amount of facial contact experienced at each orientation, which is limited at a diagonal orientation. It is expected that significant stiffening will occur at both orientations at displacements greater than $2.0t_r$ once full facial contact has been made. This stiffening effect is beneficial at large displacement amplitudes as it acts to limit the maximum displacement of the isolation layer. It is postulated that SU-FREI bearings will achieve greater effective stiffness and damping as the orientation angle approaches 45 degrees.

Using the calculated effective stiffness and damping values, it was possible to estimate the effective base isolated period under DBE and MCE conditions. At both parallel and diagonal orientations the effective base isolated period was lengthened to greater than 1 second for the considered low rise structure. There are subtle differences in dynamic properties of SU-FREI bearings at diagonal and parallel orientations. Despite these differences they can be effectively used to base isolate a low rise structure with a fixed-base period of ≈ 0.2s at either orientation. Although a specific example was used for these calculations, SU-FREI bearings can be designed to accommodate various structures in regions with higher seismic accelerations.

Table 3.1 Parallel (0°) orientation effective stiffness and effective damping values from cyclic testing on Bearings MB1-1, MB1-4, and MB1-2

		MB1-1		MB1-4		MB1-2	
Displacement Amplitude (t_r)	Cycle	Effective Stiffness (N/mm)	Effective Damping (%)	Effective Stiffness (N/mm)	Effective Damping (%)	Effective Stiffness (N/mm)	Effective Damping (%)
0.25	1	176.0	13.8	163.6	13.6	174.1	14.0
	2	171.1	14.8	154.4	14.4	163.1	15.1
	3	168.5	15.0	152.9	13.9	161.5	14.4
0.50	1	132.4	13.4	123.2	12.8	130.0	12.9
	2	125.3	12.8	116.4	12.0	122.4	12.1
	3	123.6	12.8	114.7	11.9	120.6	11.9
0.75	1	107.2	12.2	100.2	11.6	105.7	11.5
	2	100.2	11.9	94.5	11.0	99.2	11.1
	3	98.6	11.8	93.0	10.9	97.5	11.1
1.00	1	92.7	11.4	86.9	10.8	90.8	10.8
	2	87.5	10.9	82.1	10.3	85.8	10.3
	3	85.7	10.9	80.1	10.2	84.6	10.3
1.50	1	75.6	11.7	70.9	11.3	74.2	11.3
	2	70.3	10.4	66.3	9.8	69.5	9.9
	3	68.3	10.3	64.5	9.7	67.6	9.7
2.00	1	79.9	10.0	74.4	9.8	78.0	9.9
	2	74.6	8.8	68.5	8.7	72.6	8.7
	3	72.6	8.6	66.7	8.5	71.0	8.4

Table 3.2 Diagonal (45°) orientation effective stiffness and effective damping values from cyclic testing on Bearings MB3-1, MB1-4, and MB3-4

		MB3-1		MB3-4	
Displacement Amplitude (tr)	Cycle	Effective Stiffness (N/mm)	Effective Damping (%)	Effective Stiffness (N/mm)	Effective Damping (%)
0.25	1	202.2	14.4	182.3	14.1
	2	193.0	15.1	173.3	15.3
	3	190.4	14.7	171.8	15.4
0.50	1	153.0	13.9	138.9	14.0
	2	143.9	12.7	131.2	12.9
	3	140.9	12.7	128.7	13.0
0.75	1	124.7	12.4	115.2	12.5
	2	116.6	11.6	108.4	11.7
	3	114.2	11.5	106.2	11.6
1.00	1	107.8	11.7	99.8	11.8
	2	102.1	10.9	94.1	11.0
	3	99.6	10.7	92.3	10.9
1.50	1	87.9	12.8	82.2	12.7
	2	82.5	10.9	77.2	10.8
	3	79.6	10.6	74.7	10.5
2.00	1	74.6	13.0	70.1	12.9
	2	68.4	11.5	64.4	11.3
	3	65.4	11.1	61.8	11.0

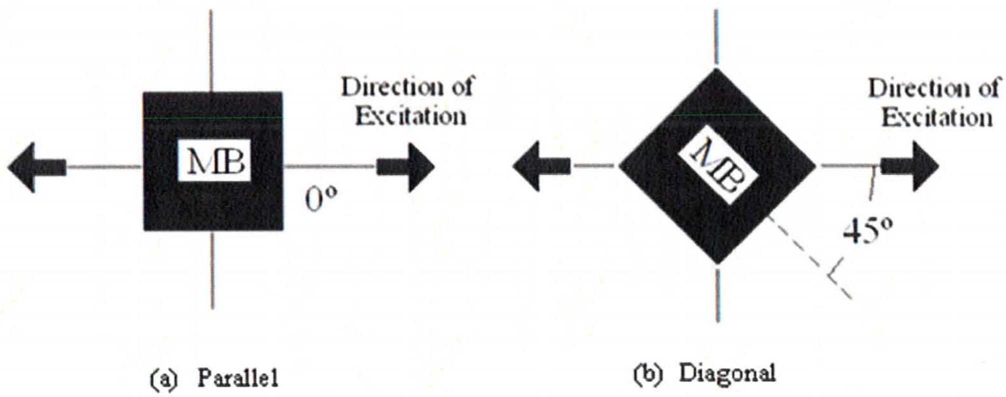

Figure 3.1 Bearing Sample orientation with respect to the direction of excitation for the parallel and diagonal case

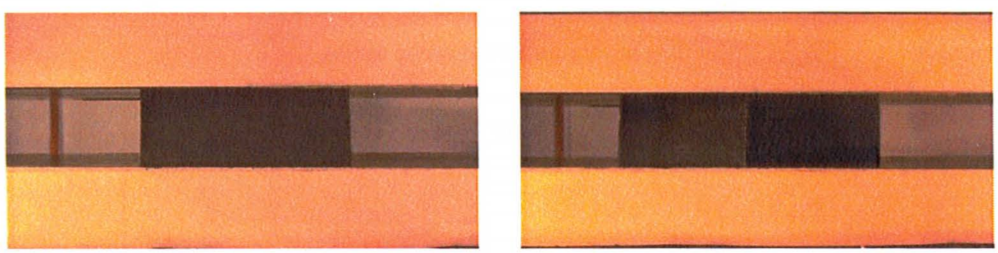

(a) Parallel (b) Diagonal

Figure 3.2 Side view of SU-FREI bearing at rest ($0t_r$)

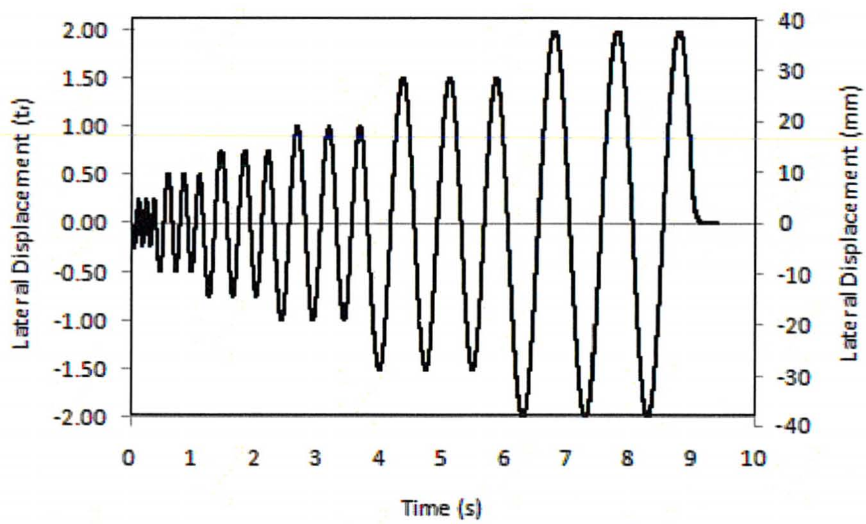

Figure 3.3 Displacement time history for lateral cyclic testing

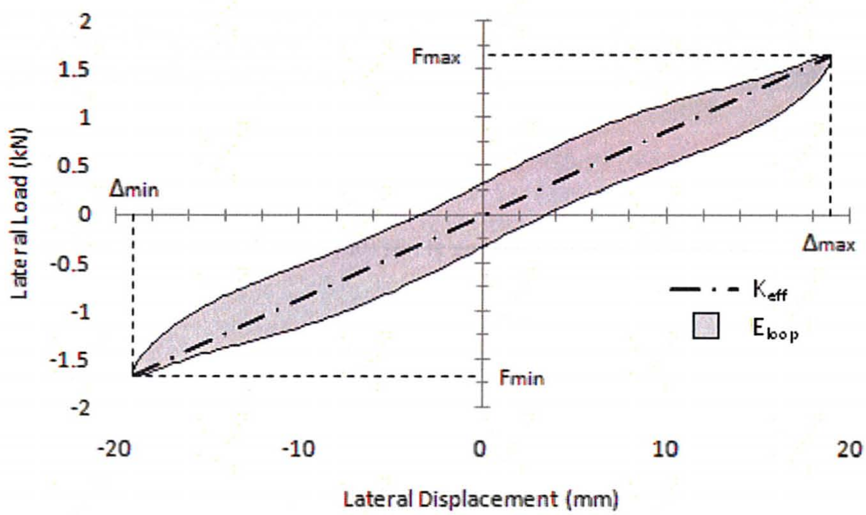

Figure 3.4 Location of maximum and minimum displacement and lateral force in a fully reversed hysteresis loop

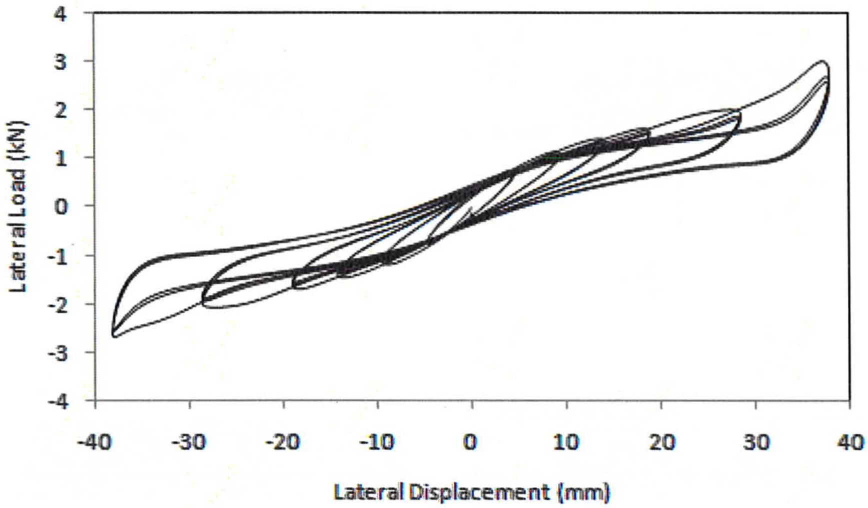

(a) MB1-1: Parallel (0°)

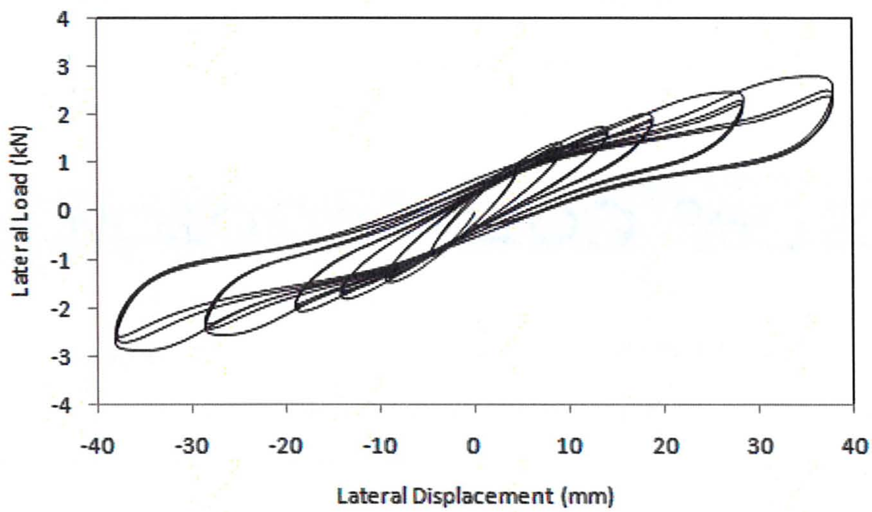

(b) MB3-1: Diagonal (45°)

Figure 3.5 Hysteresis loops for Bearing: a) MB1-1 (0°) and b) MB3-1 (45°) for all cycles

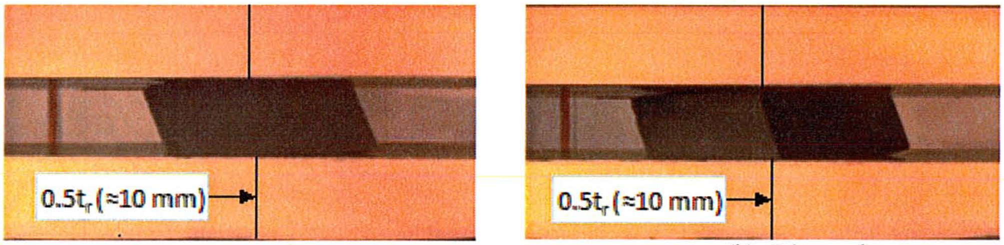

(a) Parallel (b) Diagonal

Figure 3.6 Side view of SU-FREI bearing at $0.5t_r$ (≈9.5 mm) lateral displacement

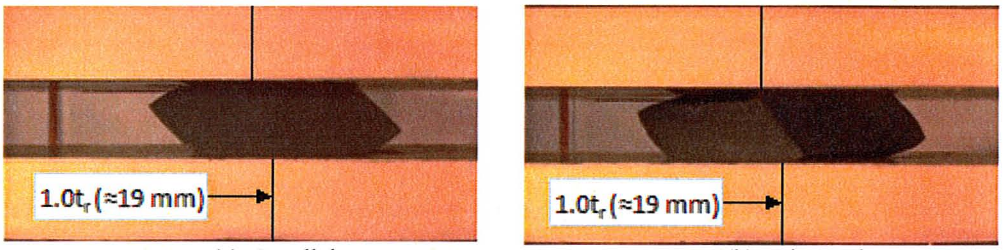

(a) Parallel (b) Diagonal

Figure 3.7 Side view of SU-FREI bearing at $1.0t_r$ (≈19 mm) lateral displacement

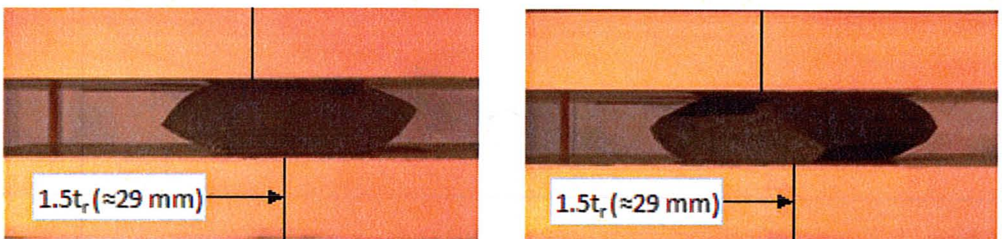

(a) Parallel (b) Diagonal

Figure 3.8 Side view of SU-FREI bearing at $1.5t_r$ (≈28.6 mm) lateral displacement

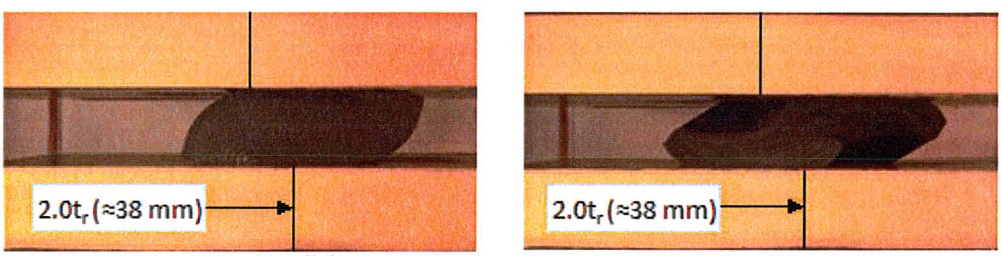

(a) Parallel (b) Diagonal

Figure 3.9 Side view of SU-FREI bearing at $2.0t_r$ (≈38.1 mm) lateral displacement

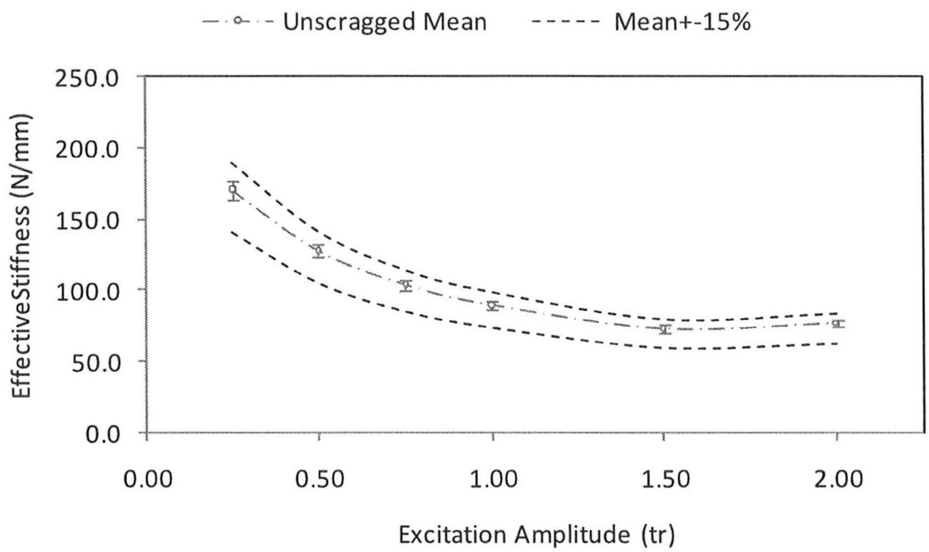

(a) Unscragged

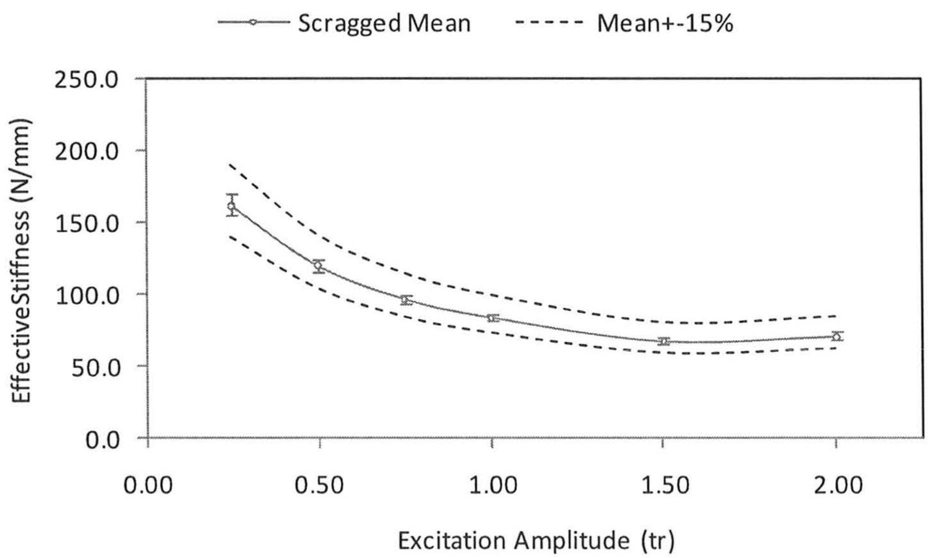

(b) Scragged

Figure 3.10 Effective stiffness at a parallel (0°) orientation for SU-FREI bearings MB1-1, MB1-2, and MB1-4: (a) Mean unscragged effective stiffness plotted with ±15% of the mean effective stiffness of all three cycles; (b) Mean scragged effective stiffness plotted with ±15% of the mean effective stiffness of all three cycles.

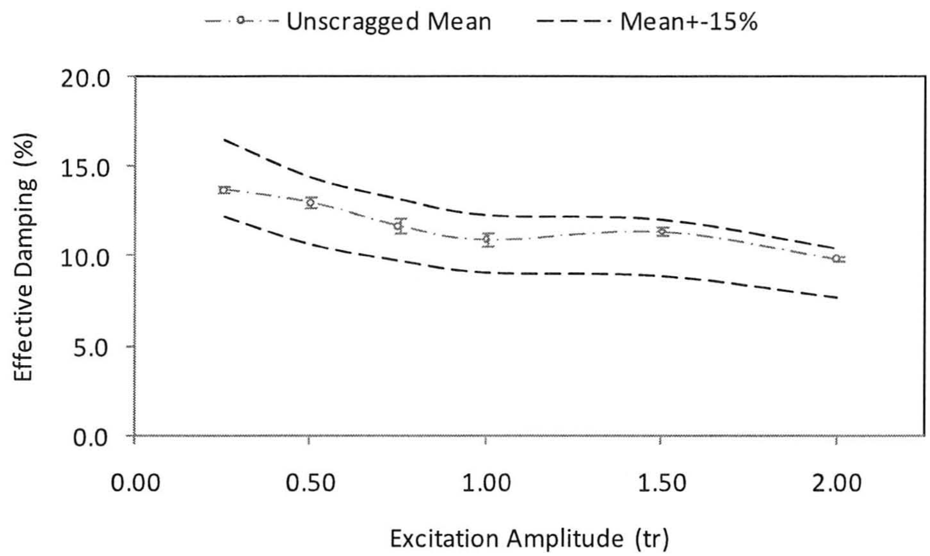

(a) Unscragged

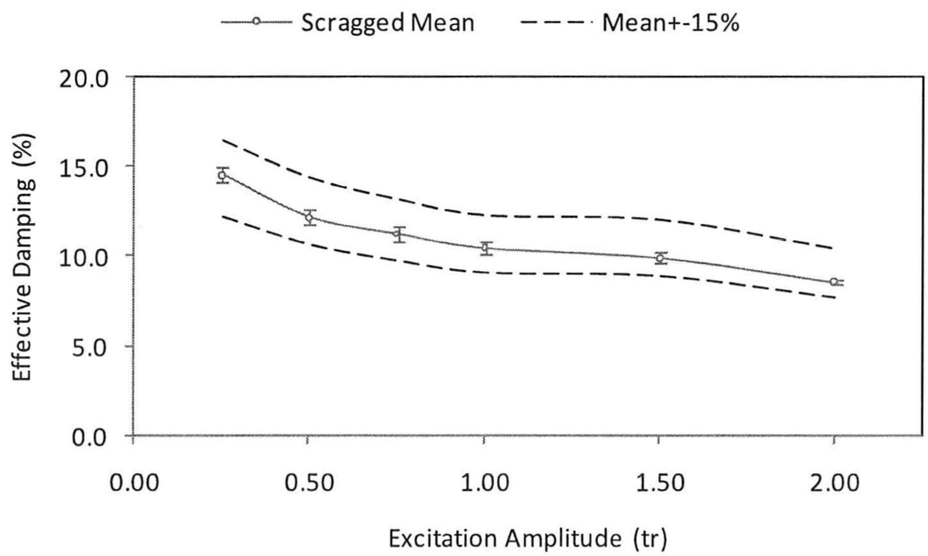

(b) Scragged

Figure 3.11 Effective damping at a parallel (0°) orientation for SU-FREI bearings MB1-1, MB1-2, and MB1-4: (a) Mean unscragged effective damping plotted with ±15% of the mean effective damping of all three cycles; (b) Mean scragged effective damping plotted with ±15% of the mean effective damping of all three cycles.

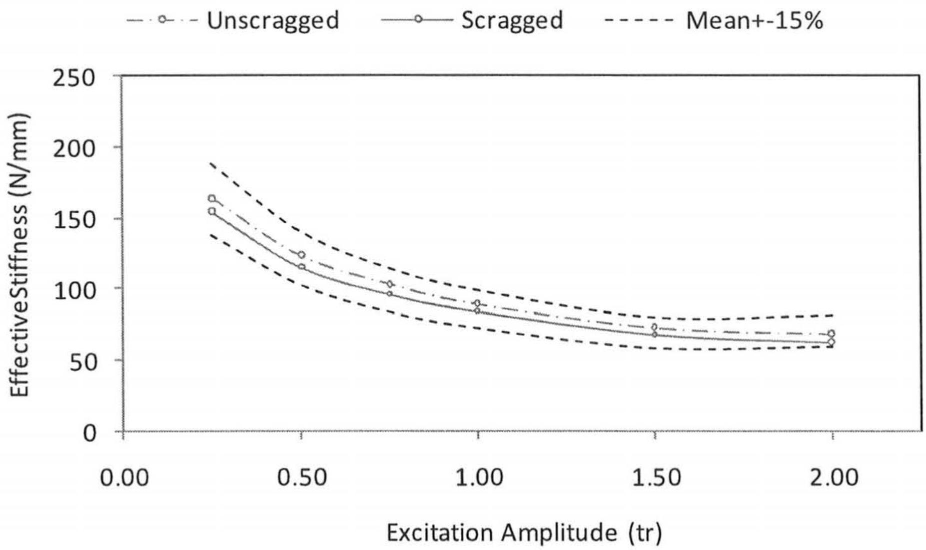

Figure 3.12 Effective stiffness at a parallel orientation for bearing HB1-3 comparing the unscragged effective stiffness to mean scragged effective stiffness averaged over the 2nd and 3rd cycles. (Toopchi-Nezhad, Tait, & Drysdale, 2008b). Mean ±15% determined from average of all 3 cycles of bearings MB1-1, MB1-2, MB1-4, and HB1-3.

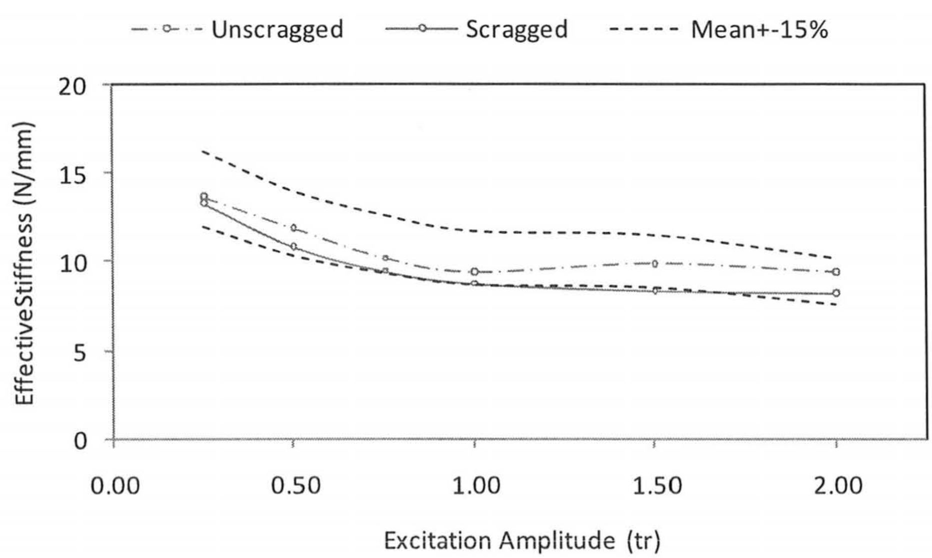

Figure 3.13 Effective damping at a parallel orientation for bearing HB1-3 comparing the unscragged effective damping to mean scragged effective damping averaged over the 2nd and 3rd cycles. (Toopchi-Nezhad, Tait, & Drysdale, 2008b). Mean ±15% determined from average over all 3 cycles from bearings MB1-1, MB1-2, MB1-4, and HB1-3.

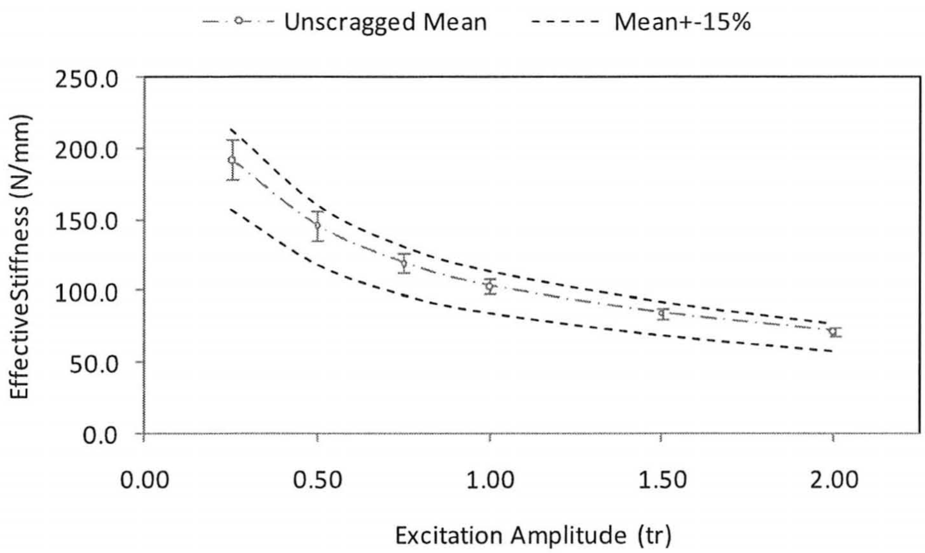

(a) Unscragged

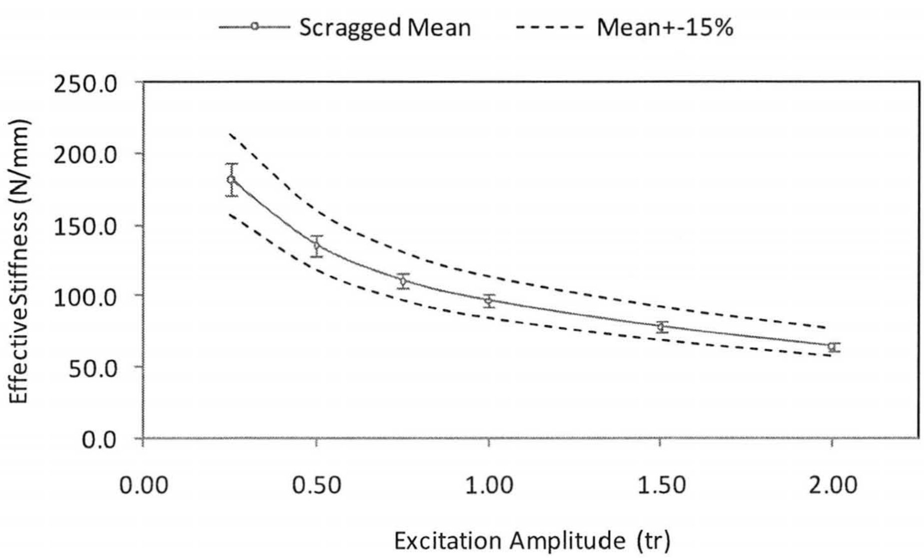

(b) Scragged

Figure 3.14 Effective stiffness at a diagonal (45°) orientation for SU-FREI bearings MB3-1 and MB3-4: (a) Mean unscragged effective stiffness plotted with ±15% of the mean effective stiffness of all three cycles; (b) Mean scragged effective stiffness plotted with ±15% of the mean effective stiffness of all three cycles.

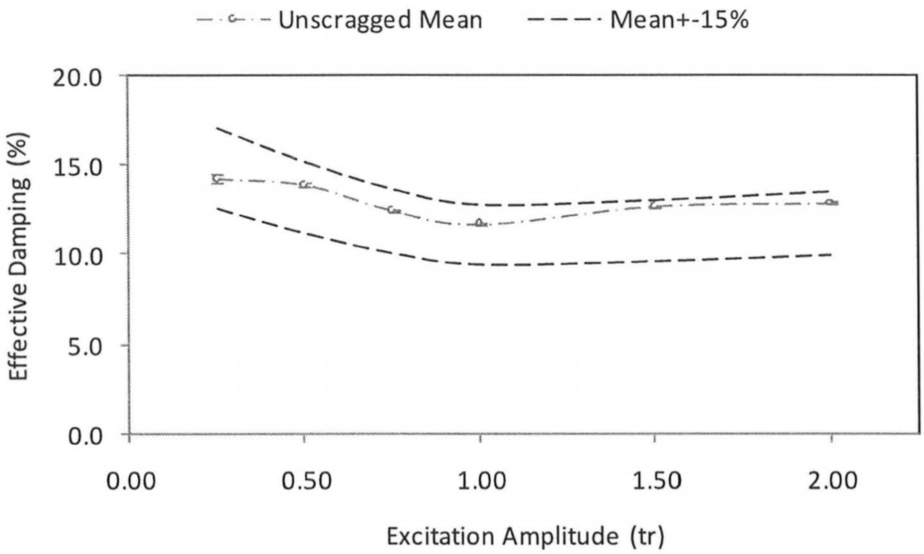

(a) Unscragged

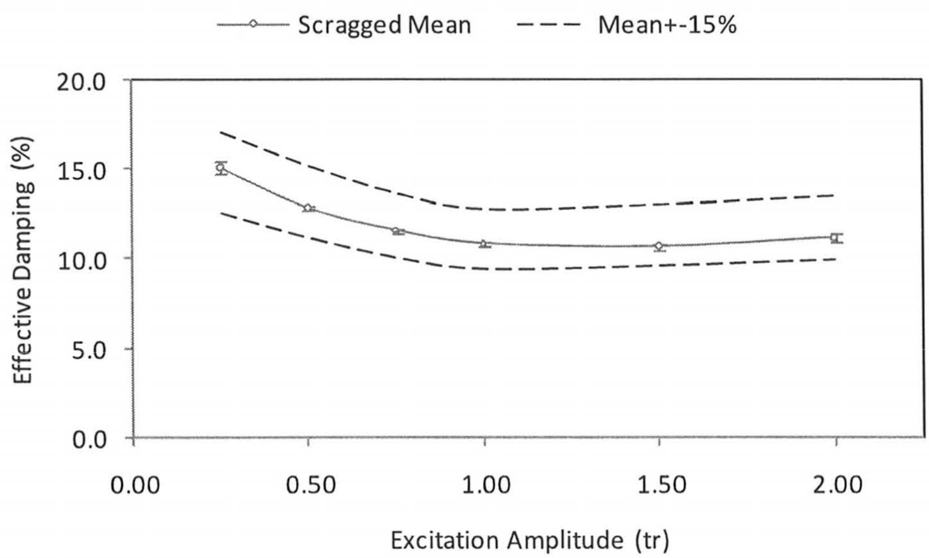

(b) Scragged

Figure 3.15 Effective damping at a diagonal (45°) orientation for SU-FREI bearings MB3-1 and MB3-4: (a) Mean unscragged effective damping plotted with ±15% of the mean effective damping of all three cycles; (b) Mean scragged effective damping plotted with ±15% of the mean effective damping of all three cycles.

Chapter 4. Stability

The objective of this chapter is to investigate the stability of SU-FREI bearings. In order to accomplish this, two different testing programs were utilized. The first testing program studies the effect of increasing the axial load on a bearing sample under lateral excitation at constant displacement amplitude. This testing program provides insight into the dynamic properties of SU-FREI bearings under a variety of axial load conditions and is a novel approach for determining the axial load corresponding to the initiation of hysteretic instability. As a supplemental investigation, two SU-FREI bearings were subjected to monotonic shear testing.

4.1 Testing Procedure

4.1.1 Dynamic Buckling

A total of five unscragged bearings were tested to determine the influence of axial load on the dynamic properties of SU-FREI bearings under cyclic loading. These properties included the effective lateral stiffness and the effective damping achieved. The objective of this study was to determine the axial load that an SU-FREI loses stability under sinusoidal lateral excitation. This loss of stability under lateral excitation has been termed *dynamic buckling*. Dynamic buckling refers to the loss of positive incremental load resisting capacity during cyclic testing. SU-FREI bearing samples were tested under several combinations of axial load and displacement amplitude.

Each ¼ scale SU-FREI bearing specimen was placed into the test setup and centered at a parallel orientation with respect to the direction of excitation. Once the sample was in place, an axial load P was applied. The bearing was then subjected to two fully reversed cycles of lateral displacement at an amplitude u while the axial load P was maintained. The average rate of displacement was maintained at a constant 76 mm/s similar to the cyclic testing performed in Chapter 3. The axial load was then completely removed and the sample inspected for any sign of damage, typically in the form of delamination. The first test on an unscragged SU-FREI bearing was performed at the smallest excitation amplitude and lowest axial load combination. The resulting lateral force-displacement hysteresis was visually inspected for stable hysteretic behaviour. If the bearing showed positive incremental force resisting capacity throughout both fully reversed cycles the bearing was tested again at the same displacement amplitude u and the next highest incremental axial load P. This process was repeated at the same lateral excitation amplitude u until hysteretic instability was observed. At this point the excitation amplitude was increased to the next highest incremental excitation amplitude and the process was repeated starting with the lowest axial load P. This allowed for the effect of excitation amplitude on the critical load to be examined.

The original testing program consisted of four displacement amplitudes (0.5tr, 1.0tr, 1.5tr, and 2.0tr) and five possible axial loads (7.84kN, 30kN, 60kN, 90kN, and 120kN) resulting in a possible 20 combinations. After preliminary testing it was found that axial loading above 90kN was unnecessary as instability typically occurred prior to this axial load level. For lateral excitation of 2.0t_r it was found that instability occurred at axial loads slightly larger than 60 kN but lower than 90 kN. For this reason, bearings tested at an amplitude of 2.0t_r underwent a maximum possible axial load of 75 kN. The maximum incremental axial load applied to a specimen at a given lateral excitation amplitude was dependant on the observed lateral force-displacement hysteresis loops. The testing program was conducted to minimize the total number of tests performed on each bearing while still obtaining the critical load at each amplitude.

Bearing MB1-3 was the first bearing tested and was the only bearing tested at all four displacement amplitudes. The results of these tests were used to decide the final testing program used for the remaining four ¼ scale SU-FREI bearings. MB1-3 was tested under 17 combinations of lateral displacement and axial load. The results of these tests provided insight into the range of axial load P required for the onset of hysteretic instability at each of the four lateral displacement amplitudes. Instability was not observed in the bearing at an excitation amplitude of 0.5t_r at an axial load of P = 120 kN. An axial load of 120 kN was the limit of the test setup capacity. From these results, it was decided that further testing at an amplitude of 0.5t_r would not yield the desired hysteretic instability without exceeding the limits of the test setup. No further stability testing was performed at an amplitude of 0.5t_r on SU-FREI bearings in this study.

Hysteretic instability was observed at the remaining three amplitudes during testing of MB1-3. Therefore, subsequent bearings were only tested at amplitudes of 1.0t_r, 1.5t_r, and 2.0t_r. Following bearing MB1-3 each bearing underwent a total of approximately 12 combinations of axial load and lateral excitation instead of 17. The final testing history for each SU-FREI bearing is provided in Table 4.1. This table provides the details of each test performed in sequence on all five bearings used in this investigation.

4.1.2 Rollout

Two partially scragged bearings (MB2-2 and MB2-3) were selected for the rollout testing program. This test did not require the use of unscragged bearings due to the extremely large lateral displacements involved. Both bearings had undergone the same testing history prior to rollout testing in order to maintain consistency. The maximum lateral displacement the bearings had been subjected to previously was 1.5t_r. Additionally, neither bearing had been placed under an axial load greater then design axial pressure. Prior to rollout testing both MB2-2 and MB2-3 were subjected to serviceability testing at 0.15t_r and 0.35t_r as well as fatigue testing at 1.5t_r. Neither bearing showed any signs of damage through visual inspection or through analysis of the prior test results. For these reasons they were considered acceptable for rollout testing.

The rollout tests performed in this study were modeled after the provisions of ISO 22762 (2005). The rollout test is used to investigate the ultimate shear properties of seismic protection isolators. Each bearing was vertically loaded with the design axial pressure of 1.6 MPa. Once the load was applied, it was held constant while unidirectional lateral displacement was applied to the bearing at a constant displacement rate of 76 mm/s. According to the provisions of ISO 22762 (2005) the lateral displacement should continue until failure occurred. For safety reasons it was not appropriate to allow the bearing to displace indefinitely. Instead two extreme lateral displacements were selected for rollout testing. Bearing MB2-2 was displaced to $2.75t_r$ and bearing MB2-3 was displaced to $3.0t_r$. These displacements were selected to ensure the bearing deformed past the point where the edge faces of the bearings make full contact with the test platens. Once the target displacement was achieved the bearing was returned to zero displacement and the axial load removed. The results were then analyzed to determine if the bearing buckled or failed under the imposed displacement. This was followed by a visual inspection for signs of damage or delamination.

4.2 Dynamic Buckling Tests

4.2.1 The Backbone Curve

In order to analyze the hysteresis loops obtained from the dynamic buckling tests a curve was fit to the hysteresis loops. Toopchi-Nezhad et al. (2008c) developed a method of fitting a polynomial to experimental force–displacement hysteresis data. The fitted curve represented an idealized estimate of the lateral force-displacement response of the bearing if damping was removed, which was referred to as the backbone curve. The total lateral load experienced by bearing "*i*" ($f_{b,i}$) is described by the following equation as a function of time (Toopchi-Nezhad et al., 2008c):

$$f_{b,i}(t) = f_{sb,i}(t) + f_{db,i}(t) \qquad 4.1$$

where, $f_{sb,i}$ is the stiffness force and $f_{db,i}$ is the corresponding force due to damping. The stiffness force $f_{sb,i}(t)$, is described by the following equation (Toopchi-Nezhad et al., 2008c):

$$\begin{aligned} f_{sb,i}(t) &= k_{b,i}(v_b(t))v_b(t) \\ &= (b_o + b_1 v_b(t) + b_2 v_b^2(t) + b_3 v_b^3(t) + b_4 v_b^4(t))v_b(t) \end{aligned} \qquad 4.2$$

where $k_{b,i}(v_b(t))$ is the lateral secant stiffness of the bearing as a function of lateral displacement $v_b(t)$. The five parameters b_o to b_4 can be determined from applying a least squares fit to the experimental data.

Employing this method, each backbone curve was fit to the force-displacement hysteresis of both cycles together. The fitted backbone curves used in this study represent an average of both hysteresis loops. The parameters for the backbone curves fit to the force-displacement hysteresis loops obtained from testing of bearing MB1-3 are provided in Table 4.2. Backbone curves have been plotted with their corresponding force-displacement hysteresis loops in Figure 4.1, Figure 4.2, Figure 4.3, for excitation amplitudes of 1.0tr, 1.5tr, and 2.0tr respectively. The next step in analysis is to investigate the tangential stiffness throughout the fully reversed cycles to determine the axial load at which the lateral stiffness becomes zero.

4.2.2 Tangential Stiffness

By taking the first derivative of the backbone curve, described by Equation 4.2, with respect to the lateral displacement an equation for tangential stiffness as a function of lateral displacement can be derived as shown in the following equation

$$k_{tb,i}(v_b(t)) = \frac{df_{sb,i}(t)}{dv_b(t)} \qquad 4.3$$

$$= b_o + 2b_1v_b(t) + 3b_2v_b^2(t) + 4b_3v_b^3(t) + 5b_4v_b^4(t)$$

The parameter b_o describes the tangential stiffness of bearing "*i*" at $v_b(t) = 0$ mm. Stanton et al. (1990) define the tangential stiffness at zero displacement in a force displacement hysteresis as the transverse stiffness (K_t) of the bearing. As mentioned previously, the objective of this study is to determine the axial load at which an SU-FREI bearing would no longer be able to maintain positive incremental force resisting capacity. The transverse stiffness is not necessarily the minimum tangential stiffness in every fully reversed hysteresis loop under constant axial load. However, the transverse stiffness represents the tangential stiffness at which zero lateral stiffness first occurs under increasing axial load.

The fitted backbone curves obtained from experimental testing of SU-FREI bearing MB1-3 are provided in Figure 4.4 for lateral displacement amplitudes of 0.5t_r, 1.0t_r, 1.5t_r, and 2.0t_r. The corresponding tangential stiffness results are provided in Figure 4.5 versus lateral displacement for each increment of axial load. As the axial load increases, the slope of the backbone curve at zero displacement decreases to a negative value. Under increasing axial load the transverse stiffness represents the first point where a tangential stiffness of zero is achieved for an SU-FREI bearing. This observation was made following the first round of testing performed on bearing MB1-3. The transverse stiffness obtained from the backbone curves for all five bearings showed similar trends. As the axial load increases the transverse stiffness decreases until it is either sufficiently close to a value of 0 N/mm or is negative. This behaviour appears to be isolated to the tangential stiffness at 0mm displacement. Under lesser axial load (7.84kN and 30kN) the transverse stiffness does not represent the minimum effective stiffness in a fully reversed cycle of lateral displacement (See Figure 4.5). Least squares interpolation can be used to determine the axial load corresponding to $K_t = 0$. For cases where the transverse stiffness did not quite reach a value of 0 N/mm, extrapolation was used. The axial load corresponding to a transverse stiffness of zero is the critical buckling load under dynamic excitation for an SU-FREI bearing.

4.2.3 Effect of Axial Load on Dynamic Properties

Similar to the EERC report discussed in Chapter 2 (Koh & Kelly, 1987), cyclic testing of SU-FREI bearings under a wide variety of axial loads allows insight into the effects of axial load on the dynamic characteristics. Analogous to Chapter 3, the two properties of importance are the effective stiffness and effective damping. Both of these properties are determined using the same method described previously in Chapter 3 using Equation 3.1 and 3.2.

4.3 Results of Dynamic Buckling Tests

The five ¼ scale SU-FREI bearings tested in this section are divided into two groups when analyzing the results. The reasons for this became apparent upon completion of the testing process. Three of the bearings sustained substantial delamination throughout the testing history while two of the bearings did not. The predominant reason for this is related to the manufacturing process. Since the two bearings that did not experience delamination were cut from the same sheet (MB3). The first two sheets, MB1 and MB2, were constructed simultaneously. The third sheet, MB3, was constructed once the first two were completed. The last sheet benefited from the experience gained while constructing the first two sheets. It is postulated that the final sheet of bearings were of a better quality. While discussing the five bearings, those cut from sheets MB1 and MB2 will be referred to as Set A (MB1-3, MB2-1, and MB2-4) while those cut from sheet MB3 will be referred to as Set B (MB3-2 and MB3-3).

4.3.1 Transverse Stiffness

The values of transverse stiffness obtained from each test are provided in Table 4.3 for all five bearings. This is illustrated in Figure 4.6 and Figure 4.7 for Set A and Set B, respectively. These values represent the tangential stiffness at zero displacement derived from the fitted backbone curve. In all of the ¼ scale SU-FREI bearings tested in this study it was found that transverse stiffness decreased with increasing axial load. The transverse stiffness is also observed to decrease as the excitation amplitude is increased.

Comparing Set A to Set B, it can be seen that the transverse stiffness at each combination of axial load and lateral displacement is greater in the bearings from Set B by approximately 10-15 N/mm. The lower transverse stiffness measured in bearings from Set A is attributed to the partial delamination that occurred during testing. Delamination occurs when a remote section of a rubber layer inside an SU-FREI bearing loses its bond with the adjacent carbon fiber layer as illustrated in Figure 4.10. Delamination occurred in all three bearings from Set A and first appeared following the first cyclic tests performed at the highest axial load. Subsequent tests resulted in negligible additional propagation in any delaminated areas. An example of the amount of visible delamination experienced by a ¼ scale SU-FREI bearing after the dynamic buckling test history was completed is provided in Figure 4.11 for bearing MB2-4. Although this delamination may have resulted in a decrease in transverse stiffness it did not affect the stability of the bearings. Each cycle of testing maintained both stable and symmetric hysteresis until buckling occurred. This can be seen in the hysteresis loops provided for SU-FREI bearing MB1-3 in Figure 4.1, Figure 4.2, and Figure 4.3. These hysteresis loops show symmetric behaviour throughout each fully reversed cycle. Even the cycles in which hysteretic instability is observed are symmetric.

It is also apparent from Table 4.3 that there are no recorded values for transverse stiffness of bearings from Set B at an axial load of 75 kN and an excitation amplitude of $2.0t_r$. Delamination was not observed in bearings from Set B until the final test performed at this combination of axial load and lateral displacement. This test resulted in erratic and unsymmetrical force-displacement hysteresis. Both bearings MB3-2 and MB3-3 behaved similarly during the final test in the dynamic buckling test history. Prior to the final test both bearings performed adequately with no signs of damage or delamination whatsoever. It was not until the final test that they showed erratic behaviour. It is proposed that this failure is due to a buildup in stress accumulated throughout the testing history. The buckling load for bearings from Set B at a lateral excitation amplitude of $2.0t_r$ was estimated using linear extrapolation between the 30kN and 60kN transverse stiffness data (Figure 4.7). It is highly unlikely that an unscragged bearing tested at the same combination of axial load and displacement amplitude would fail in this manner. This is further supported by the successful test results obtained from the bearings of Set A.

4.3.2 Critical Dynamic Buckling Load

The critical buckling load under dynamic excitation is determined at each lateral displacement amplitude from the transverse stiffness values. The objective was to determine the axial load at which a transverse stiffness of 0 N/mm occurred. For most displacement amplitudes a negative value of transverse stiffness was attained by increasing the axial load. For bearings MB1-3 and MB3-3 the transverse stiffness at a 90kN axial load and $1.0t_r$ displacement amplitude was sufficiently close to zero ($K_t \approx 1$ N/mm) to allow for an accurate estimate of the buckling load using extrapolation from least squares curve fitting. Interpolation was used for all other cases where a negative transverse stiffness was achieved at the highest axial load.

The critical buckling loads obtained from the transverse stiffness data are provided in Table 4.4. These values are plotted versus excitation amplitude in Figure 4.8 and Figure 4.9 for Set A and Set B respectively. From these results it is clear that the critical bucking load decreases with increasing excitation amplitude. By observing each set individually, it is evident that there is negligible variation in the calculated buckling loads. Bearings from Set B achieve average critical buckling loads that are greater than Set A by 3% at $1.0t_r$ and 14% at $1.5t_r$. Despite the comparable difference in transverse stiffness measured in the two sets of bearings, the final critical buckling loads of all five ¼ scale bearings fit within a 95% confidence interval of the mean. A buckling load at $2.0t_r$ could not be obtained from bearings MB3-2 and MB3-3 since the final test at 75 kN axial load did not yield useable results. An approximation of the critical buckling load for bearings from Set B at an excitation amplitude of $2.0t_r$ was performed using linear extrapolation of the transverse stiffness measured at 30 kN and 60 kN. This yielded an approximate critical buckling load of 76 kN at an excitation amplitude of $2.0t_r$ for bearings from Set B. The critical buckling loads for bearings from Set A represent a conservative estimate of the buckling load for SU-FREI bearings.

Predicting the critical buckling load of SU-FREI bearings under dynamic excitation between amplitudes of $1.0t_r$ to $2.0t_r$ is essential for estimating the critical load at both the design and maximum displacement of the isolation layer. The results of cyclic testing performed in Chapter 3 show that at a parallel orientation the estimated displacement of the isolation layer under a design basis earthquake (DBE) is $D_D = 1.16t_r$. The estimated displacement of the isolation layer under the maximum considered earthquake was found to be $D_M = 1.92t_r$. Using linear interpolation from the mean critical buckling loads obtained from Set A provides a conservative approximation of $P_{cr} \approx 1328$ kN at D_D, and $P_{cr} \approx 1024$ kN at D_M for full-scale SU-FREI bearings. This equates to approximately 11 and 8 times greater than the expected design axial load for the full-scale SU-FREI bearings at DBE and MCE respectively. A critical buckling load of $P_{cr} = 990 \pm 32$ kN was measured for full scale SU-FREI bearings from Set A at an excitation amplitude of $2.0t_r$. This is the lowest axial load at which buckling was observed in the bearings tested and it represents a conservative estimate that is still nearly 8 times the design axial load. From these results it is clear that SU-FREI bearings are highly resistant to buckling failure during dynamic excitation.

4.3.3 *Effect of Axial Load on Dynamic Properties*

In addition to determining the axial load at which SU-FREI bearings buckle under lateral excitation, the effects of axial load on the dynamic properties are investigated in this study. The results of the calculated values of effective stiffness and effective damping are provided in Table 4.5 to Table 4.9. Each table shows the results obtained from dynamic buckling testing of each of the five individual ¼ scale SU-FREI bearings. These results are illustrated in Figure 4.12 to Figure 4.17 where the results from Set A and Set B are compared. The first cycle of each test shows a notably larger effective stiffness and damping than the second cycle. It is clear that the ¼ scale SU-FREI bearings experience unscragged behaviour in the first cycle of each test. Furthermore, there is a distinct difference between bearings from Set A and Set B similar to what was discussed concerning the evaluation of transverse stiffness and the buckling load under dynamic excitation.

Effective stiffness versus axial load is provided in Figure 4.12, Figure 4.13, and Figure 4.14 for lateral displacement amplitudes of $1.0t_r$, $1.5t_r$, and $2.0t_r$ respectively. Similar to findings in Chapter 3, the first cycle shows unscragged behaviour while the second cycle shows scragged behaviour. The cyclic tests described previously in Chapter 3 involved cycling a bearing under increasing lateral displacements while the axial load was held constant. The first cycle performed at each amplitude achieved a higher effective stiffness than subsequent cycles. In this case multiple tests were performed at the same lateral displacement amplitude while the axial load was increased after each test. Scragging was previously described as cyclic loading at constant amplitude under tensile, compressive, or shear forces. Increasing the tensile, shear or compressive load will result in unscragged behaviour in the first cycle. The results show that the effective stiffness of the second cycle is less than the first cycle and as the axial load increases the difference between the first and second cycle increases. Under the design axial load the effective stiffness of the first cycles is between 4% and 7% greater than that of the second cycle. Under the highest axial loads this difference is as large as 20%.

Both the scragged and unscragged effective stiffness decrease with increasing axial load in all of the bearings tested. On average, SU-FREI bearings tested under axial loads from 7.8 kN to 90 kN, experienced a 35% drop in effective stiffness. This percentage drop is consistent among bearings from both Set A and Set B at amplitudes of $1.0t_r$ and $1.5t_r$. Bearings tested at an amplitude of $2.0t_r$ experienced an average 28% drop in effective stiffness between tests performed at axial loads of 7.8 kN and 60 kN. The axial load has a substantial impact on the effective stiffness of the SU-FREI bearings. Despite the loss of effective stiffness at high axial load, SU-FREI bearings maintained symmetric force-displacement hysteresis under cyclic excitation. Throughout dynamic buckling testing the effective stiffness remained positive for all tests.

Similar to the results of transverse stiffness, the effective stiffness calculated for Set A is less than Set B for every combination of axial load and lateral displacement. This result is expected for the same reasons discussed when comparing the transverse stiffness. It is also likely that the bearings from Set B are inherently stiffer based on the results of testing performed prior to any observed delamination in the bearings from Set A. Specifically the results of testing performed at a displacement amplitude of $1.0t_r$ prior to an axial load of 90 kN. These results show the same trend of higher effective stiffness in the bearings from Set B. The effective stiffness is between 16% and 30% greater on average in bearings from Set B. The greatest difference between the two sets of bearings occurs at the highest axial loads and the largest lateral displacements tested. Despite this fact, the effective stiffness of each cycle of testing fits within 15% of the mean effective stiffness taken between all five bearings. Although the adequacy check performed in Chapter 3 does not apply directly to this testing procedure it is worth noting that the effective stiffness stays within a reasonable range of the mean for all five ¼ scale SU-FREI bearings tested in this study. It should also be noted that despite this difference in effective stiffness there is still a 95% confidence that the buckling load will fall on the mean taken over all five samples.

Variations in the effective damping values between the two sets are less than variations in effective stiffness values. All five bearings subjected to the dynamic buckling test procedure experienced a substantial increase in effective damping with increasing axial load. The effective damping versus the axial load is compared in Figure 4.15, Figure 4.16, and Figure 4.17 for each amplitude of lateral displacement. The corresponding effective damping values are provided in Table 4.5 to Table 4.9 for each bearing. The effective damping of all five bearings is consistent up to an axial load of 60 kN for amplitudes of $1.0t_r$ and $1.5t_r$ and an axial load of 30 kN for an amplitude of $2.0t_r$. At an amplitude of $1.0t_r$ the SU-FREI bearings underwent an average increase in effective damping of 11% to 16% as the axial load increased from 7.8 kN to 60 kN. Under the same range of axial loads and a lateral excitation amplitude of $1.5t_r$ bearings displayed an increase in effective damping from 11% to 17%. Finally under axial loads from 7.8 kN to 30 kN and lateral displacement amplitude of $2.0t_r$ SU-FREI bearings show an average increase from 10% to 13% effective damping. Effective damping between the two sets of bearings is within 10% of each other during these load-displacement combinations.

Differences between Set A and Set B become more pronounced under the highest axial loads and lateral displacements. At the highest axial load tested, the average effective damping measured in bearings from Set A is 25% and 37% for excitation amplitudes of $1.0t_r$ and $1.5t_r$ respectively. Comparatively, the measured effective damping in bearings from Set B was 21% at $1.0t_r$ and 25% at $1.5t_r$. Furthermore, at an axial load of 60 kN and lateral displacement amplitude of $2.0t_r$ the average effective damping is 27% in Set A and 19% in Set B. At the highest axial loads and largest lateral displacements, bearings from Set A achieve greater effective damping than those from Set B. It is postulated that the additional damping achieved by bearings in Set A is caused by the delamination that led to reduced effective stiffness. Under the highest axial load and lateral displacement tested, the bond between the rubber layers and the adjacent layers of fiber reinforcement in each bearing are subjected to the highest levels of shear stress. It is plausible that any delaminated sections in a bearing from Set A would add to the total damping due to slipping of delaminated rubber against adjacent carbon fiber layers. In order for slip to occur the frictional forces between the two layers needs to be overcome.

4.4 Rollout Tests

Rollout is defined by ISO 22762 as the instability of a dowelled or recessed bearing under shear displacement. SU-FREIs are designed to undergo stable behaviour as they rollover, however, at extreme lateral displacement it is possible that rollout instability may occur. Ultimate shear property testing was performed on two ¼ scale SU-FREI bearings which had undergone previous testing at mid-range lateral displacements under design axial load. This test was performed as an additional investigation of the stability of SU-FREI bearings. It was expected that these bearings would not fail due to instability under the design axial load at previously investigated lateral displacement amplitudes. These tests were used to investigate the performance of bearings at extreme lateral displacements. Two displacements were selected and one bearing was tested at each displacement.

The performance of bearings subjected to rollout testing was evaluated by inspecting the recorded lateral force-displacement curve. In a typical test the axial load is held constant while the sample is displaced laterally at a constant rate until failure occurs in the bearing. Failure in this test is typically defined as either buckling or breaking of the bearing. The onset of buckling occurs when a bearing experiences a lateral stiffness of zero. At this point the bearing has lost its force resisting capacity. The objective of the buckling test is to determine the lateral displacement value a bearing will fail under design axial load (δ_{max}).

4.5 Results of Rollout Tests

The lateral force-displacement curve for rollout tests performed on ¼ scale SU-FREI bearings MB2-2 and MB2-3 are provided in Figure 4.18. MB2-2 was displaced to 2.75t_r (≈ 52 mm) while bearing MB2-3 was displaced to 3.00t_r (≈ 57 mm). The lateral force-displacement curves show negligible variation between the two bearings and positive force resisting capacity throughout the test (See Figure 4.19). Rollout instability was not observed during either test. At approximately 2.75t_r the tangential stiffness begins a decreasing trend which may lead to instability upon further displacement. Unfortunately no remaining suitable ¼ scale SU-FREI bearing samples were available to perform a test at a lateral displacement greater than 3.0t_r. Although rollout instability was not observed during these tests, the results provide a shear profile showcasing the three stages of rollover experienced by SU-FREI and how the lateral effective stiffness is affected.

Lateral effective stiffness versus lateral displacement is provided in Figure 4.20. Similar to what has been discussed previously concerning rollover deformation, the effective stiffness decreases substantially as the SU-FREI bearing is displaced laterally. Facial contact between the vertical faces of the bearing perpendicular to the direction of excitation and the upper and lower boundaries began at $\delta_{ic} \approx 1.7t_r$ (33 mm). This corresponds to the location of the minimum effective stiffness measured in either bearing (≈ 78 N/mm). As the vertical faces make further contact the effective stiffness increases until full contact is made. This displacement is denoted as δ_{fc} and is observed at approximately 2.5t_r (47 mm). Once full facial contact is made the additional effective stiffness has been fully developed. For lateral displacements greater than δ_{fc}, the effective stiffness is constant in both SU-FREI bearings tested. An increase of approximately 20% was observed in the effective stiffness of each bearing following full contact of the vertical faces compared to the minimum effective stiffness measured at δ_{ic}.

Upon completion of rollout testing, both bearings were inspected for signs of damage or delamination. Bearing MB2-3 exhibited minor delamination as illustrated in Figure 4.21. Both of these displacements represent conditions in excess of maximum expected lateral displacements encountered by an SU-FREI bearing. Rollout instability lateral displacement (δ_{max}) was not encountered at displacements up to 3.0 t_r.

4.6 Summary and Concluding Remarks

This chapter has provided a thorough investigation into the stability of SU-FREI bearings. Two test procedures were utilized to explore stability under different conditions. The first method, the dynamic buckling test, investigated stability of ¼ scale SU-FREI bearings under sinusoidal lateral excitation and increasing axial load. The second method, the rollout test, investigated the stability of ¼ scale SU-FREI bearings under design axial load and constant lateral displacement rate. The objective of both tests was to determine the conditions under which an SU-FREI bearing will lose stability.

4.6.1 Dynamic Buckling Tests

The dynamic buckling tests subjected ¼ scale SU-FREI bearings to rigorous testing during which delamination was observed in bearings from two of the three manufactured sets. Bearings which experienced delamination achieved lower effective and transverse stiffness while still maintaining both stable and symmetric lateral force-displacement hysteresis. This difference in lateral stiffness did not have significant affect on the critical buckling load of bearings. Bearings that experienced delamination achieved critical buckling loads from 3% to 14% less than those that did not experience delamination. The buckling loads from all five bearings were still within a 95% confidence interval of the mean taken between all five ¼ scale SU-FREI bearings. The bearings from Set A experienced delamination throughout the dynamic buckling test while Set B did not. For this reason critical buckling loads obtained from bearings from Set A are taken as a conservative estimate of the buckling load of SU-FREI bearings under dynamic excitation.

As the axial load is increased the effective stiffness decreases and the effective damping increases. On average, SU-FREI bearings showed a 35% reduction in effective stiffness when the axial load was increased from 7.8 kN to 90 kN. Lower effective stiffness (16% to 30%) was observed in SU-FREI bearings which experienced delamination. Under the same range of axial loads the effective damping doubled in most SU-FREI bearings. At amplitudes of 1.5t_r and

2.0t_r SU-FREI bearings that underwent delamination achieved more than three times the effective damping at the highest axial load. Both effective stiffness and effective damping showed the most variation while SU-FREI bearings were subjected to the highest axial loads and largest lateral displacements. In general delamination led to lower effective stiffness and higher effective damping.

Under dynamic excitation the critical buckling load was greater at lower amplitudes of lateral displacement. At lateral displacement amplitude of 0.5t_r there were no signs of instability during testing up to axial loads equal to 15 times the design load. Testing performed on ¼ scale SU-FREI bearings from Set A at lateral displacement amplitudes of 1.0t_r, 1.5t_r and 2.0t_r yielded critical buckling loads of approximately 11, 10, and 8 times the design axial load respectively. Predicting the critical buckling load of SU-FREI bearings under dynamic excitation between amplitudes of 1.0t_r to 2.0t_r is essential for estimating the critical load at the estimated displacement of the isolation layer under DBE and MCE conditions. The critical axial load for the full scale isolation system at the design (D_D) and maximum (D_M) displacements of the isolation layer were approximately 10.6 and 8.2 times the design axial load respectively. Under dynamic excitation SU-FREI bearings are extremely resistant to buckling instability. At the largest displacement tested, the critical load is well in excess of axial loads expected to be encountered by any individual SU-FREI bearings.

4.6.2 Rollout Tests

Rollout testing was performed on ¼ scale SU-FREI bearings up to lateral displacements on 2.75t_r and 3.0t_r. Both of the SU-FREI bearings maintained positive lateral stiffness throughout rollout testing. Negligible delamination was observed at a displacement of 3.0t_r. Otherwise no outward signs of damage were apparent upon completion of rollout testing in either bearing. Under the design axial load SU-FREI bearings are more than adequate at maintaining stability at extreme lateral displacements. An added benefit of the unbonded boundary conditions is the additional lateral effective stiffness gained when facial contact is made between the vertical faces of the bearing and the upper and lower boundaries. The effective stiffness reaches a minimum prior to the onset of facial contact. The effective stiffness increases by 20% once full facial contact has been made. Rollout instability was not observed during rollout tests performed up to a lateral displacement of 3.0t_r.

Table 4.1 Test history of bearings tested under the dynamic buckling test program.

Amplitude (% tr)	MB1-3		MB2-1		MB2-4		MB3-2		MB3-3	
	Test No.	Axial Load (kN)	Test No.	Axial Load (kN)	Test No.	Axial Load (kN)	Test No.	Axial Load (kN)	Test No.	Axial Load (kN)
50	1	*7.84*	-	-	-	-	-	-	-	-
	2	*30*	-	-	-	-	-	-	-	-
	3	*60*	-	-	-	-	-	-	-	-
	4	*90*	-	-	-	-	-	-	-	-
	5	*120*	-	-	-	-	-	-	-	-
100	6	*7.84*	*1*	*7.84*	*1*	*7.84*	*1*	*7.84*	*1*	*7.84*
	7	*30*	*2*	*30*	*2*	*30*	*2*	*30*	*2*	*30*
	8	*60*	*3*	*60*	*3*	*60*	*3*	*60*	*3*	*60*
	9	90	4	90	4	90	4	90	4	90
150	10	*7.84*	5	*7.84*	5	*7.84*	5	*7.84*	5	*7.84*
	11	*30*	*6*	*30*	*6*	*30*	*6*	*30*	*6*	*30*
	12	*60*	*7*	*60*	*7*	*60*	*7*	*60*	*7*	*60*
	13	90	8	90	8	90	8	90	8	90
200	14	*7.84*	9	*7.84*	9	*7.84*	9	*7.84*	9	*7.84*
	15	*30*	10	*30*	10	*30*	10	*30*	10	*30*
	16	*60*	11	*60*	11	*60*	11	*60*	11	*60*
	17	75	12	75	-	-	12	75	12	75

Table 4.2 Backbone-curve parameters for bearing MB1-3

Amplitude	Axial Load (kN)	Curve Parameters				
		b0	b1	b2	b3	b4
0.5tr	7.84	1.25E-01	1.25E-04	1.77E-04	-1.62E-06	-1.70E-06
	30	1.00E-01	1.06E-04	3.29E-04	-1.37E-06	-1.65E-06
	60	7.19E-02	1.16E-04	4.77E-04	-1.50E-06	-2.22E-06
	90	4.81E-02	1.23E-04	6.68E-04	-1.58E-06	-3.76E-06
	120	4.84E-02	1.02E-04	3.16E-04	-1.31E-06	-1.37E-06
1.0tr	7.84	1.01E-01	5.42E-06	-1.48E-04	-1.73E-08	2.54E-07
	30	6.94E-02	8.26E-06	-2.69E-05	-2.64E-08	1.07E-07
	60	3.13E-02	8.87E-06	1.08E-04	-2.83E-08	-4.71E-08
	90	1.04E-03	1.73E-05	2.17E-04	-5.50E-08	-2.05E-07
1.5tr	7.84	8.31E-02	6.14E-07	-8.58E-05	-8.57E-10	7.24E-08
	30	5.66E-02	1.03E-06	-4.53E-05	-1.43E-09	5.65E-08
	60	1.79E-02	2.27E-06	2.57E-05	-3.16E-09	1.64E-08
	90	-1.66E-02	4.10E-06	7.04E-05	-5.68E-09	-7.69E-09
2.0tr	7.84	7.41E-02	1.66E-07	-6.89E-05	-1.30E-10	3.98E-08
	30	4.69E-02	4.07E-07	-4.66E-05	-3.19E-10	3.29E-08
	60	1.65E-03	1.93E-06	1.41E-06	-1.51E-09	1.64E-08
	75	-2.51E-02	3.60E-06	2.65E-05	-2.79E-09	8.12E-09

Table 4.3 Transverse stiffness values for each test performed on SU-FREI bearings MB1-3, MB2-1, MBs-4, MB3-2, and MB3-3.

Excitation Amplitude	Axial Load (kN)	Transverse Stiffness (N/mm)				
		Set A			Set B	
		MB1-3	MB2-1	MB2-4	MB3-2	MB3-3
1.0tr	7.84	100.7	112.1	109.9	123.3	113.5
	30	69.4	82.0	78.3	90.6	89.6
	60	31.3	35.5	33.3	43.5	43.8
	90	1.0	-2.8	-5.9	-2.3	1.3
1.5tr	7.84	83.1	86.3	84.9	96.3	92.6
	30	56.6	61.9	58.2	71.8	71.8
	60	17.9	19.7	15.3	30.5	31.6
	90	-16.6	-26.0	-30.6	-12.0	-10.4
2.0tr	7.84	74.1	79.5	75.8	86.2	83.3
	30	46.9	55.0	49.5	65.4	65.1
	60	1.6	6.2	-2.8	21.0	24.9
	75	-25.1	-19.7	-	-	-

Table 4.4 Critical dynamic buckling loads of each SU-FREI bearing. *Values obtained through linear extrapolation using data from 30 kN and 60 kN tests.

Amplitude	Critical Load (kN)				
	Set A			Set B	
	MB1-3	MB2-1	MB2-4	MB3-2	MB3-3
1.0tr	91.8	88.2	85.4	89.6	92.2
1.5tr	74.7	72.7	69.8	81.5	82.4
2.0tr	62.1	63.8	59.7	74*	79*

Table 4.5 Effective stiffness and effective damping from dynamic buckling tests on bearing MB1-3

Axial Load (kN)	Cycle	0.5tr Effective Stiffness (N/mm)	0.5tr Effective Damping (%)	1.0tr Effective Stiffness (N/mm)	1.0tr Effective Damping (%)	1.5tr Effective Stiffness (N/mm)	1.5tr Effective Damping (%)	2.0 tr Effective Stiffness (N/mm)	2.0 tr Effective Damping (%)
7.84	1	137.4	12.3	84.0	11.7	64.3	11.6	62.8	11.4
	2	129.0	11.2	80.7	10.5	61.9	10.5	59.8	10.5
30	1	124.3	13.0	77.8	13.1	61.0	14.0	54.1	15.5
	2	116.6	12.5	73.8	12.8	58.0	13.5	49.7	15.5
60	1	106.5	16.1	70.2	16.7	56.9	18.1	46.5	24.5
	2	95.4	15.5	64.0	16.7	50.2	19.5	39.6	28.8
75	1	-	-	-	-	-	-	38.5	37.4
	2							33.8	45.0
90	1	90.9	18.2	62.4	22.0	45.1	30.8	-	-
	2	75.3	18.3	52.1	24.5	35.9	40.4		
120	1	84.1	18.2	-	-	-	-	-	-
	2	61.9	19.1						

Table 4.6 Effective stiffness and effective damping from dynamic buckling tests on bearing MB2-1

Axial Load (kN)	Cycle	1.0tr Effective Stiffness (N/mm)	1.0tr Effective Damping (%)	1.5tr Effective Stiffness (N/mm)	1.5tr Effective Damping (%)	2.0 tr Effective Stiffness (N/mm)	2.0 tr Effective Damping (%)
7.84	1	97.7	12.3	68.2	11.3	68.9	11.3
	2	91.3	10.1	65.5	10.1	65.2	10.0
30	1	89.8	12.7	65.0	13.2	59.1	14.3
	2	85.3	11.6	62.3	12.5	54.9	13.9
60	1	78.9	17.1	60.2	17.9	49.3	24.8
	2	72.8	15.2	54.3	17.9	42.8	28.8
75	1	-	-	-	-	43.0	37.6
	2					38.0	47.2
90	1	63.6	23.6	45.7	32.8	-	-
	2	55.8	23.4	37.1	41.0		

Table 4.7 Effective stiffness and effective damping from dynamic buckling tests on bearing MB2-4

		1.0tr		1.5tr		2.0 tr	
Axial Load (kN)	Cycle	Effective Stiffness (N/mm)	Effective Damping (%)	Effective Stiffness (N/mm)	Effective Damping (%)	Effective Stiffness (N/mm)	Effective Damping (%)
7.84	1	96.2	12.1	66.8	11.0	64.6	10.8
	2	90.0	9.7	64.1	9.9	61.7	9.8
30	1	88.5	12.4	64.4	13.1	56.1	14.4
	2	84.1	11.3	61.7	12.3	52.0	14.3
60	1	77.3	16.8	59.6	17.7	47.0	24.9
	2	71.5	14.9	53.5	18.0	39.3	30.5
90	1	61.3	24.2	44.7	33.6	-	-
	2	53.6	24.2	36.8	41.4		

Table 4.8 Effective stiffness and effective damping from dynamic buckling tests on bearing MB3-2

		1.0tr		1.5tr		2.0 tr	
Axial Load (kN)	Cycle	Effective Stiffness (N/mm)	Effective Damping (%)	Effective Stiffness (N/mm)	Effective Damping (%)	Effective Stiffness (N/mm)	Effective Damping (%)
7.84	1	109.6	13.6	80.5	11.8	80.3	10.7
	2	101.8	11.0	76.6	10.4	77.1	9.3
30	1	100.6	13.4	76.9	13.1	71.9	12.9
	2	95.2	12.5	73.7	12.2	67.3	12.1
60	1	89.7	16.9	73.0	16.1	61.2	19.6
	2	82.9	15.4	66.8	15.5	55.1	20.2
90	1	74.8	21.4	60.1	23.1	-	-
	2	66.4	21.0	52.3	25.4		

Table 4.9 Effective stiffness and effective damping from dynamic buckling tests on bearing MB3-3

Axial Load (kN)	Cycle	1.0tr Effective Stiffness (N/mm)	1.0tr Effective Damping (%)	1.5tr Effective Stiffness (N/mm)	1.5tr Effective Damping (%)	2.0 tr Effective Stiffness (N/mm)	2.0 tr Effective Damping (%)
7.84	1	106.6	13.4	78.0	11.6	77.8	10.7
	2	98.9	11.1	74.4	10.3	74.5	9.3
30	1	99.2	13.2	75.5	13.0	71.0	12.8
	2	93.9	12.2	72.0	12.1	65.8	12.1
60	1	88.6	16.7	71.8	16.2	62.9	17.3
	2	82.1	15.1	65.0	15.7	55.2	17.8
90	1	73.6	21.3	59.1	23.9	-	-
	2	65.7	20.5	50.6	26.2		

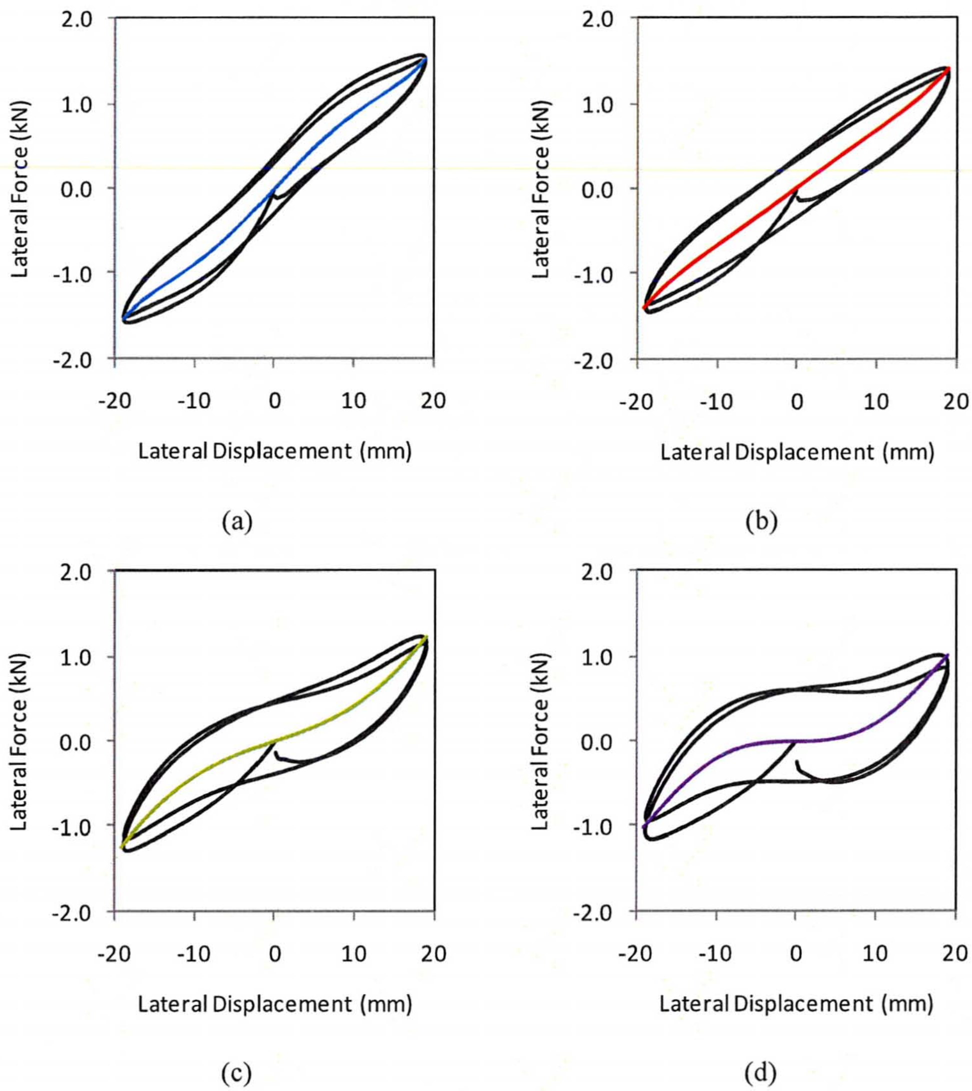

Figure 4.1 Force-displacement hysteresis for bearing MB1-3 at $1.0t_r$ displacement amplitude under axial loads of: (a) 7.84 kN; (b) 30kN, (c) 60kN; (d) 90 kN. Each hysteresis is plotted with its respective fitted curve

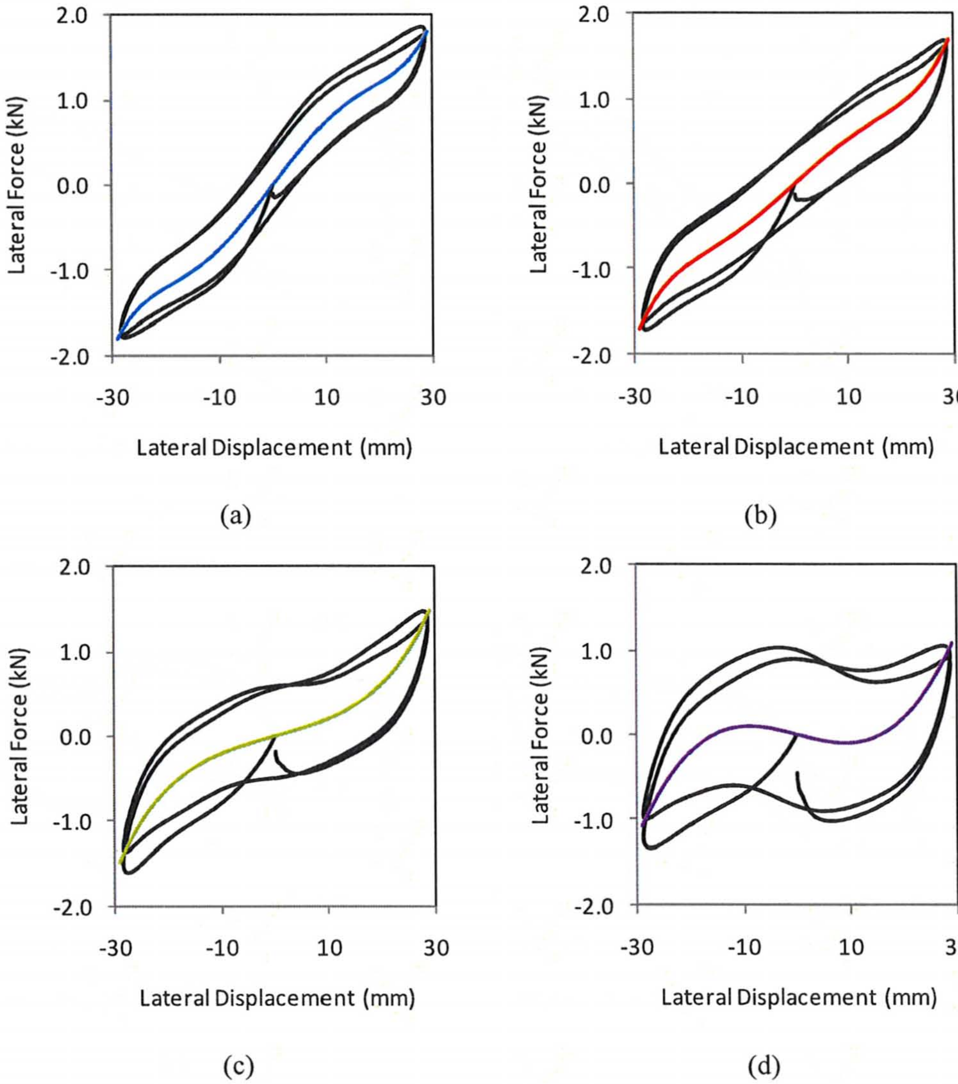

Figure 4.2 Force-displacement hysteresis for bearing MB1-3 at 1.5t_r displacement amplitude under axial loads of: (a) 7.84 kN; (b) 30kN, (c) 60kN; (d) 90 kN. Each hysteresis is plotted with its respective fitted curve

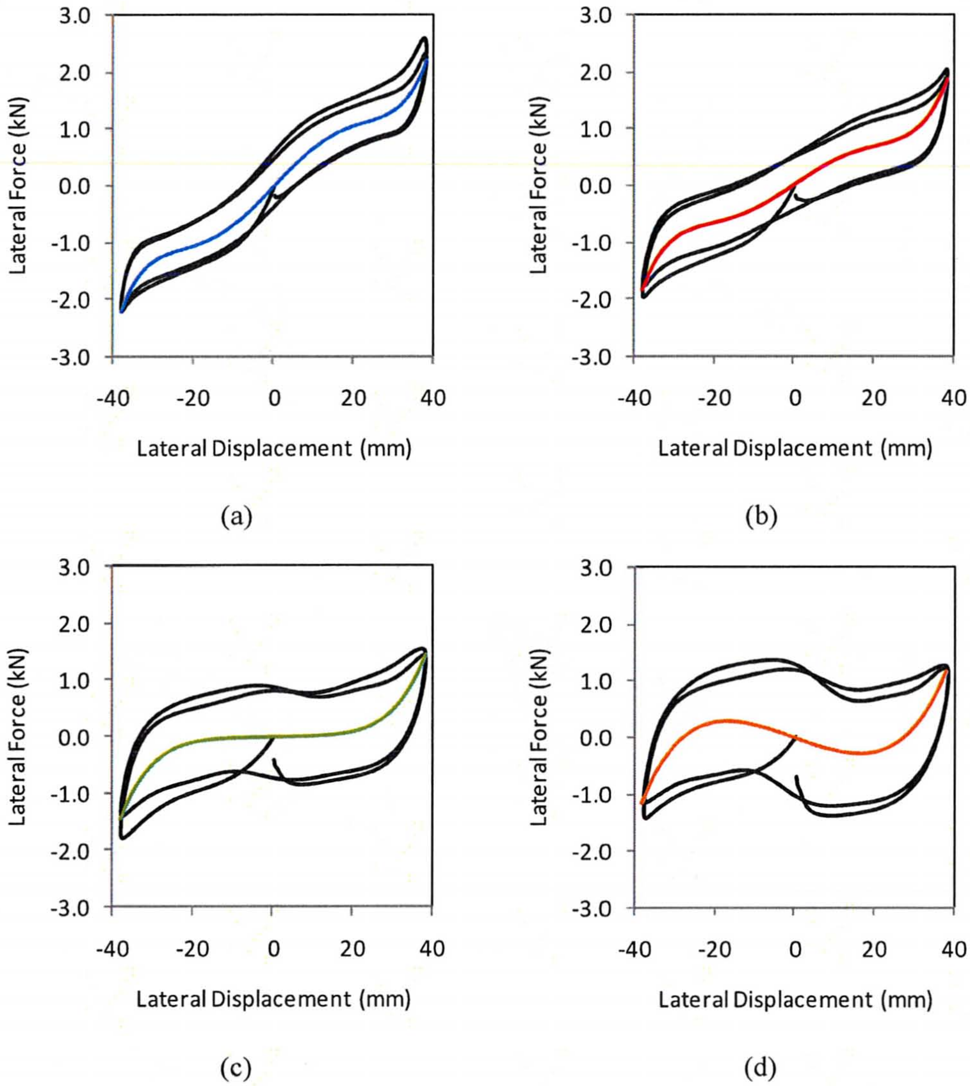

Figure 4.3 Force-displacement hysteresis for bearing MB1-3 at 2.0t_r displacement amplitude under axial loads of: (a) 7.84 kN; (b) 30kN, (c) 60kN; (d) 75 kN. Each hysteresis is plotted with its respective fitted curve

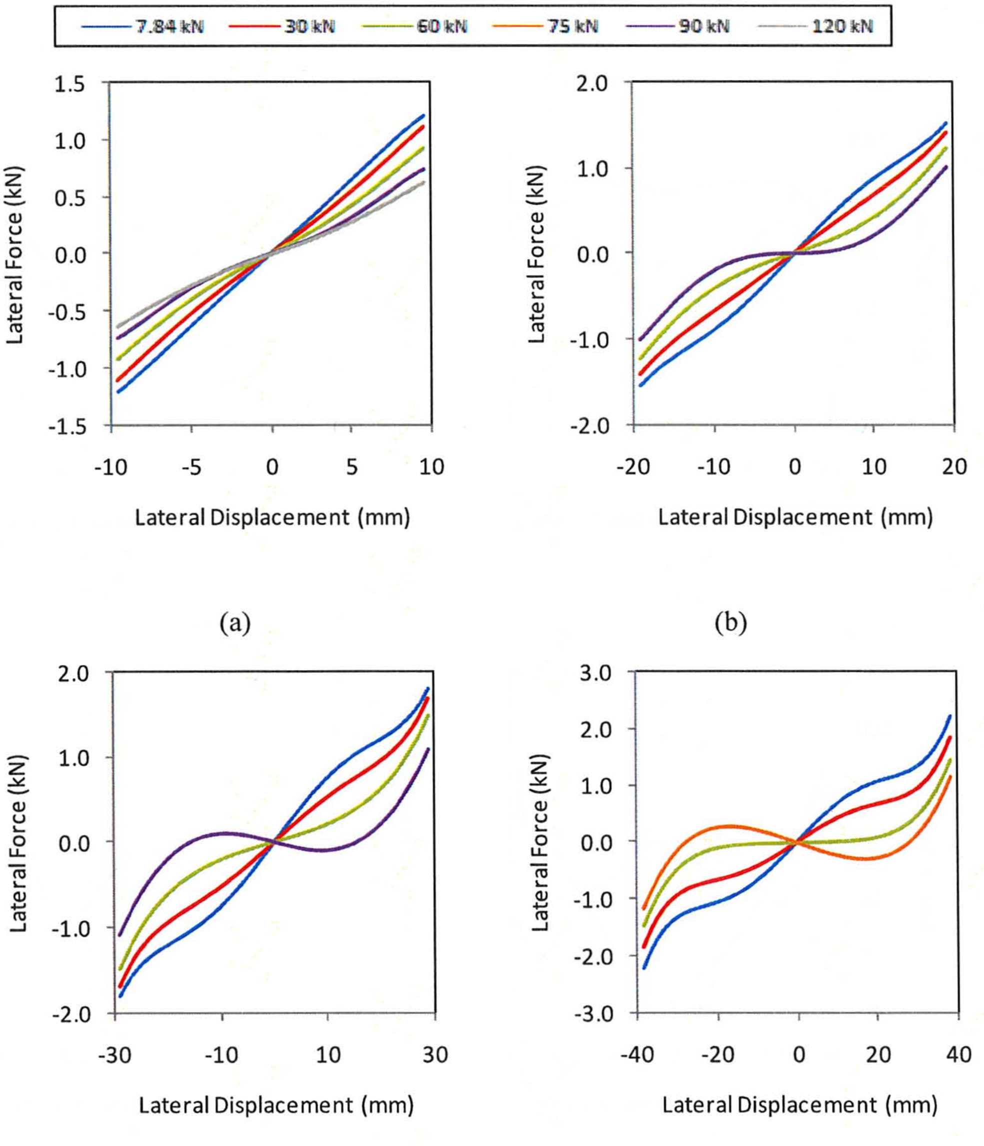

(a) (b)

(c) (d)

Figure 4.4 Backbone curves of force-displacement hysteresis for SU-FREI bearing MB1-3 at displacement amplitudes of: (a) $0.5t_r$; (b) $1.0t_r$; (c) $1.5t_r$; (d) $2.0t_r$

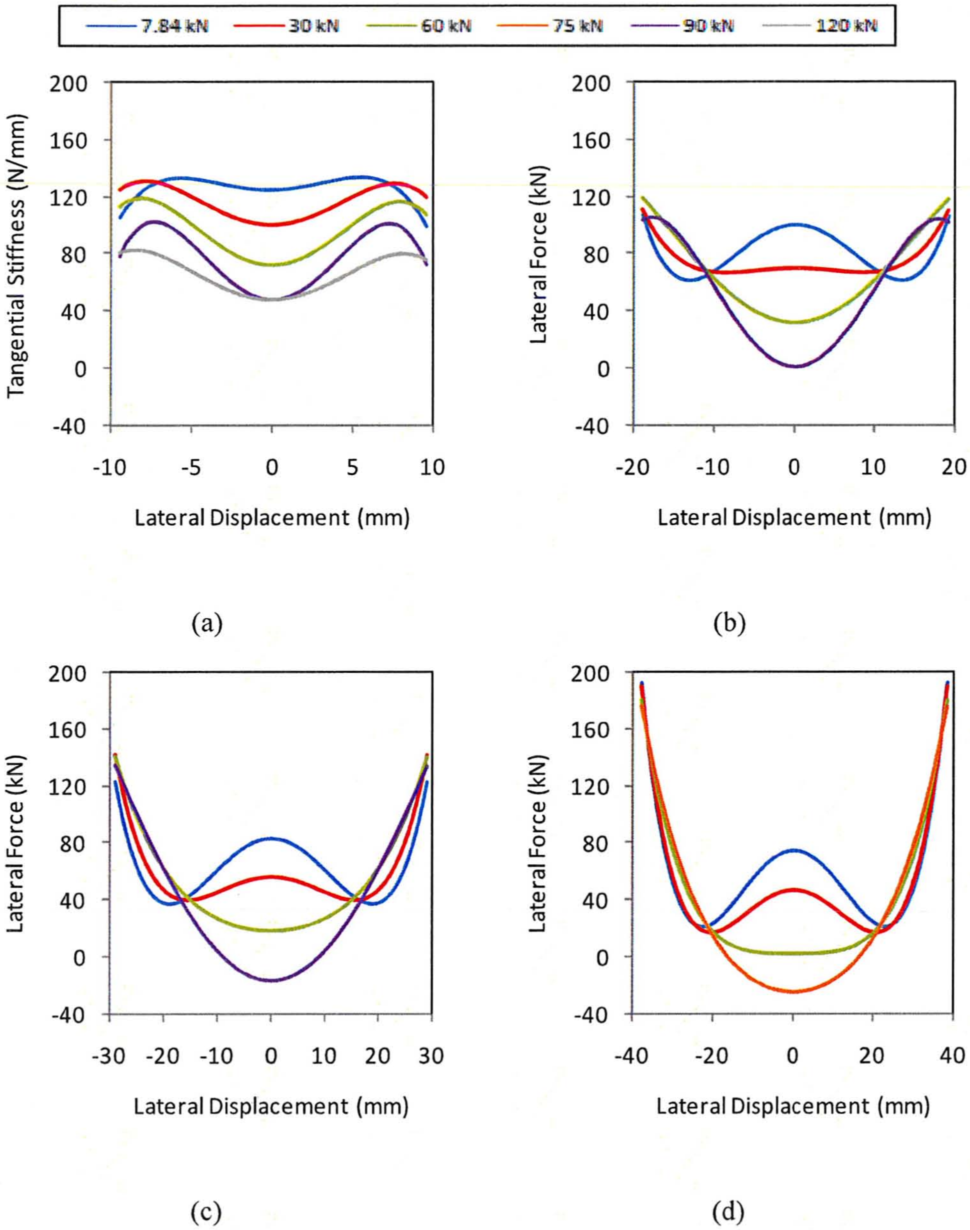

Figure 4.5 Tangential stiffness obtained from the first derivative of the fitted curve from the load displacement hysteresis of SU-FREI bearing MB1-3 at displacement amplitudes of: (a) $0.5t_r$; (b) $1.0t_r$; (c) $1.5t_r$; (d) $2.0t_r$

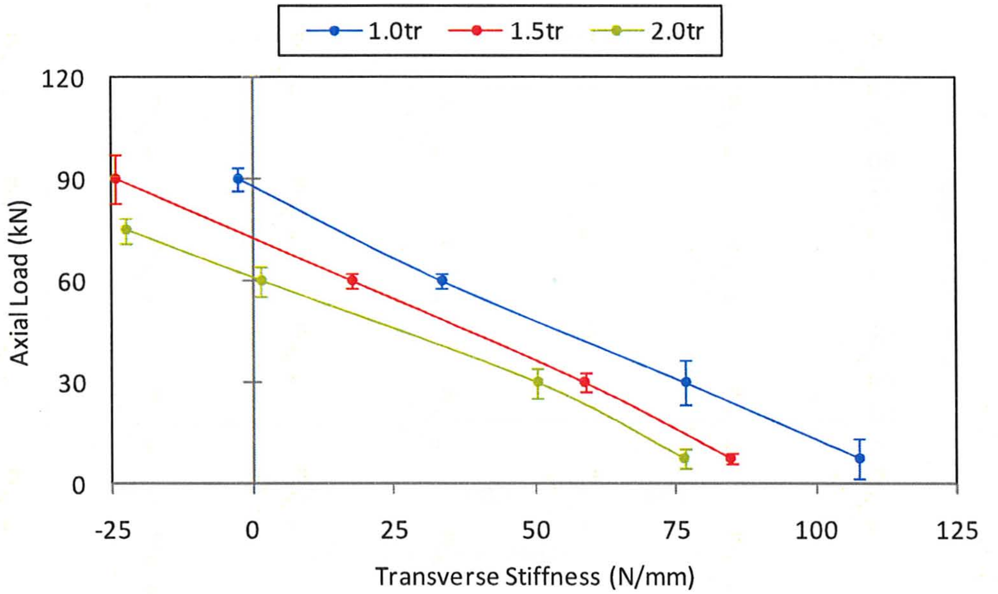

Figure 4.6 Transverse stiffness versus axial load for SU-FREI bearings in Set A: MB1-3, MB2-1, and MB2-4

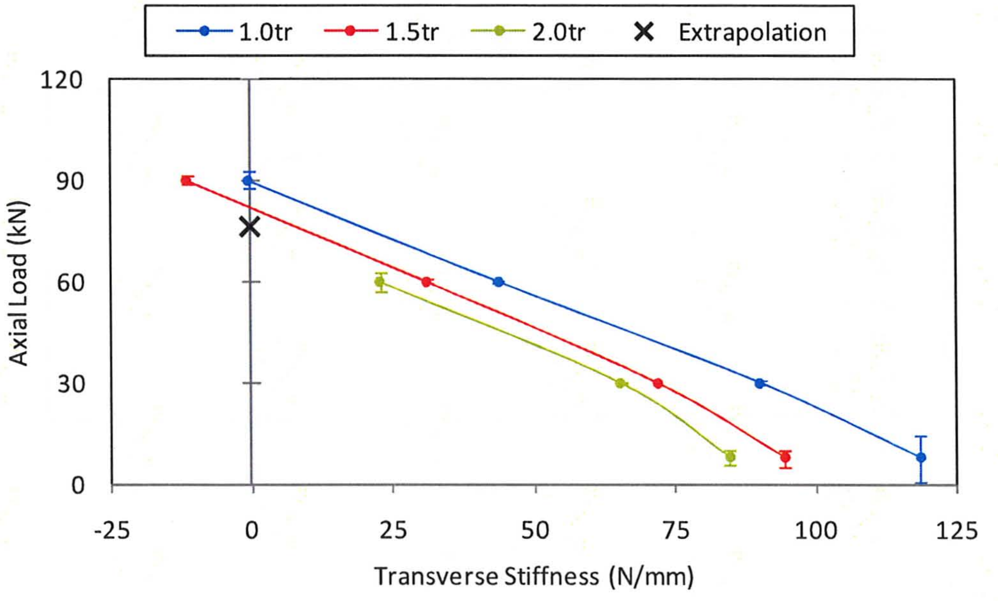

Figure 4.7 Transverse stiffness versus axial load for SU-FREI bearings in Set B: MB3-2 and MB3-3.

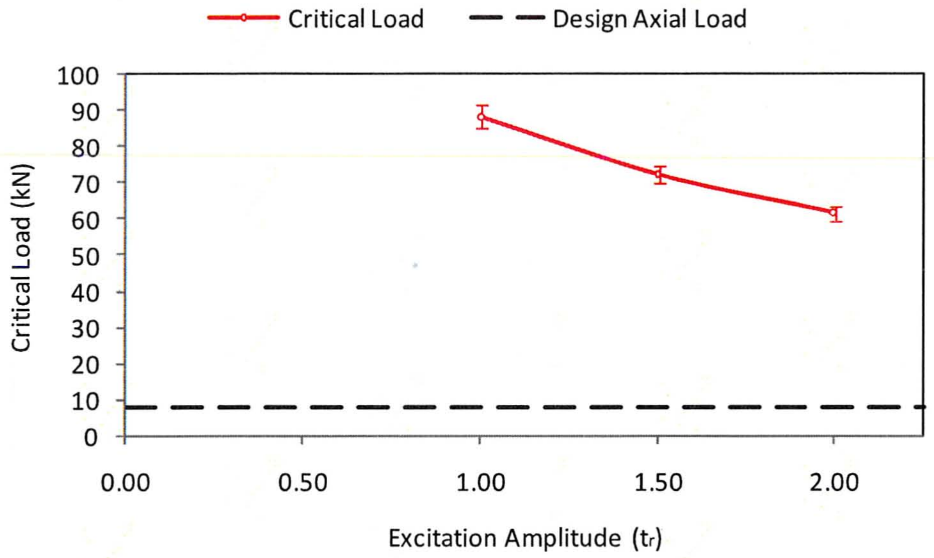

Figure 4.8 Average critical load during dynamic excitation versus excitation amplitude for SU-FREI bearings in Set A: MB1-3, MB2-1 and MB2-4

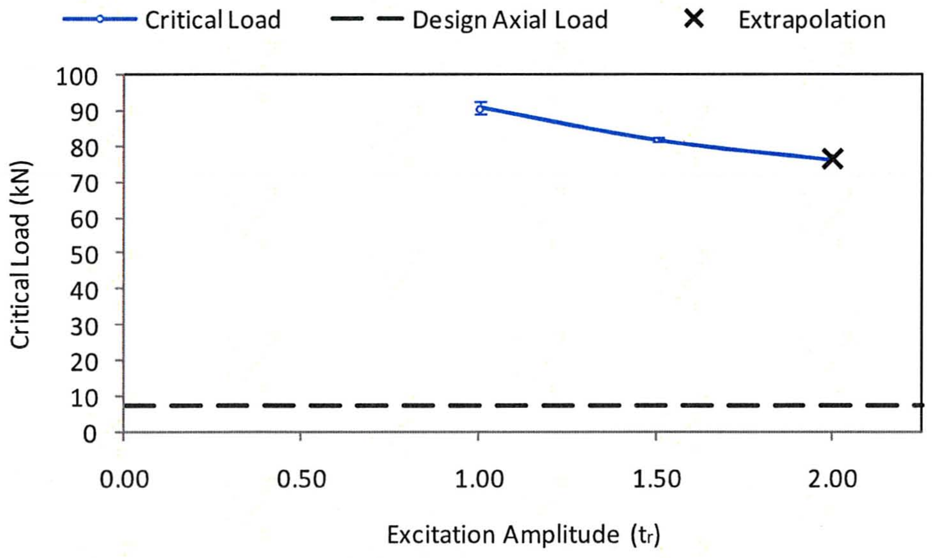

Figure 4.9 Average critical load during dynamic excitation versus excitation amplitude for SU-FREI bearings in Set B: MB3-2 and MB3-3.

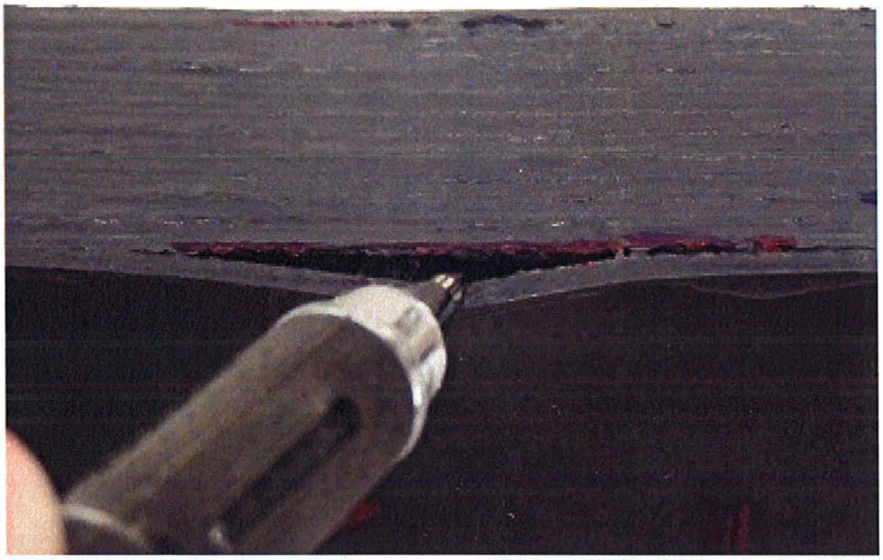

Figure 4.10 Close up of delamination sustained by a ¼ scale SU-FREI bearing during a dynamic buckling test

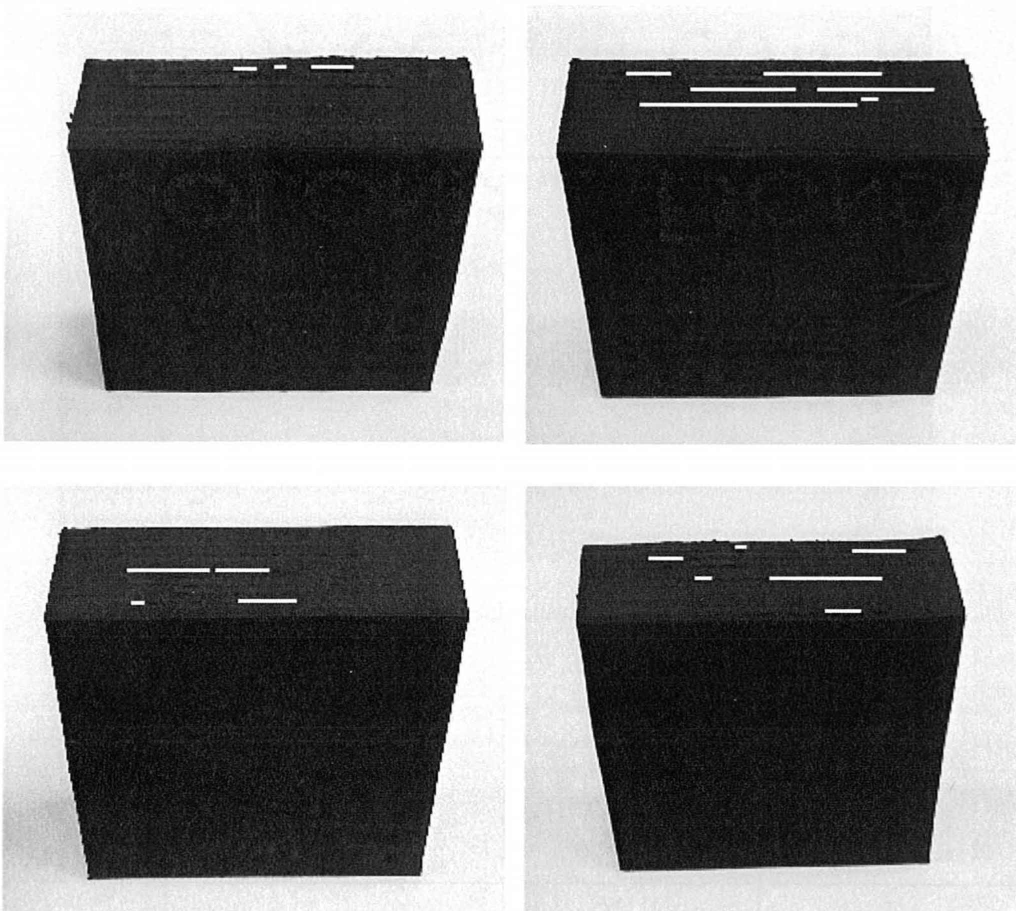

Figure 4.11 Highlighted areas detail where delamination occurred along the edge faces of bearing MB2-4 following the completion of the buckling test history

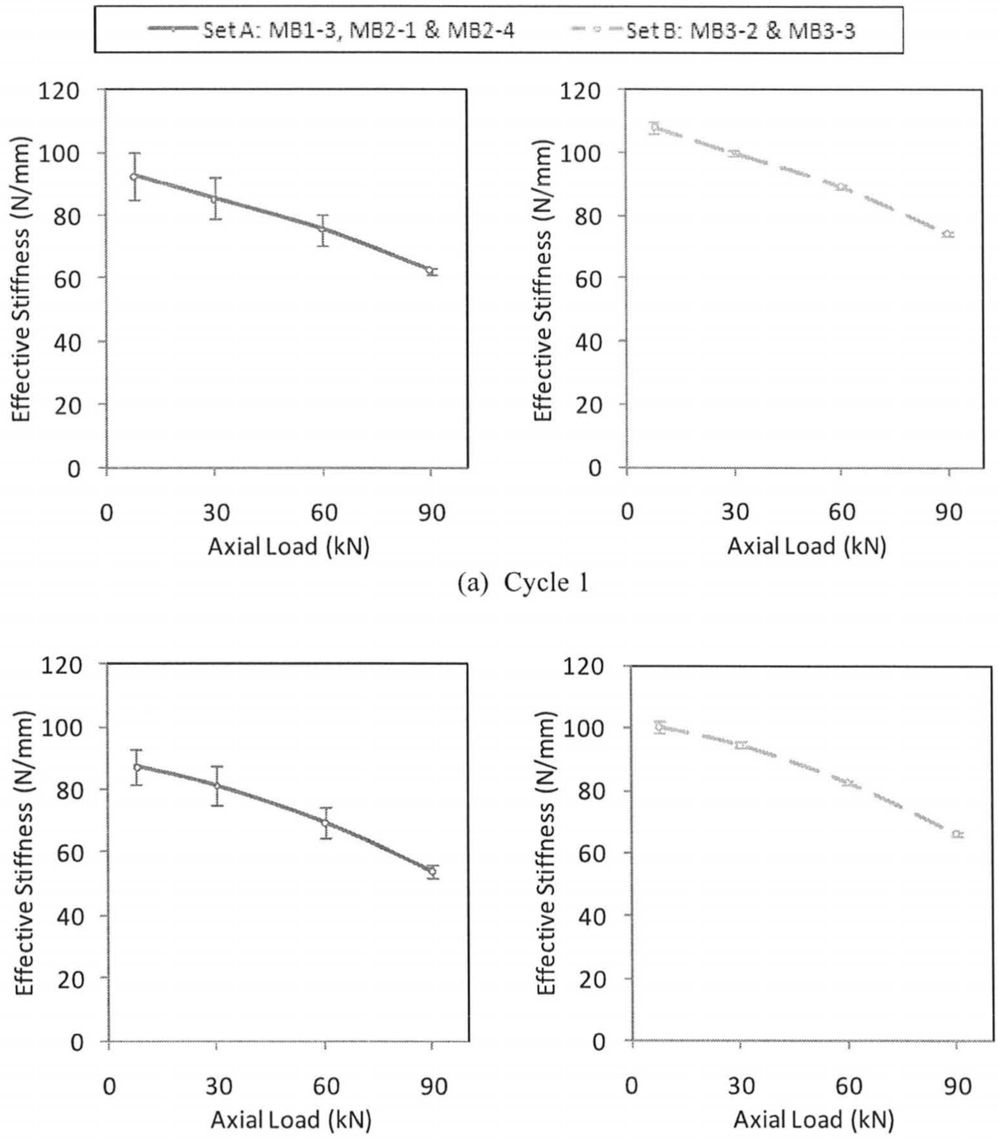

(a) Cycle 1

(b) Cycle 2

Figure 4.12 Average effective stiffness versus axial load for SU-FREI bearings MB1-3, MB2-1 MB2-4, MB3-2, and MB3-3 cycled at lateral excitation of $1.0t_r$

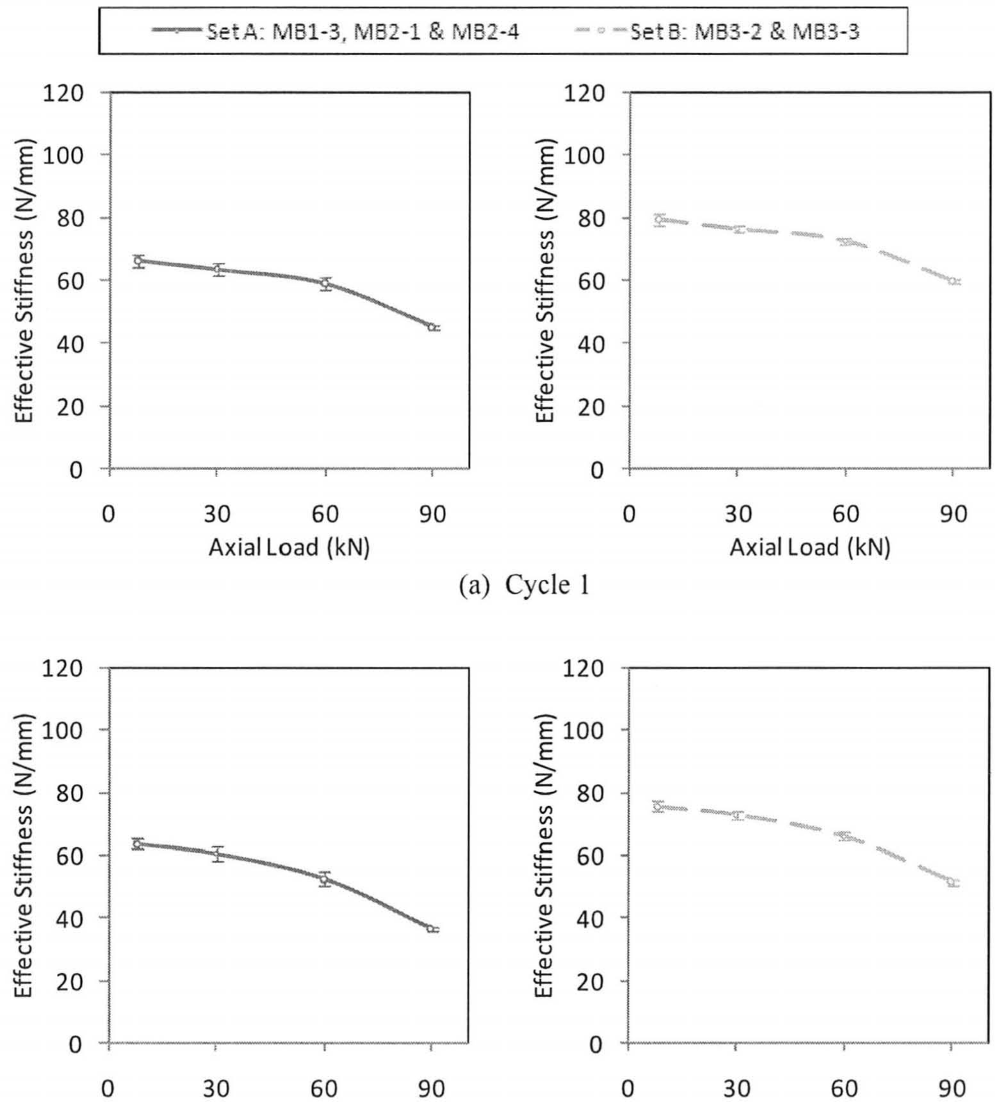

(a) Cycle 1

(b) Cycle 2

Figure 4.13 Average effective stiffness versus axial load for SU-FREI bearings MB1-3, MB2-1 MB2-4, MB3-2, and MB3-3 cycled at lateral excitation of $1.5t_r$

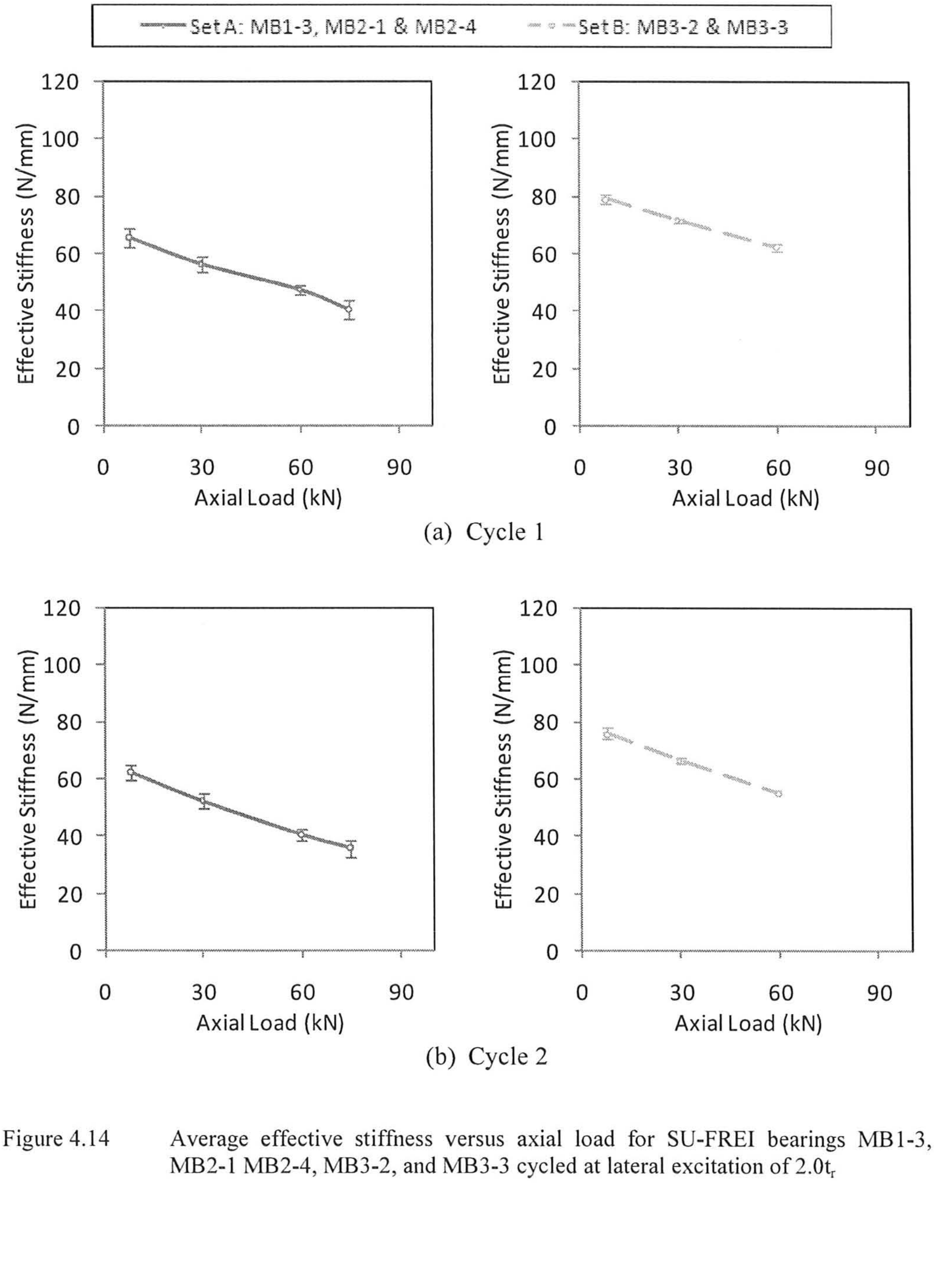

(a) Cycle 1

(b) Cycle 2

Figure 4.14 Average effective stiffness versus axial load for SU-FREI bearings MB1-3, MB2-1 MB2-4, MB3-2, and MB3-3 cycled at lateral excitation of $2.0t_r$

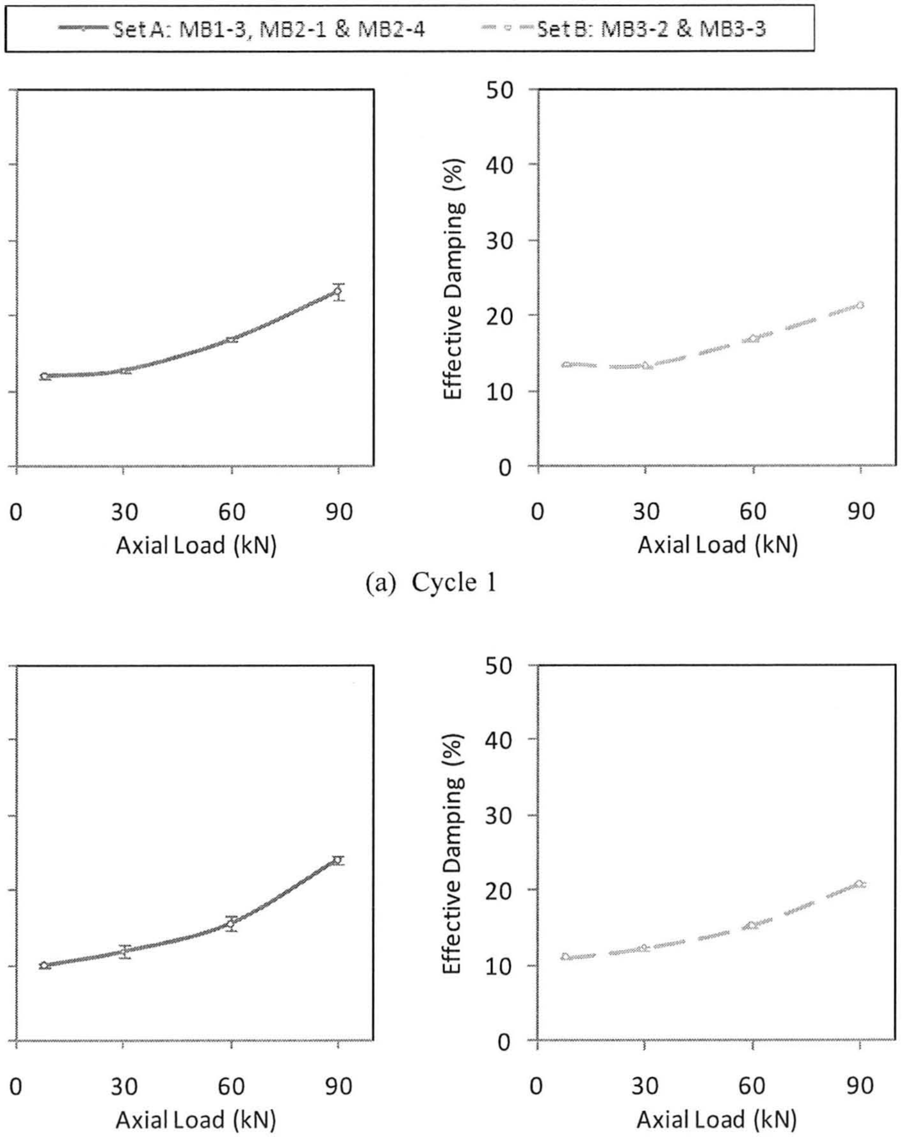

(a) Cycle 1

(b) Cycle 2

Figure 4.15 Average effective damping versus axial load for SU-FREI bearings MB1-3, MB2-1 MB2-4, MB3-2, and MB3-3 cycled at lateral excitation of $1.0t_r$

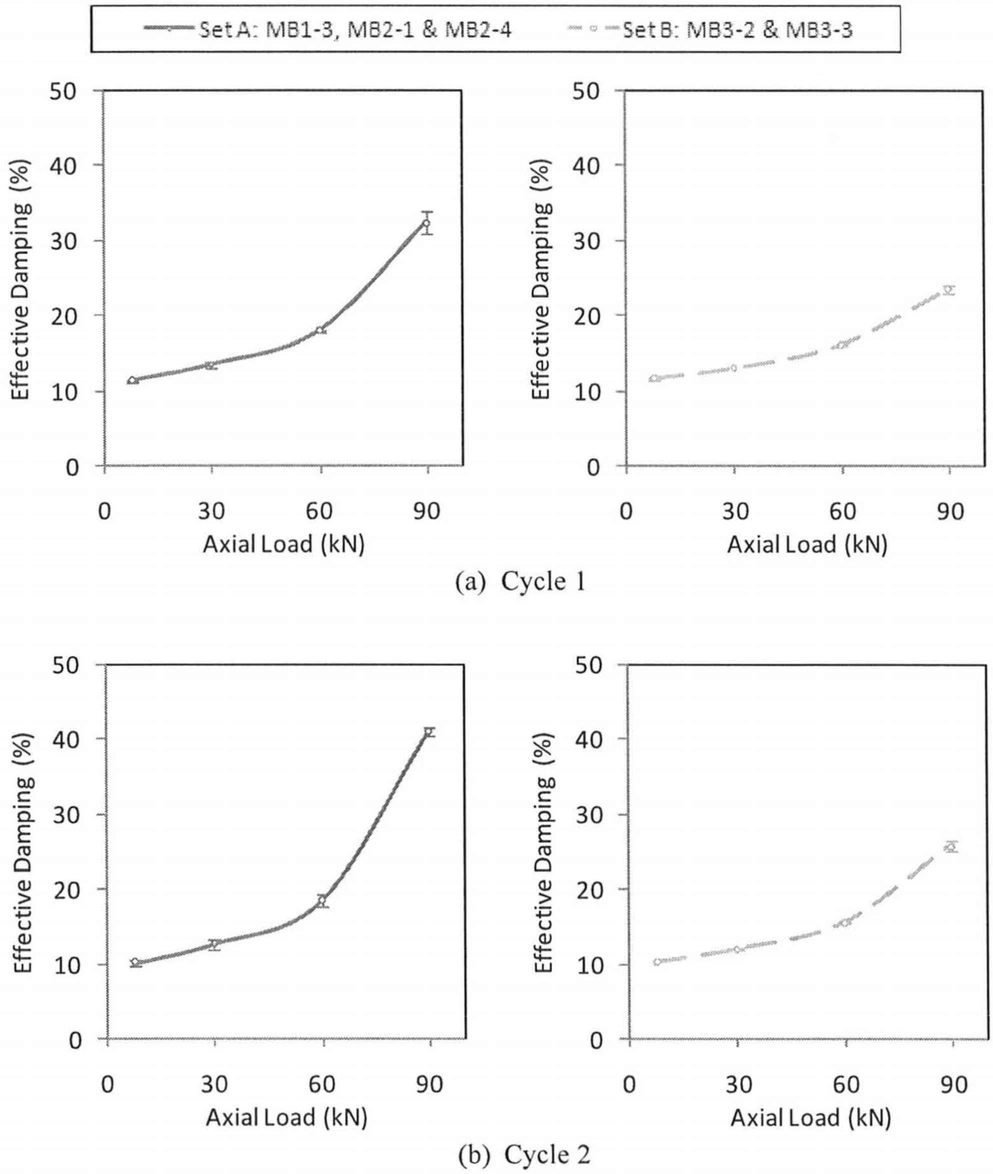

Figure 4.16 Average effective damping versus axial load for SU-FREI bearings MB1-3, MB2-1 MB2-4, MB3-2, and MB3-3 cycled at lateral excitation of $1.5t_r$

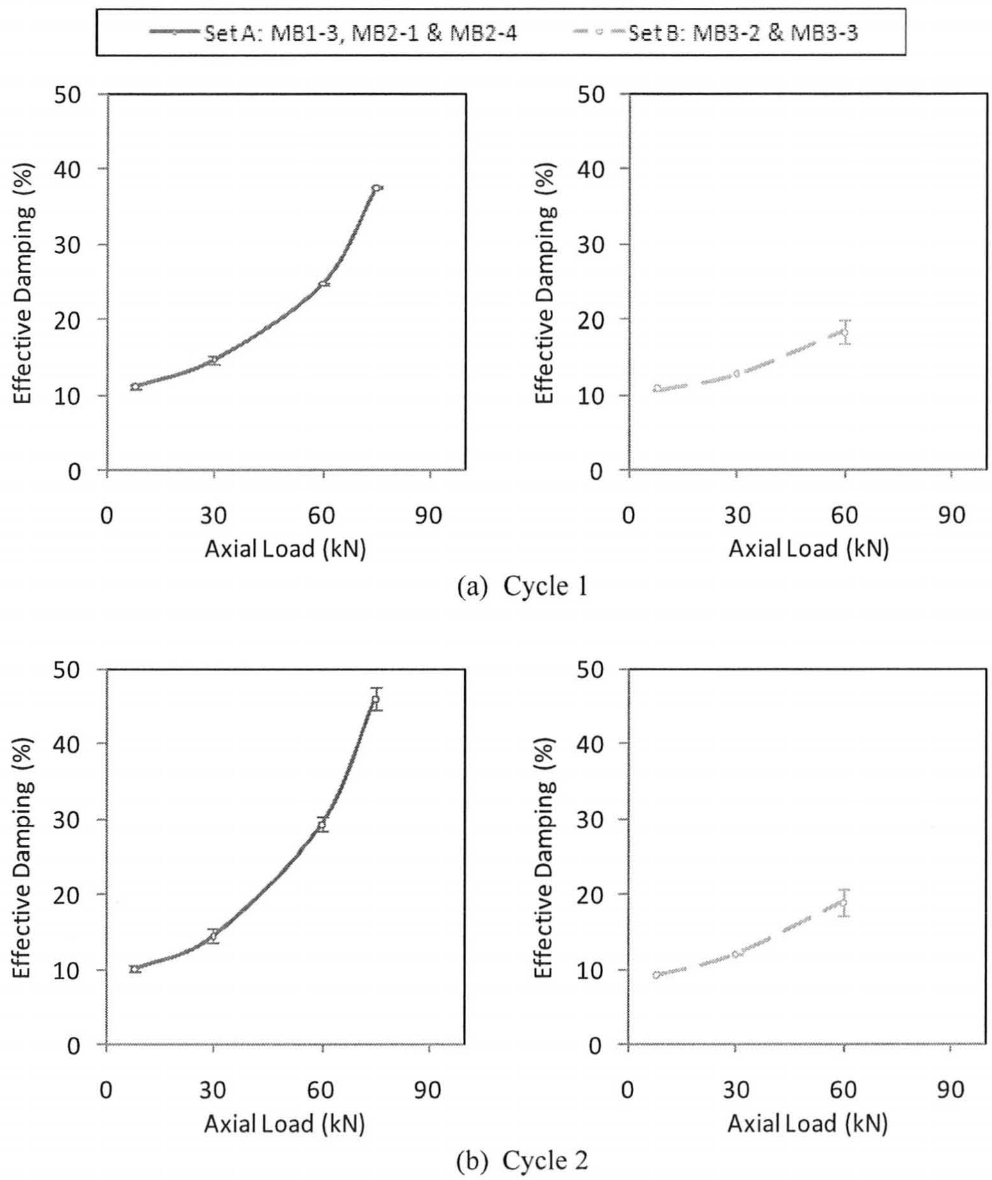

Figure 4.17 Average effective damping versus axial load for SU-FREI bearings MB1-3, MB2-1 MB2-4, MB3-2, and MB3-3 cycled at lateral excitation of $2.0t_r$

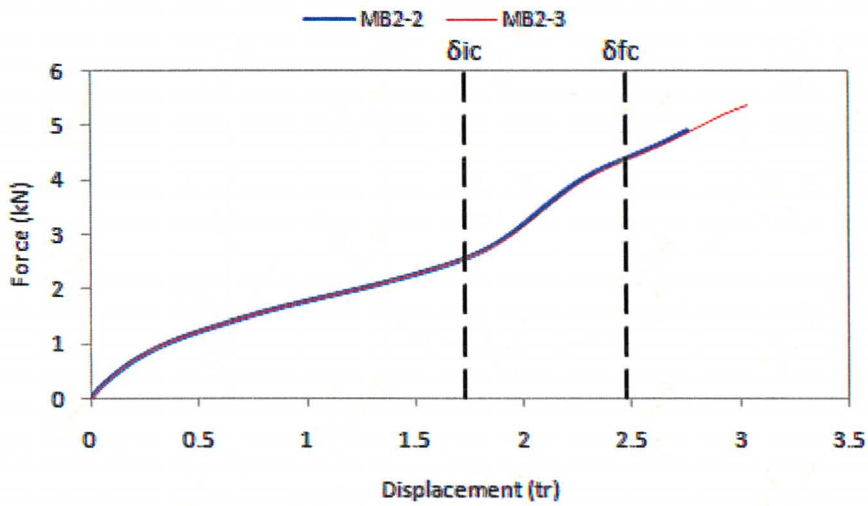

Figure 4.18 Lateral force versus displacement for rollout tests performed on MB2-2 and MB2-3 to maximum displacements of $2.75t_r$ and $3.0t_r$ respectively. The location of initial facial contact of the vertical faces δ_{ic} and full facial contact δ_{fc} are also provided

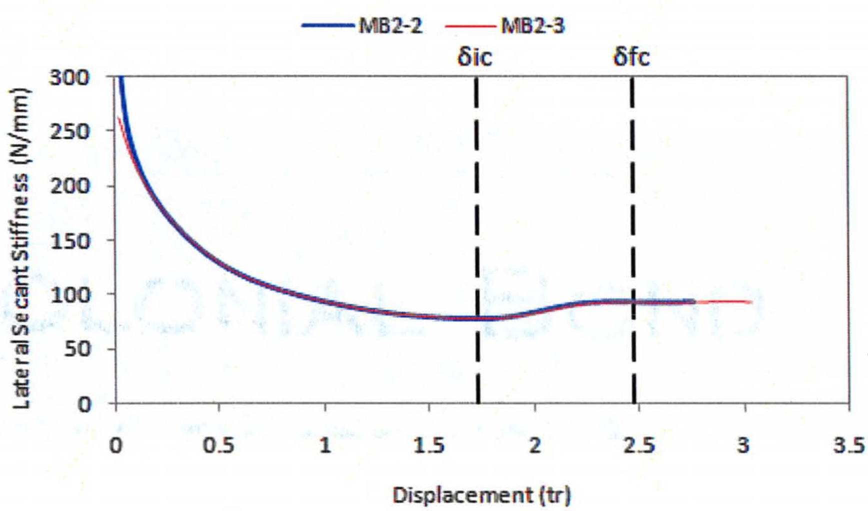

Figure 4.19 Lateral secant stiffness versus displacement for rollout tests performed on MB2-2 and MB2-3 to maximum displacements of $2.75t_r$ and $3.0t_r$ respectively. The location of initial facial contact of the vertical faces δ_{ic} and full facial contact δ_{fc} are also provided

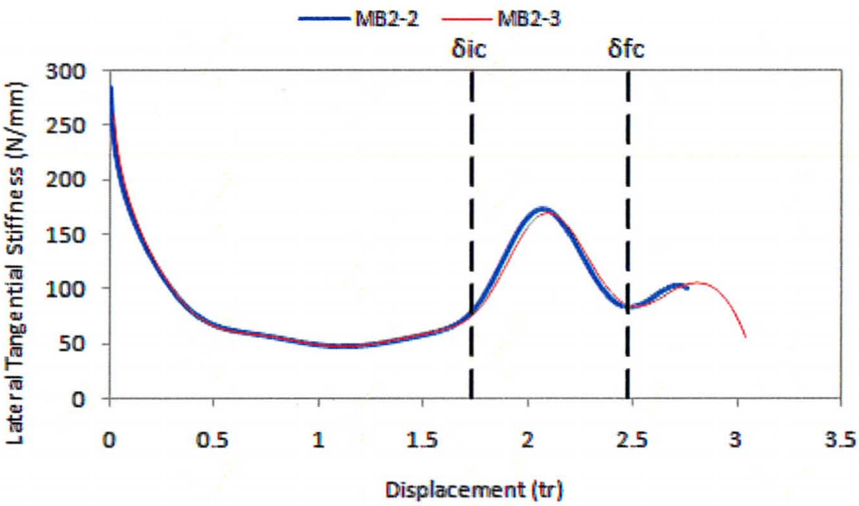

Figure 4.20 Lateral tangential stiffness versus displacement for rollout tests performed on MB2-2 and MB2-3 to maximum displacements of $2.75t_r$ and $3.0t_r$ respectively. The location of initial facial contact of the vertical faces δ_{ic} and full facial contact δ_{fc} are also provided

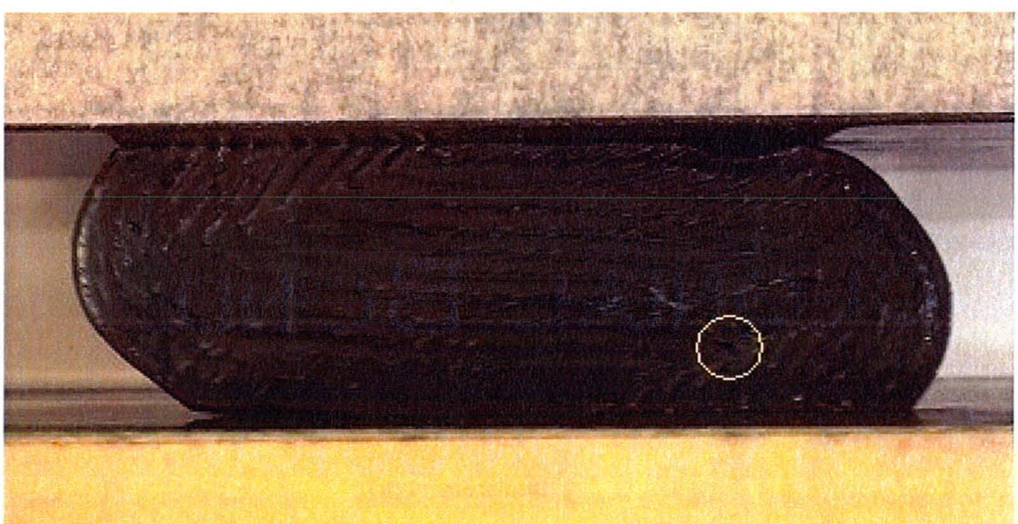

Figure 4.21 Delamination observed in bearing MB2-3 at a lateral displacement of $3.0t_r$

Chapter 5. Serviceability and Fatigue

This chapter outlines serviceability and fatigue tests performed on SU-FREI bearings. Both of these tests involve lateral cyclic testing under constant design axial load. The difference between these tests and previous cyclic tests is the number of fully reversed lateral cycles. Both tests were performed in order to show that SU-FREI bearings are capable of maintaining acceptable performance under serviceability and fatigue conditions.

5.1 Testing Procedure

5.1.1 Serviceability

In order to investigate the performance of SU-FREI bearings under serviceability conditions the design wind force was determined for a typical low-rise structure. An equivalent lateral displacement was estimated based on the design wind force. Two displacements were selected to bracket the expected displacement. Each ¼ scale SU-FREI bearing was subsequently tested at both of these lateral displacement amplitudes in sequence. Since the design wind force is determined using the dimensions and properties of a specific structure, bracketing the estimated lateral deflection under design wind forces allowed for a wider range of study. The objective of this investigation is to show that the dynamic properties of ¼ scale SU-FREIs will become stable under repeated cycling. According to ASCE 7-05, serviceability testing requires that bearings are subjected to 20 fully reversed cycles.

The first step was to estimate an approximate design wind force for a typical structure isolated using SU-FREI bearings. The wind design force was calculated using the provisions from the structural commentaries of the NBCC (2005). Although typical base isolated structures will have a height less than 120 m with a height to width ratio less than 4, they are susceptible to vibrations due to the introduction of the isolation layer. For this reason it is necessary to use the dynamic procedure to estimate design wind load (NRC, 2006). This procedure is typically employed for tall buildings and slender structures. The dimensions and specifications of a two-storey structure used during shake table testing of ¼ scale SU-FREI bearings by Toopchi-Nezhad (2008) were used for the design wind force calculation. The full scale test structure has measurements of 6 m by 5 m at the base with a 6.5 m height. The isolation system for this structure is composed of four bearings with one SU-FREI bearing located at each corner. The total weight of the full scale structure is approximately 502 kN based on the design axial load applied to four full scale SU-FREI bearings.

The design wind pressure p_e was calculated using the following equation from the NBCC (2005):

$$p_e = I_w q C_e C_g C_p \qquad 5.1$$

where I_w is the importance factor for wind which is taken as 1.0 for normal importance for serviceability purposes. The 1 in 10 year return period wind velocity pressure q was taken as 0.36 kPa for Vancouver (NBCC, 2005). A conservative exposure factor of C_e= 1.0 was selected which represents open or standard exposure. The gust factor C_g is a factor of a number of properties including the fundamental frequency and the effective damping of the system. Finally, the external pressure coefficient $C_p$was taken as 1.2. This calculation accounts for an extremely conservative design wind pressure which corresponds to a low-rise isolated structure subjected to wind with no impedance from surrounding geography or neighboring structures. Once the design wind pressure was calculated the corresponding design wind force (F_w) was calculated using

$$F_w = p_e bh \tag{5.2}$$

where b is the longest plan dimension and h is the height of the structure. Additional detail regarding the dynamic procedure used here can be found in Part 4 of Division B (NBCC 2005).

Both the fundamental frequency and the effective damping of the isolation layer were used to determine the design wind pressure. The fundamental frequency (f_n) of the isolated structure was determined using

$$f_n = \frac{1}{2\pi}\sqrt{\frac{K_{eff,T}}{M_T}} \tag{5.3}$$

where $K_{eff,T}$ is the total lateral effective stiffness of an isolation layer composed of 4 full-scale SU-FREI bearings and M_T is the total mass in kg of the structure (≈51,000 kg). The effective stiffness and damping of the isolation layer were determined by fitting a curve to the data obtained through cyclic testing in Chapter 3 using least squares fitting. Assuming that lateral displacement under the design wind load will occur predominantly in the isolation layer, the maximum displacement of the isolation layer (Δ_{max}) under the design wind force was calculated using the following equation:

$$\Delta_{max} = \frac{F_W}{K_{eff,T}} \tag{5.4}$$

Since the effective stiffness and damping of the SU-FREI bearings are dependent on lateral displacement, it was necessary to employ and iterative procedure to determine the maximum displacement. First a displacement was selected and the corresponding effective stiffness and damping of the isolation layer were determined through interpolation of the least squares fit. The design wind force calculated using these values would yield a new maximum displacement which was then used to determine the effective stiffness and damping for the next iteration. This process was repeated until convergence was achieved.

The wind design load was estimated at 39.2 kN for the specified structure located in Vancouver. Under the wind design load the displacement of the isolation layer was calculated as $\approx 0.2t_r$. Based on this result the two displacement amplitudes selected were $0.15t_r$ and $0.35t_r$. Each bearing was subjected to 20 fully reversed cycles at each amplitude in ascending sequence. Due to the low lateral displacement required for these tests it was possible to cycle the bearings at their natural frequency. Bearings were cycled at a frequency of 2.31 Hz and 2.08 Hz at amplitudes of $0.15t_r$ and $0.35t_r$ respectively. The natural frequency at each amplitude was estimated using Equation 5.3 and the results obtained from cyclic testing performed in Chapter 3. In between each test the bearing was removed from the setup and inspected for any signs of damage or delamination.

5.1.2 Fatigue

The fatigue testing procedure from ASCE 7-05 (2005) was used in this study. Similar to the calculations for serviceability testing, the dimensions of the structure used in shake table testing by Toopchi-Nezhad (2008) are used here. The fatigue test requires that each bearing undergoes fully reversed lateral excitation at the total design displacement D_{TD} while the axial design load is held constant. The number of cycles is dictated by the results of the following equation so long as it is no less than 10 cycles.

$$Number\ of\ Cycles = 30\frac{S_{D1}}{S_{DS}B_D} \tag{5.5}$$

these terms were previously defined in Chapter 3. The total design displacement is an amplification of the design displacement D_D described by Equation 3.3. Total design displacement is calculated by

$$D_{TD} = D_D\left[1 + y\frac{12e}{b^2 + d^2}\right] \tag{5.6}$$

where y is the distance from the centre of rigidity to the element of interest perpendicular to the direction of excitation. In this case y is the same for all bearings and is equal to $\approx$ 2.8 m assuming the longest plan dimension is perpendicular to excitation. The terms b and d are the shortest and longest plan dimensions respectively (6.0 m and 5.6 m). The term e describes the actual eccentricity between the centre of rigidity of the isolation system and the structures centre of mass measured perpendicular to the direction of excitation. Since there is no eccentricity, only the accidental eccentricity was used. Accidental eccentricity is defined as 5% of the longest plan dimension. This resulted in e = 0.3 m based on the dimensions of the structure.

The number of cycles calculated using Equation 5.5 resulted in a total of 11.6 cycles which was rounded up to 12. Since the calculated number of cycles was greater than 10 it was suitable for fatigue testing purposes. Using a design displacement of $D_D \approx 88$ mm (calculated in Chapter 3) for SU-FREI bearings at a parallel orientation, the resulting total design displacement becomes $D_{TD} \approx 102$ mm or $1.33t_r$. This was increased to a value of $1.5t_r$ for fatigue testing since these calculations were performed for one specific structure. Each bearing underwent 12 fully reversed cycles of lateral displacement at an amplitude of $1.5t_r$ under constant design axial load. The displacement amplitude used in this test was too large to allow for cycling at the natural frequency of the bearing. For fatigue testing, the average displacement rate of the plate was once again set at ≈ 76 mm/s. Each of the four ¼ scale bearings used for fatigue testing underwent a single fatigue test under these conditions at a parallel orientation.

5.2 Results of Serviceability Testing

Serviceability testing was performed on two ¼ scale SU-FREI bearings (MB2-2 and MB2-3). The resulting force-displacement hystereses were analyzed in a similar manner to cyclic tests performed in Chapters 3 and 4. Effective stiffness and effective damping were calculated using Equation 3.1 and 3.2. From previous discussion on scragging of rubber it is expected that the variation in dynamic properties of these bearings will become negligible after the second or third cycle. Effective stiffness and damping values calculated for each cycle of testing are provided in Table 5.1 for MB2-2 and Table 5.2 for MB2-3. The force-displacement hysteresis loops for these tests are provided in Figure 5.1 for tests at $0.15t_r$ and Figure 5.2 for tests at $0.35t_r$. The first cycle in the force-displacement hysteresis is substantially larger than subsequent cycles, which have minor visible variation. Positive incremental force resisting capacity is maintained throughout each fully reversed cycle satisfying cyclic test requirements of the ASCE (2005)

Effective stiffness is plotted versus cycle number in Figure 5.3. There is negligible difference between the effective stiffness measured in MB2-2 and MB2-3 at both amplitudes. Furthermore, from the 3rd cycle on, the effective stiffness shows negligible degradation with subsequent lateral cycling. At an amplitude of $0.15t_r$ there is a 6% decrease in effective stiffness between the 1st and 3rd cycles. Comparatively, between the 3rd cycle and the 20th cycle the average decrease in effective stiffness is only 4%. At a displacement of $0.35t_r$, both bearings showed a decrease in effective stiffness of 8% between the 1st and 3rd cycles; and 5% between the 3rd and 20th cycles. The average scragged effective stiffness from the 3rd cycle on is: ≈ 189 N/mm at an amplitude of $0.15t_r$; and ≈ 140 N/mm at an amplitude of $0.35t_r$. Effective damping versus cycle number is illustrated in Figure 5.4 for both MB2-2 and MB2-3. The effective damping remains nearly constant throughout all 20 cycles of lateral displacement with less than 5% variation from the mean. The average effective damping is 14% at an amplitude of 0.15 t_r and 12% at an amplitude of $0.35t_r$. The unscragged first cycles had a similar effective damping compared to subsequent cycles during serviceability testing.

5.3 Results of Fatigue Testing

A total of four ¼ scale SU-FREI bearings (MB2-2 MB2-3, MB3-1, and MB3-4) were subjected to the fatigue testing procedure. Each bearing underwent 12 fully reversed cycles of lateral displacement at an amplitude of $1.5t_r$ while constant axial load was applied. All four bearings had previously undergone cyclic testing under constant design axial load. Bearings MB2-2 and MB2-3 were tested previously for serviceability at amplitudes up to $0.35t_r$. Alternatively, bearings MB3-1 and MB3-4 were subjected to cyclic testing at amplitudes exceeding $1.5t_r$ at a diagonal orientation with respect to the direction of excitation. Despite their previous testing histories, all four bearings are expected to exhibit unscragged behaviour in the first cycle of this test. None of the bearings tested here had been cycled at $1.5t_r$ at a parallel orientation prior to this test.

Lateral force-displacement hysteresis loops are provided in Figure 5.5 for bearings from sheet MB2 and Figure 5.6 for bearings from sheet MB3. All four bearings exhibit a larger first cycle while subsequent hysteresis loops fall on top of each other. Bearings MB2-2 and MB2-3 display a slightly larger first loop than the bearings MB3-1 and MB3-4. Differences between the scragged loops of these bearings are not visibly apparent from the force-displacement hysteresis loops. The calculated values of effective stiffness and effective damping for all four bearings are provided in Table 5.3. Effective stiffness versus cycle number is illustrated in Figure 5.7. The effective stiffness from all four bearings is within 5% of the mean effective stiffness at each cycle. The average effective stiffness over the scragged cycles of testing (cycle 2-12) is $\approx$ 69 N/mm for ¼ scale SU-FREI bearings cycled at an amplitude of $1.5t_r$. This result is consistent with the average effective stiffness recorded at this amplitude for bearings tested in Chapter 3.

Effective damping versus cycle number is illustrated in Figure 5.8. There is less than 10% variation of the measured effective damping values for each bearing from the mean effective damping. A closer look at Table 5.3 reveals that bearings from sheet MB2 have an average effective damping of 10% while the bearings from sheet MB3 have an average effective damping of 11%. While these results are close, additional damping in MB3-1 and MB3-4 may be a result of previous cycling at high lateral displacement amplitudes. The range of effective damping measured during fatigue testing at an amplitude of $1.5t_r$ is consistent with the results obtained during cyclic testing along a parallel orientation performed in Chapter 3 at this amplitude.

The force-displacement plots show positive incremental force resisting capacity throughout each fully reversed cycle of fatigue testing. This satisfies code requirements (ASCE, 2005) regarding cyclic tests. In addition, there are two specific provisions regarding test specimen adequacy outlined in ASCE 7-05 with regards to fatigue testing. The first requires that there is no greater than a 20% decrease in the initial effective stiffness over the cycles of the fatigue test. Similarly, it requires that there is no greater than a 20% decrease in effective damping. The first condition is satisfied by the SU-FREI bearings tested which experienced an 18% average decrease between the 1st and 12th cycle. The effective damping, on the other hand, decreased by: 23% in MB2-2 and MB2-3; and 36% in MB3-1 and MB3-4. It should be noted that this decrease occurs in the unscragged first cycle. Scragged effective damping is nearly constant in all four of the bearings tested between the 2nd cycle and the 12th cycle. This is illustrated in Figure 5.8 and supported by Table 5.3. The scragged properties of SU-FREI bearings under fatigue test conditions were well within the tolerable limits of ASCE 7-05.

5.4 Summary and Concluding Remarks

This chapter investigated the performance of SU-FREI bearings under serviceability and fatigue conditions. The objectives of these tests are to show acceptable response characteristics in SU-FREI bearings. Where applicable, the design code provisions of ASCE 7-05 were used to evaluate the performance of SU-FREI bearings.

5.4.1 Serviceability Tests

Serviceability testing revealed that lateral effective stiffness decreases under repeated cycling at constant displacement amplitude and design axial load. This decrease in effective stiffness is most prominent in the first three cycles of testing. Between the first unscragged cycle and the third cycle of testing there is a 6% to 8% decrease in effective stiffness. The scragged cycles of serviceability testing from the 3rd cycle through to the 20th show a negligible decrease in effective stiffness in the range of 3% to 5%. Unlike the effective stiffness, the number of cycles performed has negligible effect on the effective damping. The measured effective damping from serviceability testing is nearly constant with less than 5% variation from the mean. Variations in effective stiffness and damping as a result of serviceability testing are well within tolerable limits. Positive force resisting capacity was maintained throughout serviceability tests satisfying the provisions of ASCE 7-05. SU-FREI bearings were subjected to larger displacements then the design wind force would have generated. Their performance during this test provides adequate evidence that they are more than capable of acceptable serviceability performance under design wind force conditions.

5.4.2 Fatigue Tests

Similar to the results of serviceability testing, repeated lateral cycling at the total design displacement resulted in a decrease in effective stiffness. Between cycle one and cycle twelve, the SU-FREI bearings experienced an average decrease in effective stiffness of 18%. This decrease in effective stiffness is within the tolerable range outlined by the ASCE (2005). The largest decrease in effective stiffness occurred in the first 2-3 cycles. Scragged cycles (2-12) achieved consistent effective stiffness within 5% of the mean in all four ¼ scale SU-FREI bearings tested. Both the unscragged and scragged effective stiffness remained within acceptable limits as per the ASCE (2005). There is a substantial (30%) decrease in effective damping between the first and second cycle. Despite the difference in unscragged effective damping between the first and second cycle of fatigue testing, the scragged cycles showed nearly constant effective damping within 3% of the mean. The difference in unscragged properties is to be expected. The SU-FREI bearings showed acceptable scragged performance throughout fatigue testing at an amplitude of $1.5t_r$.

Table 5.1 Effective stiffness and effective damping from serviceability testing of MB2-2 at lateral displacements of $0.15t_r$ and $0.35t_r$

Cycle	0.15tr Effective Stiffness (N/mm)	0.15tr Effective Damping (%)	0.35tr Effective Stiffness (N/mm)	0.35tr Effective Damping (%)
1	205.4	14.2	156.0	12.4
2	197.8	14.3	147.4	12.3
3	194.2	14.2	144.6	12.2
4	193.3	14.3	143.5	12.1
5	191.8	14.4	142.4	12.1
6	190.0	13.9	142.2	12.2
7	190.3	14.0	141.6	12.2
8	190.5	14.2	141.0	12.1
9	189.9	13.8	140.7	12.1
10	189.1	14.1	140.6	12.1
11	189.3	14.2	139.9	12.1
12	188.7	14.0	139.8	12.3
13	188.8	14.4	139.6	12.1
14	188.0	14.4	139.5	12.1
15	186.9	13.7	138.8	12.1
16	185.9	14.1	139.0	12.1
17	186.0	14.1	138.9	12.0
18	185.9	14.2	138.6	12.2
19	187.8	14.0	138.3	12.0
20	187.2	13.8	138.1	11.6

Table 5.2 Effective stiffness and effective damping from serviceability testing of MB2-3 at lateral displacements of $0.15t_r$ and $0.35t_r$

	0.15tr		0.35tr	
Cycle	Effective Stiffness (N/mm)	Effective Damping (%)	Effective Stiffness (N/mm)	Effective Damping (%)
1	208.7	14.6	156.6	12.2
2	197.9	14.3	147.6	12.2
3	195.4	14.1	145.5	12.1
4	192.9	14.3	143.8	12.1
5	192.5	14.1	143.1	12.2
6	191.3	14.2	142.3	12.2
7	190.3	14.1	141.9	12.2
8	190.2	14.0	141.2	12.0
9	189.9	14.1	141.2	12.2
10	189.5	14.0	140.8	12.1
11	188.4	14.1	140.4	12.3
12	188.5	14.1	140.1	12.1
13	187.9	14.1	139.8	12.1
14	188.0	14.0	139.8	12.1
15	187.7	13.9	139.6	12.1
16	187.7	14.0	139.1	12.1
17	187.1	14.0	139.1	12.2
18	187.7	13.9	138.9	12.1
19	186.4	14.0	138.9	12.1
20	186.7	13.3	138.4	11.6

Table 5.3 Effective stiffness and damping from fatigue testing of bearings MB2-2, MB2-3, MB3-1, and MB3-4

	MB2-2		MB2-3		MB3-1		MB3-4	
Cycle	Effective Stiffness (N/mm)	Effective Damping (%)	Effective Stiffness (N/mm)	Effective Damping (%)	Effective Stiffness (N/mm)	Effective Damping (%)	Effective Stiffness (N/mm)	Effective Damping (%)
1	79.5	12.8	79.7	12.7	81.0	13.0	74.5	12.8
2	73.0	9.9	73.2	9.8	75.5	10.9	70.6	11.1
3	70.7	9.7	70.9	9.5	73.5	10.8	68.8	10.9
4	69.5	9.6	69.7	9.5	72.4	10.7	67.9	10.9
5	68.6	9.6	68.9	9.5	71.7	10.7	67.2	10.8
6	68.0	9.6	68.3	9.5	71.1	10.7	66.7	10.8
7	67.5	9.6	67.7	9.5	70.6	10.7	66.2	10.8
8	67.1	9.6	67.3	9.5	70.3	10.7	65.9	10.8
9	66.7	9.6	67.0	9.4	69.9	10.6	65.6	10.7
10	66.4	9.5	66.7	9.4	69.6	10.6	65.4	10.8
11	66.1	9.5	66.4	9.4	69.4	10.6	65.1	10.7
12	65.9	9.4	66.1	9.3	69.1	10.4	64.9	10.5

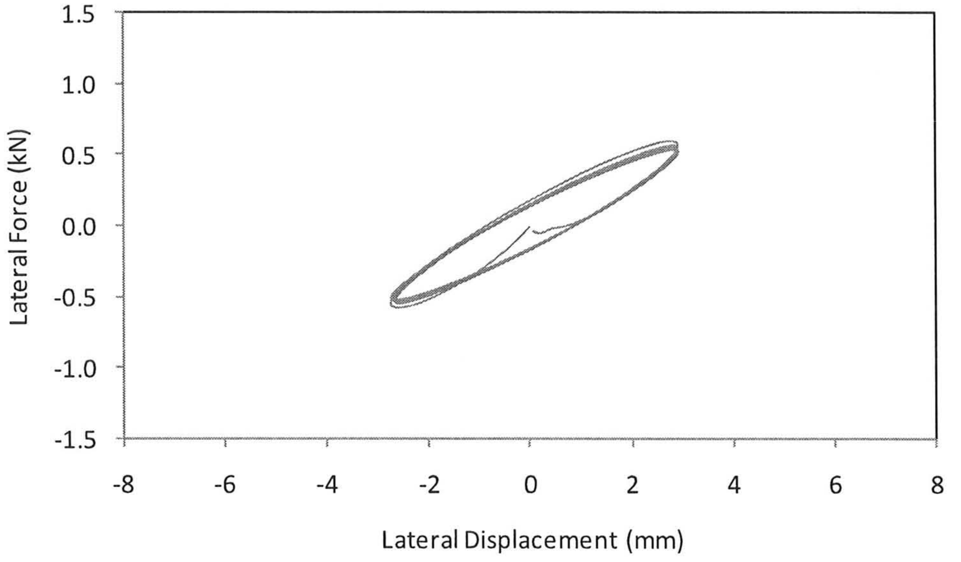

(a) MB2-2

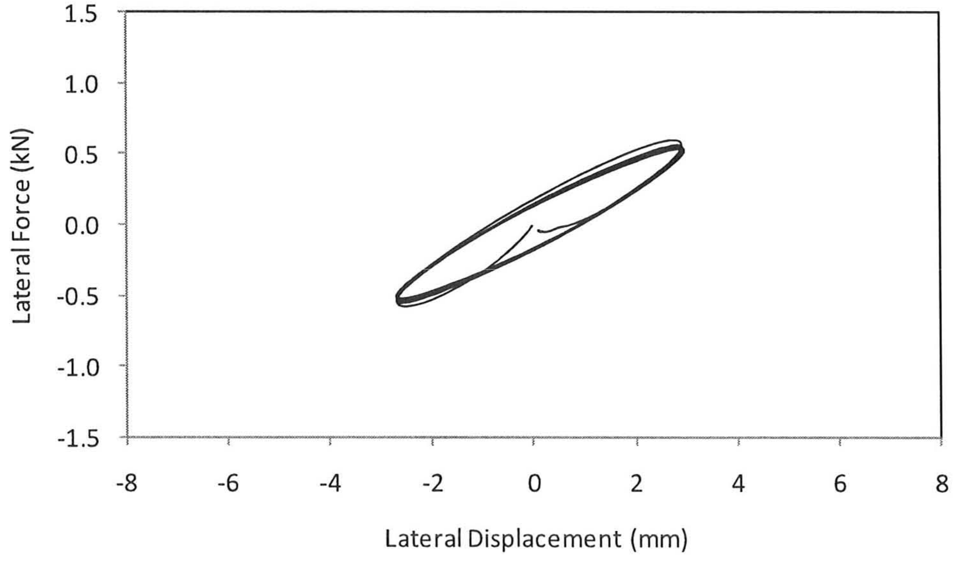

(b) MB2-3

Figure 5.1 Force displacement hysteresis from serviceability testing performed on ¼ scale SU-FREI bearings:(a) MB2-2 and (b) MB2-3 at a lateral displacement amplitude of $0.15t_r$

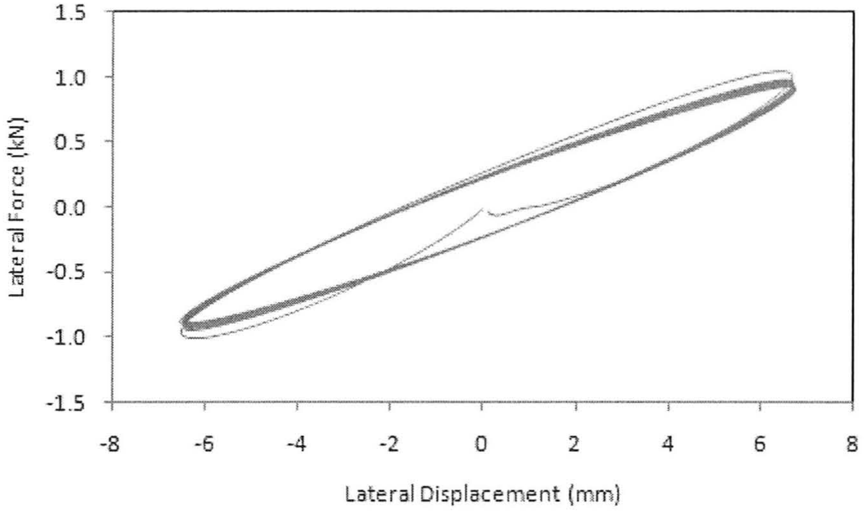

(a) MB2-2

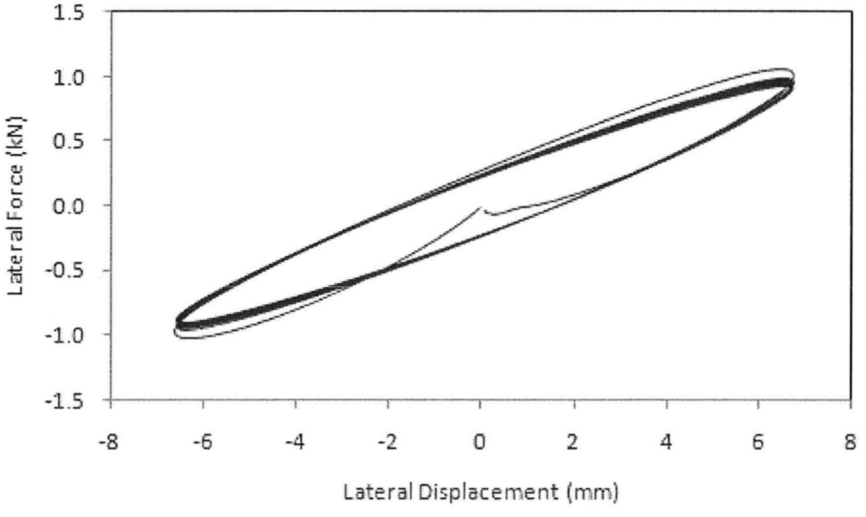

(b) MB2-3

Figure 5.2 Force displacement hysteresis from serviceability testing performed on ¼ scale SU-FREI bearings:(a) MB2-2 and (b) MB2-3 at a lateral displacement amplitude of $0.35t_r$

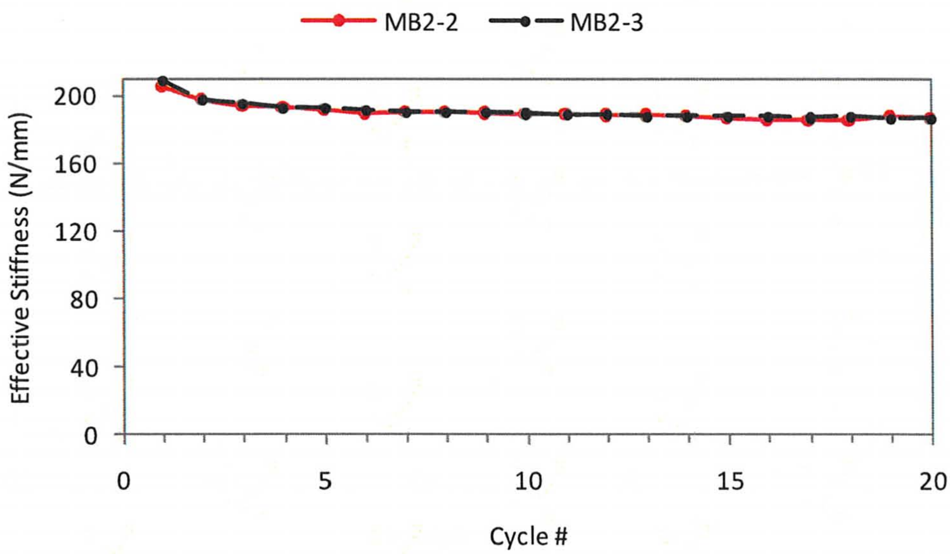

(a) $0.15t_r$

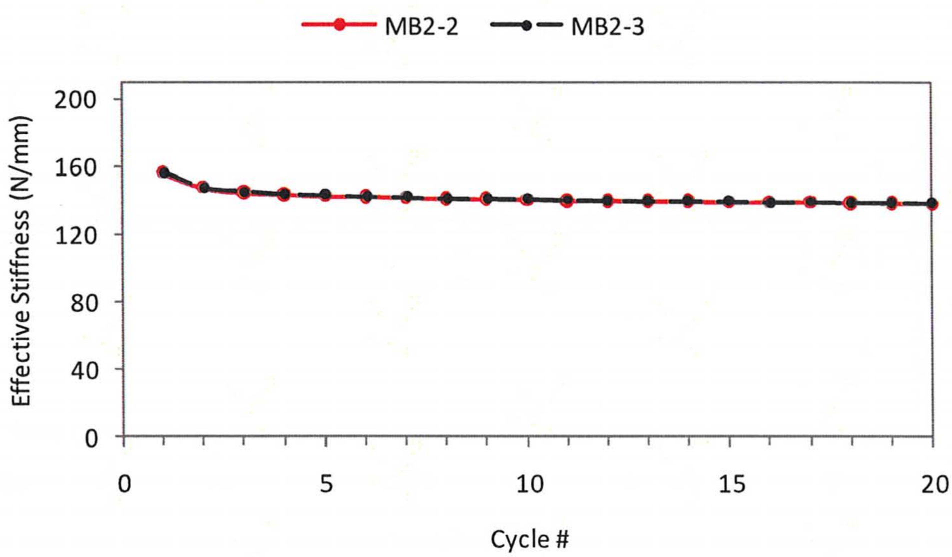

(b) $0.35t_r$

Figure 5.3 Effective stiffness versus the cycle number obtained from serviceability testing of SU-FREI bearings at lateral displacement amplitudes of $0.15t_r$ and $0.35t_r$

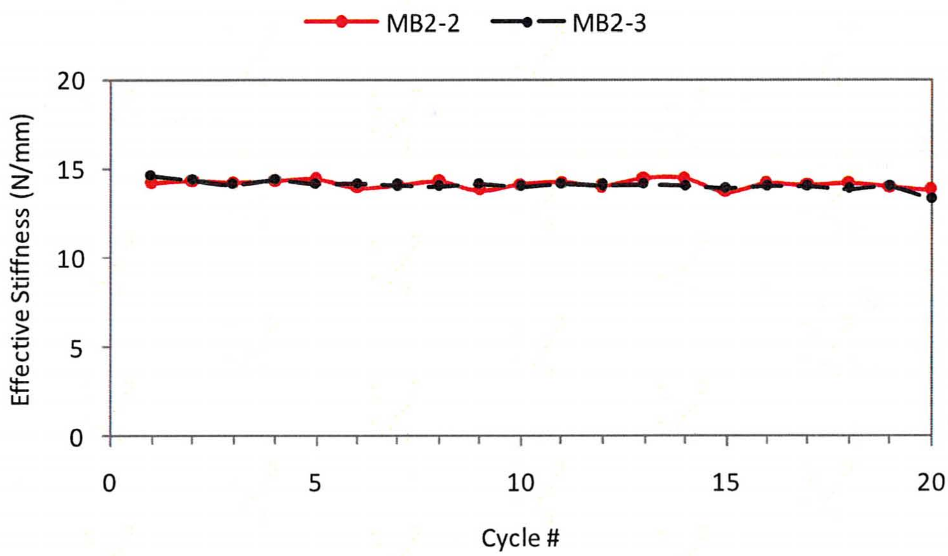

(a) $0.15t_r$

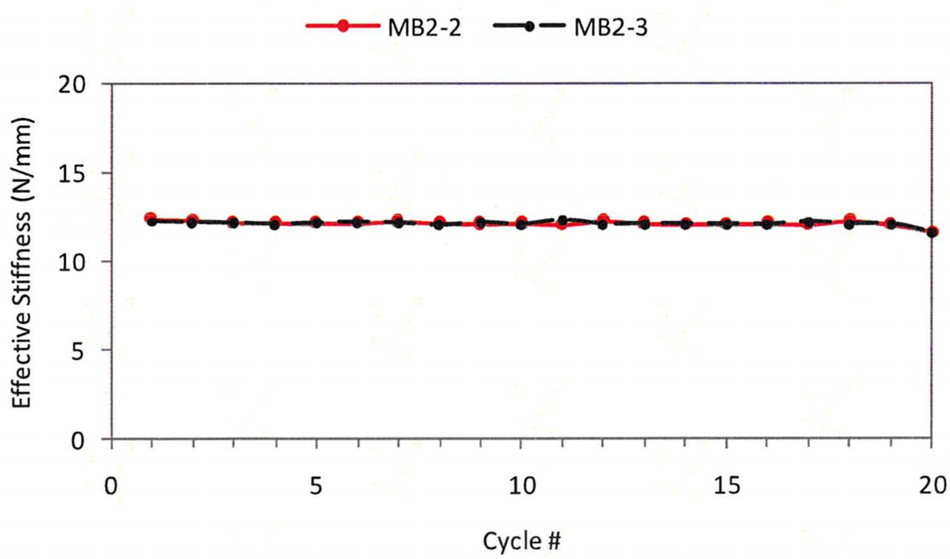

(b) $0.35t_r$

Figure 5.4 Effective damping versus the cycle number obtained from serviceability testing of SU-FREI bearings at lateral displacement amplitudes of $0.15t_r$ and $0.35t_r$

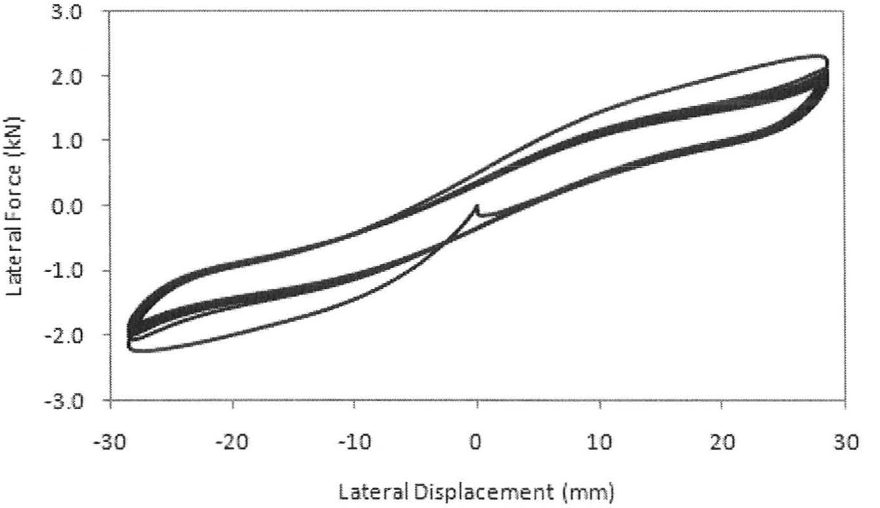

(a) MB2-2

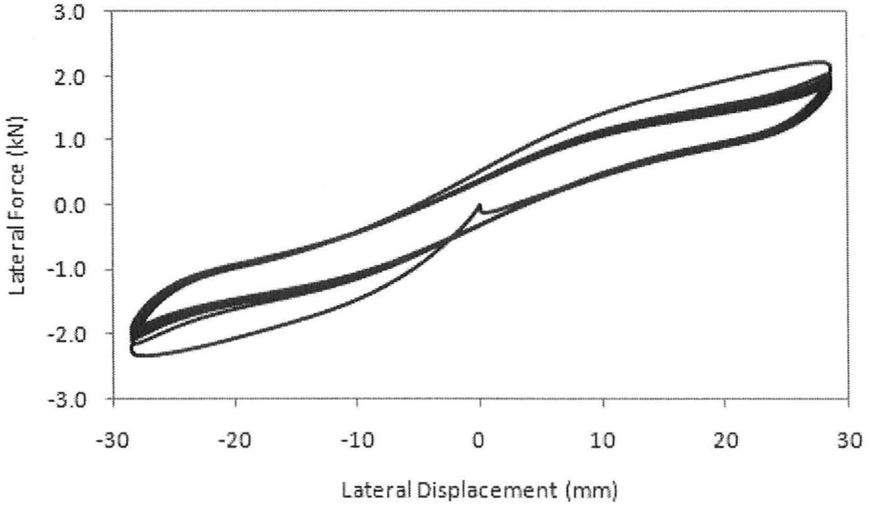

(b) MB2-3

Figure 5.5 Lateral force-displacement hysteresis from fatigue testing performed on SU-FREI bearing: (a) MB2-2, and (b) MB2-3

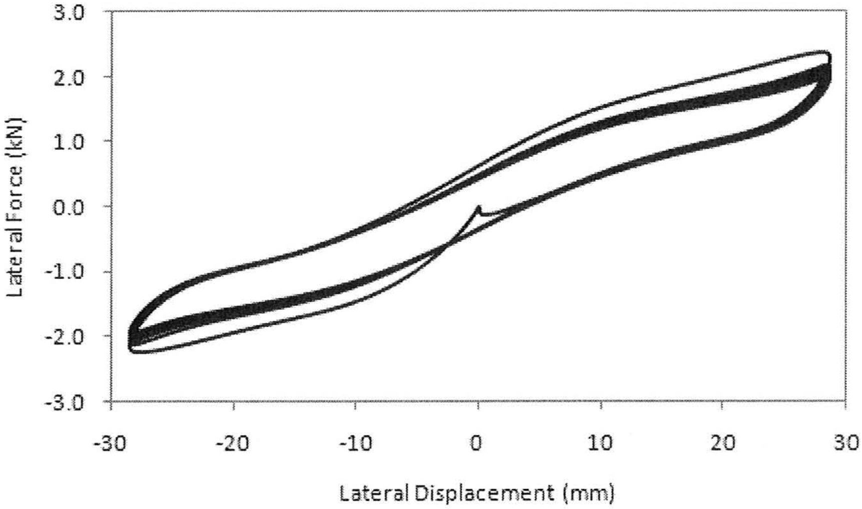

(a) MB3-1

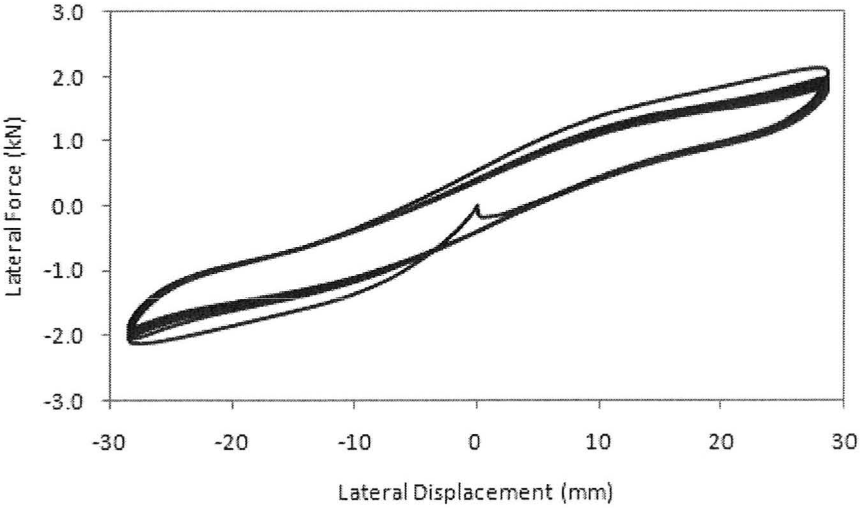

(b) MB3-4

Figure 5.6 Lateral force-displacement hysteresis from fatigue testing performed on SU-FREI bearing: (a) MB3-1, and (b) MB3-4

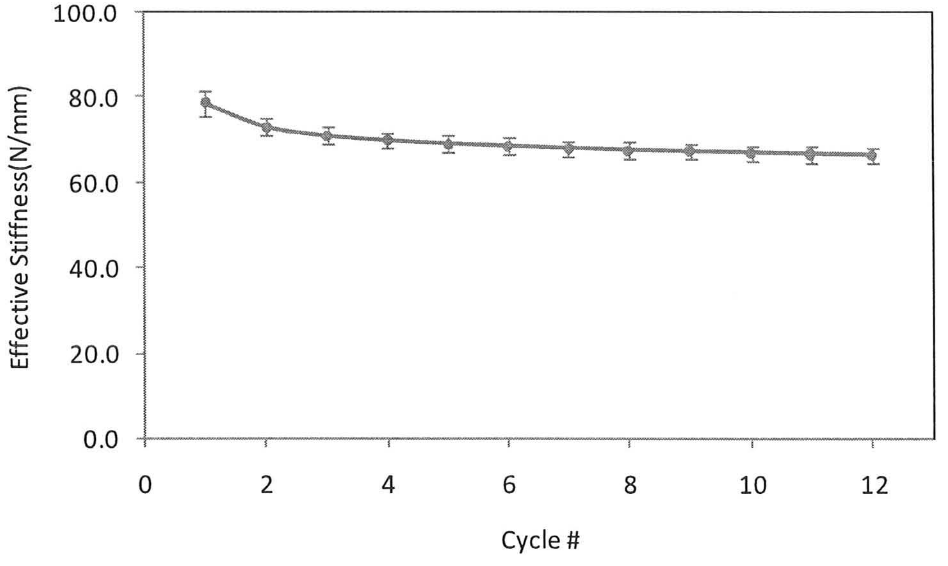

Figure 5.7 Average effective stiffness versus sycle number obtained from fatigue testing performed on ¼ scale SU-FREI bearings: MB2-2, MB2-3, MB3-1, and MB3-4

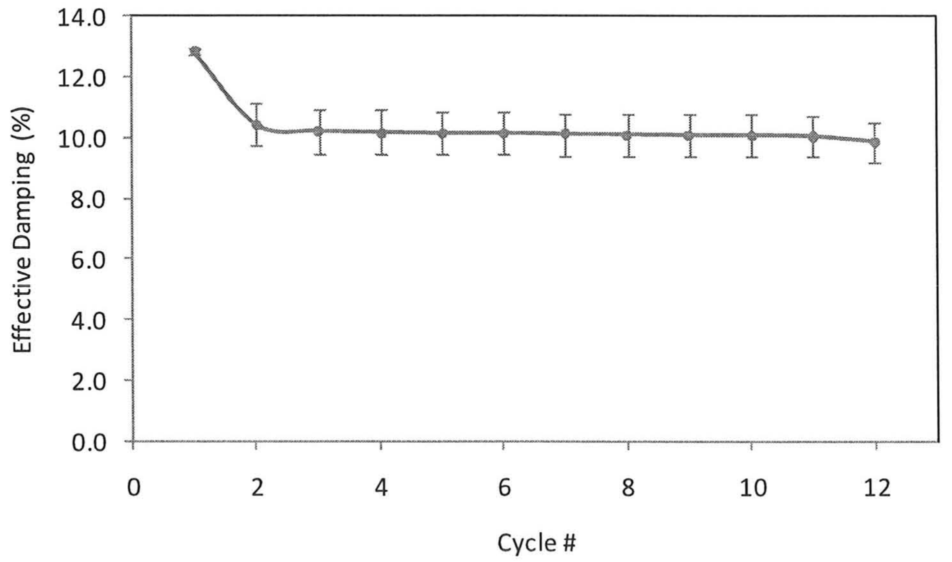

Figure 5.8 Average effective damping versus cycle number obtained from fatigue testing performed on ¼ scale SU-FREI bearings: MB2-2, MB2-3, MB3-1, and MB3-4

Chapter 6. Conclusions and Recommendations

6.1 Summary and Conclusions

The objective of the research performed in this thesis was to further investigate the performance of square SU-FREI bearings as seismic base isolators for use in low-rise structures. Several experimental tests were employed in order to achieve this. Twelve ¼ scale SU-FREI bearings were built and tested. The first test investigated the influence of orientation angle on SU-FREI performance during lateral cyclic testing. Next, the stability of SU-FREI bearings was explored under lateral cyclic excitation and rollout testing. Finally, the performance of SU-FREI bearings under fatigue and serviceability conditions was investigated.

6.1.1 Lateral Cyclic Testing at Parallel and Diagonal Orientations

The first topic of research involved lateral cyclic testing of ¼ scale square SU-FREI bearings under design axial load at parallel and diagonal orientations with respect to the direction of excitation. The following points summarize the main findings of Chapter 3:

- Comparison between orientation angles revealed that higher effective stiffness and damping is generally achieved when square SU-FREI bearings are cycled at a diagonal orientation. Code requirements regarding cyclic testing were satisfied at both orientations.
- Bearings tested at a parallel orientation achieved a longer base isolated period then those tested along a diagonal orientation. Despite this difference, SU-FREI bearings tested at both orientations achieve adequate base isolated periods longer than one second.

6.1.2 Stability of SU-FREI Bearings

The stability of square SU-FREI bearings was the next topic explored in this thesis. Two test procedures were used to investigate the stability of SU-FREI bearings. The first procedure involved lateral cyclic testing of ¼ scale bearings under increasing axial loads. A number of tests were performed at incremental lateral displacement amplitudes in order to determine the critical axial loads under which buckling occurred during dynamic excitation. The following points summarize the main findings of dynamic buckling tests performed in Chapter 4:

- Cyclic testing at high axial loads caused delamination to occur in some of the SU-FREI bearings. Delamination led to a decrease in effective stiffness and a significant increase in effective damping at high axial loads and large lateral displacements.
- The decrease in both effective and transverse stiffness, which accompanied delamination in SU-FREI bearings, had a minor effect on the critical load. Results were consistent within a 95% confidence interval of the mean.

- The critical buckling load decreases with increasing lateral displacement amplitude. At the largest displacement amplitude, the critical load achieved was measured as 8 times the design axial load.
- Dynamic buckling tests reveal that SU-FREI bearings are highly resistant to buckling instability under dynamic excitation. The axial loads required for instability to occur are significantly larger than the design axial load.

The second stability test performed on ¼ scale SU-FREI bearings was the rollout test. The following points summarize the main findings of rollout testing discussed in Chapter 4:

- Stable rollover (SR) deformation was observed in SU-FREI bearings up to lateral displacements equal to $3.0t_r$. Positive force resisting capacity was maintained during rollout tests performed up to a displacement of $3.0t_r$.
- Contact made between the vertical faces of SU-FREI bearings and the upper and lower test platens was accompanied by a significant increase in force resisting capacity in the bearing. This benefits the isolation system by acting to limit the maximum lateral displacement.

6.1.3 Serviceability and Fatigue Performance of SU-FREI Bearings

The design code provisions of ASCE 7-05 provide experimental test requirements for seismic isolators subjected to fatigue and serviceability conditions. The following points summarize the main findings of serviceability testing explored in Chapter 5:

- Effective stiffness decreases under repeated cycling at serviceability lateral displacement amplitude and design axial load. This decrease in effective stiffness is most prominent in the first three cycles of testing. Between the first unscragged cycle and the third cycle of testing there is a 6% to 8% decrease in effective stiffness.
- Between the 1st and 20th cycle of lateral displacement there is negligible variation in effective damping.

The following points summarize the main findings of fatigue testing investigated in Chapter 5:

- Repeated cycling at the total design displacement resulted in a decrease in effective stiffness. Between cycle one and cycle twelve, the SU-FREI bearings experienced an average decrease in effective stiffness of 18%. This decrease in effective stiffness is within the tolerable range outlined by the ASCE (2005).
- The scragged cycles showed nearly constant effective damping within 3% of the mean. The scragged effective damping of SU-FREI bearings is well within the tolerance set by ASCE 7-05.

Ultimately it is the intention of this research to provide further evidence that SU-FREI bearings are suitable for use as seismic isolation devices in low rise structures. Through a range of experimental test procedures, the SU-FREI bearings investigated in this study have shown satisfactory performance according to design code provisions.

6.2 Recommendations for Further Research

The following points are recommendations for future experimental research:

- During stability testing performed in this study, SU-FREI bearings underwent delamination during cyclic testing under an axial load of 90 kN. It would be beneficial to further understand the conditions that lead to delamination. This would involve material testing to determine the forces required to break the bond between elastomer layers and carbon fiber layers.
- Although delamination was visibly apparent from the outside edges of the SU-FREI bearings, the condition inside the bearing was not known. It would be of great benefit to SU-FREI bearing research if a non intrusive imaging method (MRI or CT scan) could be used to determine if an SU-FREI bearing had undergone internal delamination. Bearings would need to be scanned before and after cyclic testing to determine if any damage had occurred internally.
- Square SU-FREI performance has been evaluated through cyclic testing at parallel and diagonal orientations and shake table testing was previously performed on bearings at a parallel orientation. Ultimately bi-directional shake table testing is the next step in SU-FREI research. It is necessary to explore the performance of these bearings under simultaneous excitation along two axes.
- In order to fully understand the ultimate shear properties of SU-FREI bearings additional rollout testing needs to be performed at larger displacements. In addition, it is necessary to determine what if any effect orientation angle has on δ_{max}.

The following points are recommendations for future analytical research:

- Currently, a closed form solution for estimating the critical buckling load of SU-FREI bearings does not exist. Experimental results cannot yet be compared directly to analytical results when investigating SU-FREI stability.
- It was previously suggested that further experimental research should be performed to accurately determine under what conditions the onset of delamination occurs in SU-FREI bearings. Modeling the stress which would lead to delamination, a decrease in effective stiffness, and damping is another necessary step to understanding this phenomenon.

References

Aiken, I. D., Kelly, J. M., Clark, P. W., Tamura, K., Kikuchi, M., & Itoh, T. (1992). "Experimental studies of the mechanical characteristics of three types of seismic isolation bearings". *Proceedings, Tenth World Conference on Earthquake Engineering.* Madrid, Spain: Seismic Isolation Engineering, Inc.

ASCE. (2005). Minimum Design Loads for Buildings and other Structures. *ASCE/SEI 7-05* . New York: American Society of Civil Engineers.

Ashkezari, G. D., Aghakouchak, A. A., & Kokabi, M. (2008). "Design, manufacturing and evaluation of the performance of steel like reinforced elastomeric seismic isolators". *Journal of Materials Processing Technology , 197,* 140-150.

Buckle, I. G., & Liu, H. (1994). "Experimental determination of critical loads of elastomeric isolators at high shear strain". *NCEER Bulletin , 8* (3), 1-5.

Buckle, I. G., & Liu, H. (1993). "Stability of elastomeric seismic isolation systems". *Proceedings of the Seminar on Seismic Isolation, Passive Energy Dissipation and Active Control, Applied Technology Council Report ATC-17-1,* (pp. 293-305). Redwood City, CA.

Buckle, I., & Kelly, J. M. (1986). "Properties of slender elastomeric isolation bearings during shake table studies of a large-scale model bridge deck". *Joint Sealing and Bearing Systems for Concrete Structures (ACI)* , 247-269.

Buckle, I., & Nagarajaiah, S. (2002). "Stability of elastomeric isolators: Critical load tests and computations". *MCEER Bulletin , 16* (1), 1-4.

Buckle, I., Nagarajaiah, S., & Ferrell, K. (2002). "Stability of elastomeric isolation bearings: Experimental study". *Journal of Structural Engineering* , 3-11.

Campbell, S. D. (2004). "Carbon fiber-reinforced elastomeric pads for building isolation". *The 33rd International Congress and Exposition on Noise Control Engineering.* Prague, Czech Republic.

Carneiro, J. O., de Melo, F. J., Jalali, S., & Camanho, P. P. (2004). "Analytical dynamic analysis of earthquake base-isolation structures using time history modal superposition". *Proceedings of the Institution of Mechanical Engineers , 218,* 39-49.

Chopra, A. K. (2007). *Dynamics of Structures: Theory and Application to Earthquake Engineering 3rd ed.* New Jersey: Prentice Hall.

Connor, J. J., & Klink, B. S. (1996). *Introduction to motion based design.* Boston: Computational Mechanics Publications.

Dorfmann, A., & Ogden, R. (2004). "A constitutive model for the mullins effect with permanent set in particle-reinforced rubber". *International Journal of Solids and Structures* , 1855-1878.

Gent, A. N. (1964). "Elastic stability of rubber compression springs". *Journal of Mechanical Engineering Science* , *6* (4), 318-326.

Imbimbo, M., & Kelly, J. M. (1998). "Influence of material stiffening on stability of elastomeric bearings at large displacements". *Journal of Engineering Mechanics* , 1045-1049.

Imbimbo, M., & Kelly, J. M. (1997). "Stability aspects of elastomeric isolators". *Earthquake Spectra* , *13* (3), 431-449.

ISO. (2005). Elastomeric seismic-protection isolators. *ISO 22762* . Geneva: International Organization for Standardization.

Kang, B.-S., Kang, G.-J., & Moon, B.-Y. (2003). "Hole and lead plug effect on fiber reinforced elastomeric isolator for seismic isolation". *Journal of Materials Processing Technology* , 592-597.

Kelly, J. M. (1999). "Analysis of fiber-reinforced elastomeric isolators". *Journal of Seismology and Earthquake Engineering* , *2* (1), 19-34.

Kelly, J. M. (1991). "Base isolation: Origins and development". *EERC News* , *12* (1).

Kelly, J. M. (2003). "Tension buckling in multilayer elastomeric bearings". *Journal of Engineering Mechanics* , 1363-1368.

Kelly, J. M. (1997). *Earthquake-resistant design with rubber, 2nd ed.* London: Springer-Verlag Limited.

Kelly, J. M., & Takhirov, S. M. (2001). "Analytical and Experimental Study of Fiber-Reinforced Elastomeric Isolators". *PEER Report 2001/11*, University of California Berkely.

Kikuchi, M., & Aiken, I. D. (1997). "An analytical hysteresis model for elastomeric seismic isolation bearings". *Earthquake Engineering and Structural Dynamics* , *26*, 215-231.

Koh, C. G., & Kelly, J. M. (1988). "A simple mechanical model for elastomeric bearings used in base isolation". *International Journal of Mechanical Sciences* , *30* (12), 933-943.

Koh, C. G., & Kelly, J. M. (1987). "Effects of axial load on elastomeric isolation bearings". *EERC Report - 86/12*, University California Berkeley.

Moon, B.-M., Kang, G.-J., Kang, B.-S., & Kelly, J. M. (2002). "Design and manufacturing of fiber reinforced elastomeric isolator for seismic isolation". *Journal of Material Processing Technology , 130-131*, 145-150.

Mordini, A., & Strauss, A. (2008). "An innovative earthquake isolation system using fibre reinforced rubber bearings". *Engineering Structures* , 2739-2751.

Nagarajaiah, S., & Ferrell, K. (1999). "Stability of elastomeric seismic isolation bearings". *Journal of Structural Engineering , 125* (9), 946-954.

Naiem, F., & Kelly, J. M. (1999). *Design of Seismic Isolated Structures: From Theory to Practice.* New York: John Wiley & Sons, Inc.

NBCC. (2005). National Building Code of Canada. Ottawa: National Research Council of Canada.

NRC. (2006). User's Guide - NBC 2005 Structural Commentaries (Part 4 of Division B). Ottawa: National Research Council of Canada.

Robinson, W. H. (1982). "Lead-rubber hysteretic bearings suitable for protecting structures during earthquakes". *Earthquake Engineering and Structural Dynamics* , Vol. 10, 593-604.

Robinson, W. H. (1982). "Lead-rubber hysteretic bearings suitable for protecting structures during earthquakes". *Earthquake Engineering and Structural Dynamics* , 593-604.

Stanton, J. F., Scroggins, G., Taylor, A. W., & Roeder, C. W. (1990). "Stability of laminated elastomeric bearings". *Journal of Engineering Mechanics , 116* (6), 1351-1371.

Taylor, A. W., & Igusa, T. (2004). *Primer on Seismic Isolation.* ASCE Publications.

Toopchi-Nezhad, H. (2008). "Stable Unbonded Fiber Reinforced Elastomeric Isolators". (master's thesis, McMaster University, 2008).

Toopchi-Nezhad, H., Tait, M. J., & Drysdale, R. G. (2008c). "A novel elastomeric base isolation system for seismic mitigation of low-rise buildings". *The 14th World Conference on Earthquake Engineering.* Beijing, China.

Toopchi-Nezhad, H., Tait, M. J., & Drysdale, R. G. (2007a). "Base isolation of small low-rise buildings using fiber reinforced elastomeric bearings". *CSCE 2007 Annual General Meeting & Conference* (pp. 1-11). Yellowknife, Northwest Territories, Canada: CSCE.

Toopchi-Nezhad, H., Tait, M. J., & Drysdale, R. G. (2008b). "Lateral response evaluation of fiber-reinforced neoprene seismic isolators utilized in an unbonded application". *Journal of Structural Engineering*, *134* (10), 1627-1637.

Toopchi-Nezhad, H., Tait, M. J., & Drysdale, R. G. (2008a). "Testing and modeling of square carbon fiber-reinforced elastomeric seismic isolators". *Structural Control and Health Monitoring*, *15*, 876-900.

Toopchi-Nezhad, H., Tait, M., & Drysdale, R. G. (2007b). "Experimental study on carbon fiber-reinforced square seismic isolators". *Ninth Canadian Conference on Earthquake Engineering*, (pp. 26-29). Ottawa, Ontario, Canada.

Tsai, H.-C. (2008). "Deformation analysis of infinite-strip bearings of laminated elastic material interleaving with tension-only reinforcements". *International Journal of Solids and Structures*, *45*, 2836-2849.

Tsai, H.-C., & Kelly, J. M. (2002). "Bending stiffness of fiber-reinforced circular seismic isolators". *Journal of Engineering Mechanics*, *128* (11), 1150-1157.

Tsai, H.-C., & Kelly, J. M. (2005). "Buckling load of seismic isolators affected by flexibility of reinforcement". *International Journal of Solids and Structures*, *42*, 255-269.

Tsai, H.-C., & Kelly, J. M. (2002). "Stiffness analysis of fiber-reinforced rectangular seismic isolators". *Journal of Engineering Mechanics*, *128* (4), 462-470.

Warn, G. P., Whittaker, A. S., & Constantinou, M. C. (2007). "Vertical stiffness of elastomeric and lead-rubber seismic isolation bearings". *Journal of Structural Engineering*, 1227-1236.